DOKUZ EYLÜL UNIVERSITY
GRADUATE SCHOOL OF NATURAL AND APPLIED SCIENCES

TWO-DIMENSIONAL DOA ESTIMATION USING ARBITRARY ARRAYS

by

Peter Nyongesah OBIMO

July, 2021

İZMİR

TWO-DIMENSIONAL DOA ESTIMATION USING ARBITRARY ARRAYS

A Thesis Submitted to the
Graduate School of Natural And Applied Sciences of Dokuz Eylül University
In Partial Fulfillment of the Requirements for the Degree of Master of Science in
Electrical and Electronic Engineering

by

Peter Nyongesah OBIMO

July, 2021
İZMİR

M.Sc THESIS EXAMINATION RESULT FORM

We have read the thesis entitled "**TWO-DIMENSIONAL DOA ESTIMATION USING ARBITRARY ARRAYS**" completed by **PETER NYONGESAH OBIMO** under supervision of **ASST. PROF. DR. ÖZGÜR TAMER** and we certify that in our opinion it is fully adequate, in scope and in quality, as a thesis for the degree of Master of Science.

....

Asst. Prof. Dr. Özgür TAMER

Supervisor

....

Prof. Dr. Yeşim ZORAL

Jury Member

....

Asst. Prof. Dr. Nalan ÖZKURT

Jury Member

Prof. Dr. Özgür ÖZÇELİK
Director
Graduate School of Natural and Applied Sciences

For Truphena Martina Anyange; you are profoundly missed.

ACKNOWLEDGEMENTS

Firstly, I express my greatest honor and gratitude to the Almighty God for this far.

Secondly, I thank Türkiye Scholarships (YTB) and the Government of Kenya for the opportunity and immense support they granted me during my pursuit of this Master of Science in Electrical and Electronic Engineering degree.

In a very special way, I thank my supervisor, Asst. Prof. Dr. Özgür TAMER for his expert advice and guidance offered throughout the research period.

To my family, I heartily appreciate the invaluable sacrifices coupled with spiritual, material, and moral support which they endlessly rendered during my study period.

Besides, I thank my colleagues, friends and faculty without whom this work wouldn't have been possible.

Finally, I am very grateful to my lovely wife Winnie for the sacrifices and all the support. Her encouragement was immense and always gave me a reason to keep the faith.

Peter Nyongesah OBIMO

TWO-DIMENSIONAL DOA ESTIMATION USING ARBITRARY ARRAYS

ABSTRACT

Wireless communication is gaining popularity with plethora of applications occasioning a crunch in bandwidth capacity. This has necessitated exploitation of higher frequency bands with higher spectral availability. However, higher frequencies results in higher data rates with higher user density leading to multipath fading and cross-channel interference which degrades bit error rate (BER). This research proposes techniques of addressing these challenges through estimation of direction of arrival (DOA) of user signals.

Specifically, the research focuses on two-dimensional (2D) DOA estimation using arbitrary arrays. Description of adaptive antenna array with factors that influence DOA estimation is comprehensively covered. Consequently, for conducting DOA estimation, coprime array is considered using MUltiple SIgnal Classification (MUSIC) algorithm. Two one-dimensional (1D) DOA estimation methods; DEcompose and COMbine (DECOM) and Unfolded Coprime Linear Array (UCLA) are proposed followed by 2D DOA estimation methods, for which; Coprime L-shaped Array (CLSA) and Unfolded Coprime L-shaped Array (UCLSA) methods coupled with a novel low-complexity 2D MUSIC algorithm are considered. Finally, virtual array interpolation technique using nuclear norm minimization is used to interpolate holes in difference co-array of coprime array to increase degrees of freedom (DoF) of the array without increasing physical sensor elements.

It was established that UCLA performed better than DECOM. Equally, UCLSA outperformed CLSA. DECOM and CLSA consider each coprime sub-array separately thereby losing the intrinsic mutual information of the array, a characteristic that is preserved in UCLA and UCLSA. Virtual interpolated array exhibited greater DoF thereby resolving $2MN-N$ sources with only $M+N-1$ sensors.

Keywords: DOA estimation, DECOM, UCLA, CLSA, UCLSA, MUSIC algorithm, Virtual Array Interpolation, nuclear norm minimization

DÜZENSİZ ANTEN DİZİLERİ İLE İKİ BOYUTLU GELİŞ AÇISI KESTİRİMİ

ÖZ

Kablosuz iletişim, bant genişliği kapasitesinde bir daralmaya neden olan çok sayıda uygulama ile popülerlik kazanıyor. Bu, daha yüksek spektral kullanılabilirliğe sahip daha yüksek frekans bantlarının kullanılmasını gerektirmiştir. Bununla birlikte, daha yüksek frekanslar, daha yüksek kullanıcı yoğunluğu ile daha yüksek veri hızları ile sonuçlanır ve bu da çok yollu zayıflamaya ve bit hata oranını (BER) azaltan çapraz kanal girişimine yol açar. Bu araştırma, kullanıcı sinyallerinin geliş açısı kestiriminenin (DOA) tahmini yoluyla bu zorlukların ele alınmasına yönelik teknikler önermektedir.

Spesifik olarak, araştırma, rastgele diziler kullanarak iki boyutlu (2D) DOA dayanmaktadır. DOA tahminini etkileyen faktörlerle birlikte uyarlanabilir anten dizisinin tanımı kapsamlı bir şekilde ele alınmaktadır. Sonuç olarak, DOA tahminini yürütmek için, çoklu sinyal sınıflandırması (MUSIC) algoritması kullanılarak ortak dizi düşünülür. İki tek boyutlu (1D) DOA tahmin yöntemi; ayrıştırmak ve birleştirmek (DECOM) ve açılmamış eş asal doğrusal dizi (UCLA) ve ardından 2D DOA tahmin yöntemleri önerilmiştir, bunun için; eş asal L-şekilli dizi (CLSA) ve Katlanmamış eş asal L-şekilli dizi (UCLSA) yöntemleri, yeni bir düşük karmaşıklıklı 2D MUSIC algoritması ile birleştirildi. Son olarak, nükleer norm minimizasyonunu kullanan sanal dizi enterpolasyon tekniği, fiziksel sensör elemanlarını artırmadan dizinin serbestlik derecesini (DoF) artırmak için ortak asal dizinin fark eş dizisindeki delikleri enterpolasyon yapmak için kullanılır.

UCLA'nın DECOM'dan daha iyi performans gösterdiği tespit edildi. Aynı şekilde, UCLSA, CLSA'dan daha iyi performans gösterdi. DECOM ve CLSA, her bir asal alt diziyi ayrı ayrı ele alır ve böylece dizinin içsel karşılıklı bilgisini kaybeder; bu, UCLA ve UCLSA'da korunan bir özelliktir. Sanal enterpolasyonlu dizi, daha fazla DoF sergileyerek $2MN-N$ kaynaklarını yalnızca $M+N-1$ sensörlerle çözer.

Anahtar kelimeler: DOA tahmini, DECOM, UCLA, CLSA, UCLSA, MUSIC algoritması, Sanal Dizi İnterpolasyonu, çekirdek norm minimizasyonu

CONTENTS

Page

LIST OF FIGURES

Page

LIST OF TABLES

Page

CHAPTER ONE
INTRODUCTION

1.1 Background and Motivation

There is an avalanche of wireless devices leading to an exponential rise in data generation. The net effect being a crunch in the bandwidth capacity. Fifth generation (5G) or mm-wave communication for instance, coupled with artificial intelligence, and big data analytics is geared towards achieving diversified ecosystem through a technology called internet of everything (IoE) which will ensure interconnection of people, processes, things, and data to enable their intelligent communication with no human intervention (Santacruz et al., 2020; Kubba & Hoomod, 2019; Miraz et al., 2015). According to IDC forecasts, the interconnected devices are growing exponentially with an estimation of having 75 billion of these by 2025 which will be generating over 79.4 ZB of data (Al-Sarawi et al., 2020).

One of the drivers of the aforementioned advancements is the wireless communication technologies. In this sector, the focus is on optimizing wireless networks for enhanced capacity, fidelity, quality of service, spectral efficiency, link reliability and low-power operation. Although it might be demanding to realise all the above features in a single network, a tradeoff for an optimal operation is possible.

A number of techniques have been embraced as a means of realising the aforementioned features. These techniques include redesigning of the antenna system, employing enhanced modulation, multiple access and switching techniques, spectral efficiency algorithms, channel coding and new error correction and detection protocols (Giordani et al., 2020; Ilderem, 2019).

Redesigning of the antenna system has led to development of smart antennas (adaptive antenna arrays) that have a dynamic beam-forming characteristic, a property that enhances channel capacity and spectrum efficiency through multipath and co-channel interference suppression (Misra et al., 2018; Bhobe & Perini, 2001).

One of the parameters of an adaptive array that has realised a lot of attention recently is the direction of arrival (DOA) estimation of a user signal. This is the process of determining the direction from which propagating electromagnetic waves impinge on an antenna array. Nonuniform antenna array geometries like L-shaped array (LSA), Cross-shaped array (CSA) and sparse array geometries like nested arrays, coprime linear arrays (CLA), Coprime L-shaped arrays (CLSA) etc when used for DOA estimation, presents excellent results compared to the regular array geometries like uniform linear array (ULA), uniform circular array (UCA), uniform rectangular (planar) arrays (URA) etc which in addition, have some limitations when applied practically. This is because nonuniform arrays, have the advantage of avoiding coupling problem and at the same time providing high degrees of freedom (DOFs). Therefore, nonuniform array geometries are preferred due to enhanced performance compared to the regular ones with the same number of sensor elements, (Li et al., 2018).

There are numerous DOA estimation algorithms that have been proposed of which include: beamforming, subspace and parametric approaches. These algorithms offer varying performances in terms of estimation accuracy, resolution capability and computational complexity (Chung et al., 2014). Therefore, the choice of any algorithm would mostly depend on the performance preferences as well as limitations either in terms of resolution, computational complexity or the type of arrays to which they may be applied.

Balabadrapatruni (2012) used uniform linear array (ULA) to perform analysis on two categories of algorithms namely classical (non-subspace) e.g. Delay-and-Sum (DS), Maximum Likelihood (ML) and Capon's Minimum Variance Distortionless Response (MVDR) techniques and subspace methods e.g. Multiple Signal Classification (MUSIC), root-MUSIC and estimation of signal parameters via rotational invariance technique (ESPRIT). In his findings, he noted that the former category which depends on spatial spectrum, are simple to implement but have poor resolutions despite being suitable in circumstances where the signal properties are unknown. On the contrary, the latter - which have also been deeply analysed by Reaz et al. (2012) - have been categorised as super-resolution algorithms due to their superior performances. Other comparative studies by Dhope et al. (2013); Li et al. (1993) for instance, that majored on subspace algorithms particularly MUSIC, MVDR, State-Space Realization (SSR) and ESPRIT over ULA antenna in the presence of white Gaussian noise asserted that the subspace algorithms have greater performance in terms of sensor array processing, spectral analysis, and general parameter estimation.

While comparing MUSIC and ESPRIT algorithms over adaptive antenna arrays, Lavate et al. (2010) found out that MUSIC algorithm has a higher accuracy and stability and resolution than ESPRIT. This therefore gives MUSIC a wider application in adaptive arrays especially where user separation through SDMA for cellular communication is required. Moreover, Dongarsane & Jadhav (2011); Gupta & Kar (2015) investigated the factors that affects DOA estimation using MUSIC algorithm on ULA for which the authors opined that the resolution of DOA estimation improves as number of snapshots, number of array elements and signal-to-noise ratio (SNR) increases.

Most of the aforementioned high-resolution DOA estimation algorithms perform efficiently only on regular array geometries. However, MUSIC is regarded as one of the most representative technique due to its high resolution and flexibility for even arbitrary arrays (Sun et al., 2018). DOA analysis using arbitrary arrays is realising a lot of attention due to greater performances in two-dimensions (2D) and by applying L-shaped coprime array (CLSA) for instance, lesser computation complexity can be realised. Coprime array concept has been used by several authors in analysis of nonuniform array. For instance, Kwizera et al. (2017); Zhou et al. (2013) used DEcompose and COMbine (DECOM) method for coprime array to perform a comparison between ULA and nonuniform coprime linear array (NCLA) for which they observed that the latter's performance is superior to that of the former for DOA estimation applications. On the other hand, Unfolded Coprime Linear Array (UCLA) concept used by Zhang et al. (2020, 2019) seemed more promising than the DECOM method. In these two different scenarios, UCLA method is seen to present higher

DOF and aperture with suppressed ambiguous DOAs in the power pseudo-spectra.

In Wang et al. (2017) 2D DOA estimation of multiple signals for coprime planar arrays (CPAs) was conducted for which a computationally efficient 1D partial spectral search approach based on MUSIC algorithm was proposed. Furthermore, Yang et al. (2017) proposed a novel method for 2D DOA estimation using CLSA geometry with MUSIC algorithm with an aim of eliminating angle ambiguity. The same analysis was further advanced by Hu et al. (2015) using propagator method (PM). Their proposed methods seemed rather computationally complex as in both scenarios, conventional MUSIC method is applied. Li et al. (2018) proposed an UCLSA method for analysing L-shaped coprime arrays, a method that was also adopted by Zhang et al. (2019) but with a novel low complexity MUSIC-like algorithm method that seem promising since it offered automatic angle-pairing and low computational complexity.

In DOA estimations, the problem is not only to estimate angles of arrival (AoA), but to also find the maximum number of sources that can be resolved at the least cost possible with the lowest computations to ensure greater speeds. For this reason, virtual array interpolation has been proposed as a way of resolving more sources than sensor elements. Interpolation techniques like SS-MUSIC, positive definite Toeplitz completion, array interpolation, ℓ_1 minimization or LASSO can be used for interpolating the sensors for the holes in the co-array. The only drawback in using them is that they will require additional tuning parameters like matrix vectorisation, matrix reshaping, spatial smoothing or discretization of parameter space into a dense grid respectively resulting in computational complexity. Liu et al. (2016) proposed a novel low complexity method for interpolating the holes in the difference co-array using nuclear norm minimization. This method was also adopted by Hosseini & Sebt (2017) due to its simplicity and better performance.

This research focuses on achieving three major DOA estimation objectives namely realisation of greater DOF, superior DOA estimations using arbitrary arrays and lastly being able to resolve more sources than sensors. Therefore, coprime array geometries as well as interpolated virtual arrays will be used coupled with MUSIC algorithm.

1.2 Purpose and Aims of the Thesis

The purpose of this research is to perform two-dimensional (2D) DOA estimation of an impinging electromagnetic waves using arbitrary antenna arrays. The research focus on conducting 2D DOA estimation using coprime L-shaped array even with a missing element making them arbitrary arrays. Specifically, it shall focus on analysis of a sparse array namely unfolded coprime L-shaped array (UCLSA) for DOA estimation using MUSIC and a novel MUSIC-like algorithm which transforms a 2D spectral peak searching problem to 1D as a way of reducing the computational complexity involved in 2D estimations thereby increasing the speed, resolution and efficiency. Further, the analysis will encompass interpolation of a coprime linear array (CLA) and to apply co-array MUSIC for its DOA estimation with an aim of increasing the Degrees of Freedom (DOF) of the antenna to enable resolving of more signal sources than the number of sensor elements.

1.3 Objectives

The main objective of this research is to model and perform DOA estimation using arbitrary antenna arrays. The specific objectives include the following:

(i) To provide an understanding of adaptive beamforming, a case for smart antenna systems, and highlight its benefits in wireless communication system.

(ii) To investigate essential features that influence the source localization with an aim of capitalizing on ways of ensuring low computational complexity in determination of the angle of arrival.

(iii) To model and analyze sparse array geometry specifically coprime array using DECOM and UCLA methods for 1D and CLSA and UCLSA methods for 2D DOA estimation respectively using the coprime principle.

(iv) To perform virtual array interpolation for coprime array using nuclear norm minimization method.

(v) To utilize MUSIC algorithm, a high-resolution DOA estimation technique, to simulate and evaluate the performance of the aforementioned models in MATLAB program with a view of enhancing the robustness and capacity of the network while at the same time reducing interference.

1.4 Scope of the Thesis

The scope of this research ranges from mathematical modelling of the signal data for sparse array geometry specifically coprime array in the conventional way, novel methods for 2D MUSIC algorithm to virtual array interpolation method for enhancing the DOF and consequently aperture of the array without increasing physical sensor elements. The concept is developed from a coprime nonuniform linear array for 1D DOA estimation and improved through coprime L-shaped array for 2D DOA estimation using unfolded coprime L-shaped array (UCLSA) for 2D DOA estimation providing automatic ambiguity elimination and finally nuclear norm minimization method used for interpolation of the co-array.

1.5 Organization of the Thesis

This thesis is organised into five chapters. Firstly, chapter one presents the background and motivating factors to carry out the research. The chapter consequently proceeds to present the purpose, aims and objectives of the research. In chapter two, the description of DOA estimation including an overview of smart antenna system is presented. Further, factors that influence the performance of DOA estimation are discussed. The chapter ends by giving a perspective on the sparse arrays specifically coprime theory and L-shaped antenna arrays. In chapter three, mathematical models for three classes of array geometries:- DECOM and UCLA for 1D DOA estimation, CLSA and UCLSA for 2D DOA estimation and thirdly virtual array interpolation for co-array MUSIC algorithm are generated. The 1D geometries have been considered since they are the basis to which 2D DOA estimation is anchored. Chapter four presents the simulation results as conducted in MATLAB program. This chapter ends by presenting the discussion of the results where individual model as well as comparison among the geometry classes is conducted. Lastly, in chapter five, inferences, recommendations, conclusion and future work is presented.

CHAPTER TWO
INTRODUCTION TO DIRECTION OF ARRIVAL ESTIMATION

Since its inception in 1897 by Guglielmo Marconi who successfully transmitted telegraphy signals using electromagnetic waves to a distance of merely over 100 meters (Andersen, 2017; Falciasecca & Valotti, 2009), wireless communication has gone through major transformations to today's most preferred, most advanced and fastest growing technology. In a wireless communication system, the signals are transmitted through electromagnetic waves capable of travelling even in free space without the use of any physical medium like enhanced electrical conductors or wires.(Bhalla & Bhalla, 2010). This communication system operates through a subsystem that directs the transmitted and received electromagnetic waves called antennas.

An efficient and effective wireless communication system ensures interference suppression, capacity enhancement, power efficiency, ability to support multimedia services, spectral efficiency, quality of service (QoS), high Speeds or throughput, reliability, multiple networks compatibility and capital and operational expenditure optimization (Renukadas & Beed, 2016; Ramiro & Hamied, 2011; Saunders & Aragón-Zavala, 2007). Practically, it is not easy to achieve all of the aforementioned parameters in every single system. A trade-off is normally inevitable.

The increasing demand for the spectrum for instance, has resulted in full exploitation of the low-end spectrum leaving only one option of exploring the higher frequency bands with higher spectral availability. The major challenge is that higher frequencies results in higher data rates with higher user density leading to multipath fading and cross-interference which degrades the bit error rate (BER) which further results in poor quality of service (QoS) (Balabadrapatruni, 2012).

Multipath fading comes as a result of the transmitted signal being blocked by obstacles along the path leading to reflection, scattering and absorption as well as superimposition of undesired signals (Dai et al., 2006). As a result, the signal reaches the destination through different paths leading to phase mismatch as some paths creates delays. Consequently, co-channel interface is the inference caused between two wireless communication channels operating at the same frequency (Lee, 1986). These are illustrated in Figure 2.1.

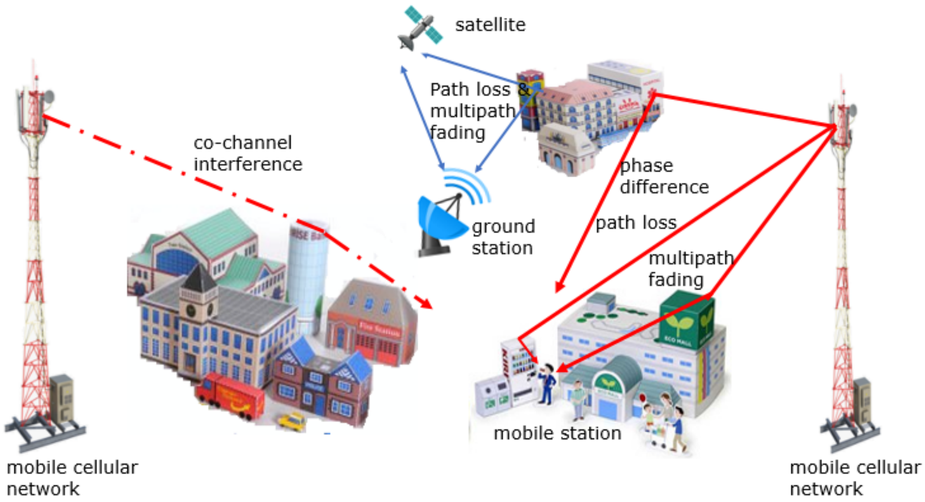

Figure 2.1 Interference in wireless communication system

The combination of these described inferences coupled with path absorption and any other cause for signal degradation is referred to as path loss. To solve the above challenges and as a way of embracing technological advancements for effective and efficient wireless communication systems, a number of techniques have been embraced among which include redesigning the antennas, employing enhanced modulation, multiple access and switching techniques, spectral efficiency algorithms, channel coding and new error correction and detection protocols.

2.1 Antenna Array

An antenna is an electrical device (circuit) that enables radiation or reception of electromagnetic signals in a wireless communication system. Balanis (2016), Balanis (1969) and Dhande (2009) elaborates the important antenna parameters as polarization, radiation pattern, half-power beam width, radiation density, radiation intensity, radiation power density, directivity, gain and bandwidth.

A set of similar or different antenna elements having individual amplitude and phase relation may be arranged in a manner to produce a certain desired radiation pattern. Such an arrangement containing N spatially separated antenna elements is referred to as an antenna array. A simple antenna array may contain as few as two elements like for the case of cellular telephony tower to as many as tens of elements as for case for radio telescope arrays with the general principle being: the more the elements, the better the performance. On the contrary, increase in the number of elements leads to computational complexity of the array. Therefore, a tradeoff is inevitable.

Phased antenna arrays are widely preferred since they provide a high gain as compared to ordinary antenna element. Importantly, they provide the capability of producing diverse, narrow and steerable beam, which means the array can be steered so that it is most sensitive in the desired direction and by so doing ensures cancellation of interfering signals from undesired directions. Figure 2.2 illustrates the two common types of uniform antenna arrays.

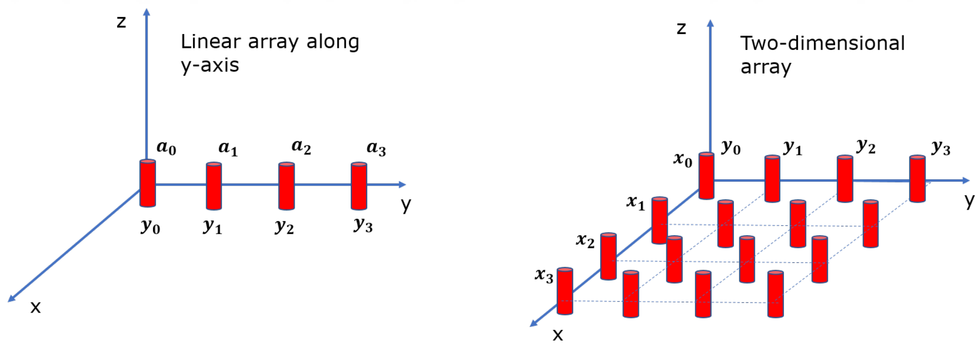

Figure 2.2 Typical uniform antenna array configurations

2.1.1 Smart Antenna

The antenna was initially thought of as a passive circuit element where its operating characteristics was predetermined at the initial design and manufacture which meant that the operating characteristics were fixed for each antenna. This kind of antenna is referred to as switched beam antenna. Currently, as a way of tackling the challenges of multipath fading, cross-interference and general path loss as highlighted in Chapter 1, the antenna is viewed as an integral part of the circuit and therefore designed in a manner that it can automatically change the direction of beam-forming (radiation pattern) thereby suppressing the interference and at the same time optimizing the capacity of the network. An antenna with such features is called an adaptive antenna system.

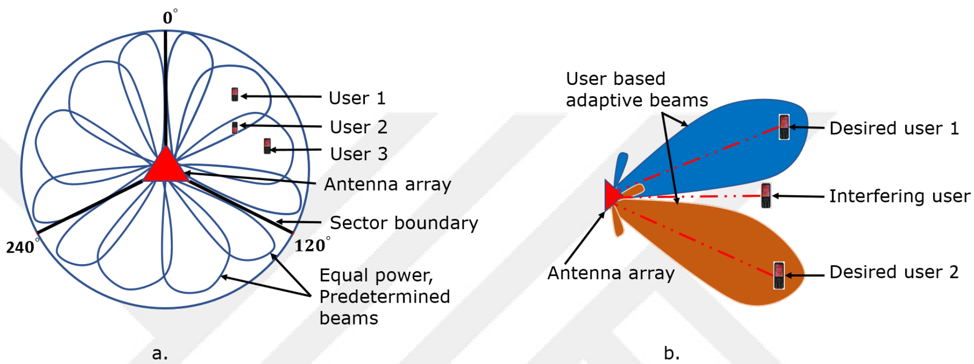

Figure 2.3 Smart antenna types: (a) Switched beam (b) Adaptive array

As illustrated in Figure 2.3 (a), a switched beam antenna radiates equally in all directions leading to interference and high power dissipation. Figure 2.3 (b) is of an adaptive array radiating along the desired user direction only and therefore able to achieve automatic interference cancellation while dissipating very low power among other positive features.

Adaptive array system is a scenario-based antenna with infinite number of beamforming patterns that are adjustable in real time. The beamforming is automatically achieved through a digital signal processor system and phase shifter for automatic adjustments (Lakshmi & Sivvam, 2017; Bellofiore et al., 2002). An adaptive array has the ability to effectively locate and track different types of signals through the use of new signal-processing algorithms thereby allowing it to dynamically minimize system interferences like multi-path and co-channel; and maximize the intended signal reception. This combination is capable of automatically detecting the direction of arrival (DOA) of the intended signals and on the other hand suppress the interfering signals and noise. Figure 2.4 shows an illustration of an adaptive array.

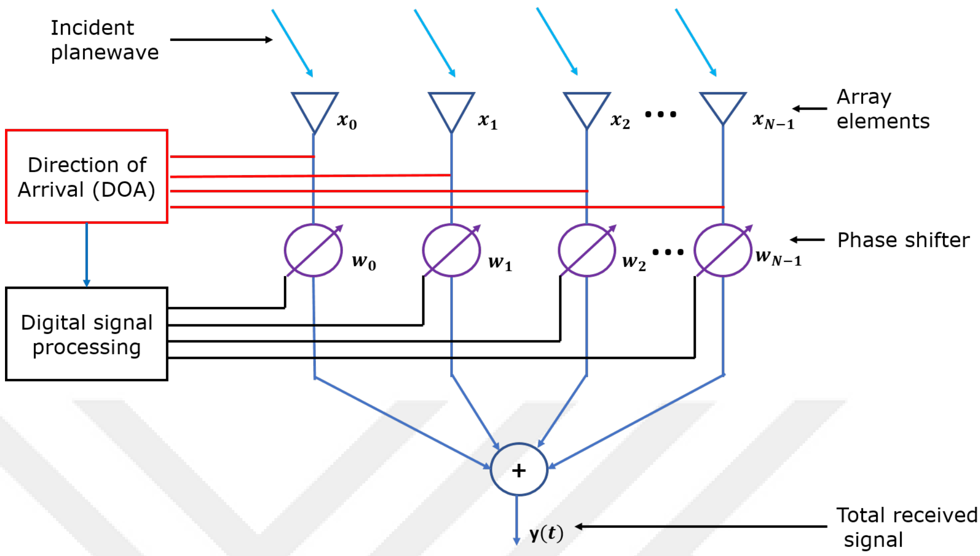

Figure 2.4 A simplified adaptive antenna array structure

2.2 DOA Estimation

Direction of arrival (DOA) is a terminology used to describe the direction from which a propagating electromagnetic wave arrives at the receiver preferable array elements. It is a localization procedure in which the azimuth and/or elevation angle(s) of the desired source signals in a wireless communication system is estimated with an aim of optimizing the performance of the system by enhancing capacity, throughput and interference cancellation (Barodia, 2017).

DOA can be estimated in 1D, where either elevation or azimuth angle is determined or 2D where both the elevation and azimuth angles are determined. Yan et al. (2015) states that in practice, 2D DOA estimation is of more importance than the former because it provides more information about the location of the incoming signals. DOA estimation is never a straight forward process. There are normally practical challenges which include decomposing multiple source signals having different amplitudes, additive white Gaussian noise corrupting the signal, clutters and signal multipath problems to deal with.

The principle of DOA estimation is important and has found applications in the fields of : wireless communications, sonar systems, geophysical applications like radio astronomy, navigation and tracking of objects and seismic estimations; signal processing in acoustics, radar tracking and rescue & emergency assistance devices as well as in biomedical engineering (Gentilho et al., 2020; Kiani & Pezeshk, 2015; Bhuiya et al., 2012).

DOA estimation is preformed by algorithms through determination of phase difference (time delay) of the arrival of signals (plane wave-front) at individual array elements. By determining this delay, it is possible to determine the angular direction from which the signal is arriving as illustrated in Figure 2.5 of uniform linear array where elements are arranged along $x-axis$ with a uniform separation distance d.

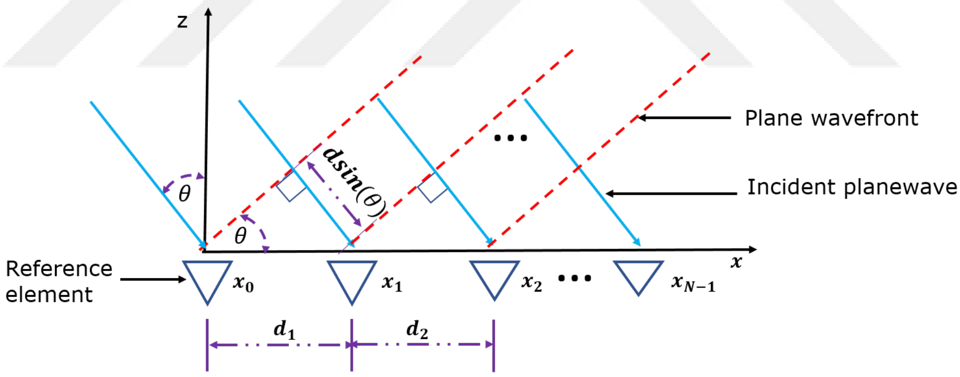

Figure 2.5 Uniform linear array

To illustrate the process of DOA estimation, it is assumed that the received signal at the reference element x_0 given by

$$S_0(t) = e^{j2\pi f_0 t} \tag{2.1}$$

Consequently, the second array element, x_1 receives the same signal after a time delay. If the time delay is τ, then the second array element receives a signal represented as

$$S_1(t) = S_0(t-\tau) = e^{j2\pi f_0 t} \, . \, e^{-j2\pi f_0 \tau} \tag{2.2}$$

Delay time, τ is given by

$$\tau = \frac{dsin\theta}{c} = \frac{dsin\theta}{f_0\lambda_0} \tag{2.3}$$

Where: c represents the velocity of electromagnetic wave with a wavelength of λ_0 and f_0 is the baseband frequency.

The problem then becomes an estimation problem since the exact difference of the plane wave-fronts cannot be determined. For 2D DOA estimation on the other hand, the receiving antenna array needs to be in at least two dimensions.

2.3 DOA Estimation Parameters

2.3.1 Coordinate System

In this thesis, 3D Cartesian plane technique which has three coordinates namely x, y, and z will be considered. This method considers the angular incoming or outgoing electromagnetic signals in a three-dimensional space. Therefore, the spatial spherical coordinates are transformed into 3D Cartesian coordinates for analysis. For the case of this thesis, again, the elevation angle will be represented by θ while the azimuth angle will be represented by ϕ. Consequently, the radial distance between the source(s) and the antenna elements will be denoted as r.

The 3D spherical representation shown in Figure 2.6 is converted through cylindrical coordinates to respective Cartesian plane coordinates given as.

$$\begin{cases} x = d_x\sin(\theta)\cos(\phi) \\ y = d_y\sin(\theta)\sin(\phi) \\ z = d_z\cos(\phi) \end{cases} \tag{2.4}$$

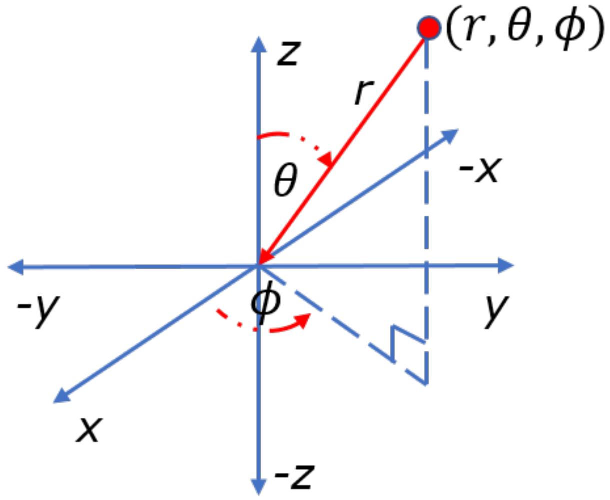

Figure 2.6 3D spherical coordinate representation

2.3.2 *Power Spectrum*

The DOA estimation method to be adopted is one based on the power spectrum peak detection. Several authors have proposed unique algorithms for estimating the peaks of the power spectrum. Since the actual power spectrum cannot be computed, an approximated values which are equally sufficient are used and are called pseudo-spectrum. The most popular pseudo-spectra used are for 1D and 2D DOAs which are determined with the number of planes the power is resolved. The illustrations are as shown in Figure 2.7.

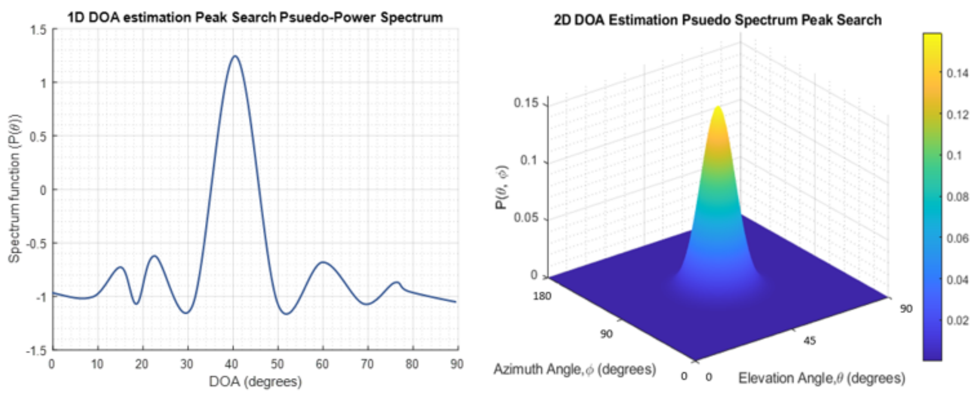

Figure 2.7 Illustration of 1D and 2D DOA estimation spectral peak searches

2.4 DOA Estimation Algorithms

Several DOA estimation algorithms have been proposed for 1D and 2D estimations (Liu et al., 2018). Devendra & Manjunathachari (2015) and Dhope et al. (2013) for instance, discussed different DOA estimation methods in detail where they categorized DOA estimation approaches into two major classes namely quadratic types and subspace decomposition types. Among the proposed algorithms, subspace-based approach is preferred due to its higher resolution and less computational complexity as opposed to maximum likelihood (ML) approach (Jaafer et al., 2018; Gentilho et al., 2020).

Several subspace DOA estimation algorithms have been developed which can further be categorized as summarized in the flow diagram of Figure 2.8. Maximum likelihood methods like Capon (Minimum Variance Distortionless Response) and Bartlett depend highly on the physical size of array aperture, leading to poor resolution and low estimation accuracy. On the other hand, subspace methods especially MUSIC is more accurate with high resolution, and at the same time not limited to physical size of array aperture (Jaafer et al., 2018; Gentilho et al., 2020; Dhope et al., 2013).

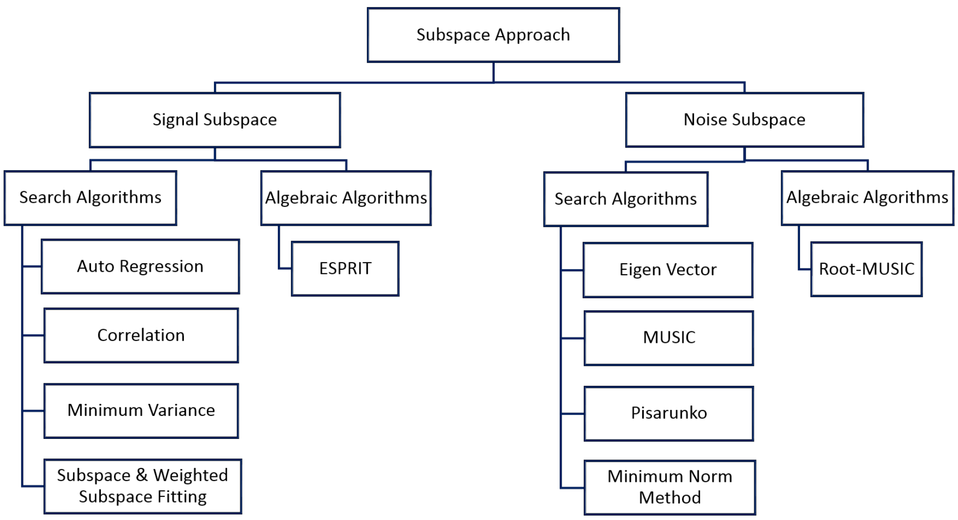

Figure 2.8 Types of subspace DOA estimation algorithms (Devendra & Manjunathachari, 2015)

2.5 MUSIC Algorithm

Multiple Signal classification (MUSIC) DOA estimation algorithm was first proposed by Schmidt in 1979 (Joshi & Dhande, 2014). This algorithm provides higher resolution based on exploiting the eigen-structure of input covariance matrix of the signal under analysis. The covariance matrix is decomposed into eigenvectors of signal and noise subspaces respectively and due to the orthogonality of the two, the direction of the source(s) is computed from the steering vectors of the noise subspace (Tayem & Kwon, 2005).

MUSIC is considered a super-resolution algorithm which is able to resolve very close sources due to the perfect orthogonality of signal and noise subspaces for scenarios where SNR is sufficiently high. Apart from presenting high resolution, MUSIC also performs better with arbitrary array geometries (Yan et al., 2015).

2.5.1 Factors Affecting MUSIC Algorithm DOA Estimation

According to Dhope et al. (2013); Gupta & Kar (2015); Sharma et al. (2015) and Barodia (2017), DOA estimation is affected by both the behavior of the incoming signals and estimation environment. The major factors that affect the resolution of estimated angle are as follows.

- Signal to Noise Ratio (SNR): For low noise environments, the resolution of the estimated DOAs is higher as opposed to when the SNR is high.
- Array Aperture: Array aperture is the effective antenna surface oriented perpendicular to the impinging electromagnetic waves. Therefore, the larger the aperture the higher the DOF and therefore higher resolution and accuracy in estimation. The aperture can physically be extended by adding more sensors although this can lead to additional hardware costs as well as slower operations due to high computational complexity for the signal processor. Another way of

extending the aperture is by extending the inter-element spacing which should be done cautiously for conventional arrays as it is bounded at half-wavelength to avoid the occurrence of cyclical ambiguous direction-cosine estimates according to spatial Nyquist sampling theorem (Zoltowski & Wong, 2000).

- Sources inter-spacing Distance: When estimating multiple number of sources, there inter-spacing distance is a factor of consideration as it determines the array geometry and the estimation algorithm that can be applied. For instance, most classical algorithms require modification to enable estimation of number of sources greater than the number of array elements.

- Number of Snapshots: Snapshots which is the number of signal samples per unit time is directly proportional to the resolution of the estimated DOA. Super resolution DOA estimators like MUSIC operate perfectly even with few snapshots. However, conventional estimators would require higher number of snapshots to perform better.

- Coherency of the signal sources: MUSIC algorithm performs for non-coherent sources. For coherent sources, the signal covariance matrix is no longer a non-singular matrix. For this condition, the original super-resolution algorithm will not be suitable.

- Inter-element Spacing: Conventionally, the sensor spacing between adjacent elements is maintained not more than half-wavelength of the propagating wave. To ensure no spatial aliasing responsible for mutual coupling and lower array aperture (Zhang et al., 2020). Mutual coupling is undesirable because it degrades the performance of the estimator. MUSIC algorithm cannot perform well with inter-element spacing of more than half wavelength. In such scenario, false peaks (ambiguous DOAs) emerge.

- Number of Array Elements: In conventional DOA estimation algorithms, the number of resolvable source DOAs are dependent on the number of array sensors. The number of sensor elements further affects the array aperture (Zhao et al., 2019).

CHAPTER THREE
METHODOLOGY

The research aims at analyzing non-regular array geometries. Coprime array, one of the sparse array geometries is analysed in detail. The aim is to perform analysis of coprime array using different methods, both 1D and 2D, including virtual array interpolation to determine how sparse arrays can be used for extended degrees of freedom (DOF) for resolving of more sources than sensors. In all the methods, MUSIC, a super resolution algorithm is used. The breakdown of the workflow is shown in Figure 3.1.

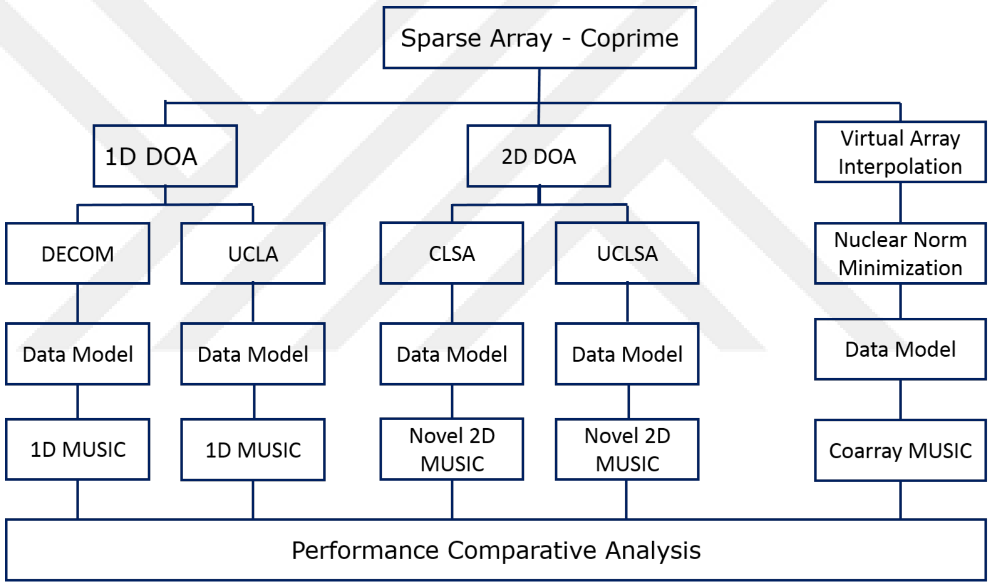

Figure 3.1 Execution procedure

3.1 Sparse Arrays

An array in which sensor elements are nonuniformly placed according to a unique principle with the aim of increasing the DOF of the antenna is referred to as sparse array (Hu et al., 2013). They can be classified as those with closed-form sensor locations like coprime arrays, generalized coprime arrays, nested arrays, and super-nested arrays and those with no closed-form sensor locations (irregular arrays) like minimum hole arrays (MHA) and minimum redundancy arrays (MRA) (Hosseini & Sebt, 2017). Sparse arrays have the advantage of resolving more signal sources than the number of sensor elements which is occasioned by their increased aperture and DOF.

3.1.1 The Coprime Concept

This is a concept of realising closed-form sparse array called coprime. It is derived from the prime number theory. The Coprime integer pairs are numbers with only integer 1 as their common divisor and no other.

The coprime array concept was first put forth by Pal & Vaidyanathan (2011) where array elements arranged according to a pair of coprime integers is analyzed in detail. Bush & Xiang (2017) expanded the concept to analyse an n-tuple array, elaborating that any n multiple number of sets of pairwise coprime integers can be modelled thereby expanding the coprime array concept from just a pair to suggesting that the set can be imagined to be as large as the largest prime number which is actually infinity.

In Qin et al. (2015), different generalised coprime configurations have been discussed for DOA estimation. Many researchers have of late given a lot of attention to coprime array concept due to its computational simplicity and ease of implementation (Zhang et al., 2020).

3.2 DECOM Method for Nonuniform Linear Array

DECOM is a diminutive of decompose and combine. This is one of the DOA estimation methods for analysing coprime linear arrays. It is performed in two steps. Firstly, the nonuniform coprime linear array (NCLA) is decomposed to its respective uniform linear sub-arrays 1 and 2 in accordance with coprime integer pair. This process allows the application of MUSIC algorithm in each sub-array separately. Secondly, DOA estimation is realised by combining the MUSIC results of the two sub-arrays (Kwizera et al., 2017; Zhou et al., 2013).

Consider two coprime integer pair M and N where $M < N$. The sensors are spaced in accordance with multiples of these integers. This arrangement has the merit of increasing the aperture area and degrees of freedom (DOF). The constraint is that the inter-sensor spacing will exceed half wavelength and therefore there tends to be occurrence of cyclical ambiguous direction-cosine estimates according to spatial Nyquist sampling theorem (Tayem & Kwon, 2005). The array geometry is shown in Figure 3.2.

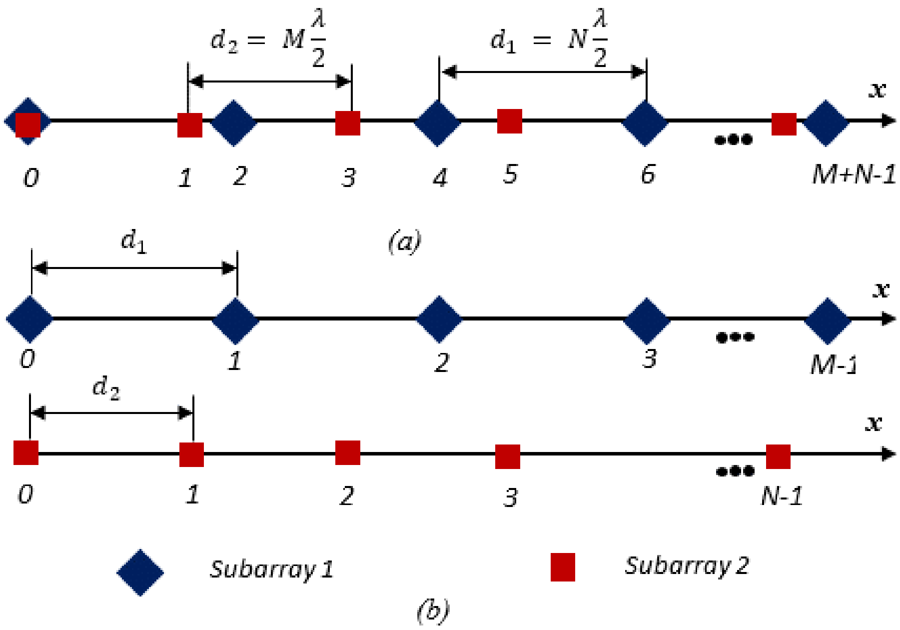

Figure 3.2 (a) Nonuniform Coprime linear array(NCLA) (b) Decomposed coprime linear sub-arrays

Generally speaking, a nonuniform linear array would require additional analysis techniques for it to be used in DOA estimation. However, with the coprime concept and the virtue that the matrices can be analyzed in a decomposed form, it is easy to analyze the nonuniform array shown in Figure 3.2(a) into its n respective uniform linear sub-array components as shown in Figure 3.2(b). Therefore, the method is referred to as DECOM because it entails decomposing the nonuniform array into its respective uniform linear arrays followed by DOA estimation through combining the MUSIC results of the linear arrays.

3.2.1 Data Model

It is assumed that P uncorrelated far-field narrowband signals $\{s_p(t)\}_{p=1}^{P}$ with same wavelength λ impinge on the nonuniform linear array in a manner that p^{th} signal makes an angle of $\{\theta_k\}_{p=1}^{P}$ where $\theta_p \in (0^0, 90^0)$ or $\phi_p \in (0^0, 180^0)$ for elevation and azimuth estimations respectively. The total received signal to the array for t^{th} snapshot can be expressed as

$$\mathbf{x}(t) = \mathbf{A}\mathbf{s}(t) + \mathbf{n}(t) \tag{3.1}$$

This is decomposed for individual signals received by each sub-array as.

$$\mathbf{x}_M(t) = \mathbf{A}_M\mathbf{s}(t) + \mathbf{n}_M(t) \tag{3.2a}$$

$$\mathbf{x}_N(t) = \mathbf{A}_N\mathbf{s}(t) + \mathbf{n}_N(t) \tag{3.2b}$$

Where: $\mathbf{s}(t) = [s_1(t), s_2(t), ..., s_P(t)]^T$ is the signal vector for $t = 1, 2, ..., J$ snapshots; $\mathbf{n}_M(t)$ and $\mathbf{n}_N(t)$ are the additive white Gaussian noise vectors assumed to have zero mean, and variance σ_n^2 and independent of sources and $\mathbf{A}$ is the manifold matrix for the respective sub-arrays given by $\mathbf{A}_M \in \mathbb{C}^{M\times P}$ and $\mathbf{A}_N \in \mathbb{C}^{N\times P}$ and are Vandermonde matrices which can be individually expressed as

$$\mathbf{A}_M = [\boldsymbol{\alpha}_M(\theta_1), \boldsymbol{\alpha}_M(\theta_2), ..., \boldsymbol{\alpha}_M(\theta_{P-1}), \boldsymbol{\alpha}_M(\theta_P)] \tag{3.3a}$$

$$\mathbf{A}_N = [\boldsymbol{\alpha}_N(\theta_1), \boldsymbol{\alpha}_N(\theta_2), ..., \boldsymbol{\alpha}_N(\theta_{P-1}), \boldsymbol{\alpha}_N(\theta_P)] \tag{3.3b}$$

The corresponding steering vectors of the above matrices along positive and negative x axis respectively is expressed for the range $p = 1, 2, ..., P$ as

$$\boldsymbol{\alpha}_M(\theta_1) = [\boldsymbol{\alpha}_M^0(\theta_p), ..., \boldsymbol{\alpha}_M^{M-1}(\theta_p)]^T \tag{3.4a}$$

$$\boldsymbol{\alpha}_N(\theta_1) = [\boldsymbol{\alpha}_N^0(\theta_p), ..., \boldsymbol{\alpha}_N^{N-1}(\theta_p)]^T \tag{3.4b}$$

Where $\boldsymbol{\alpha}_M^n(\theta_p) = e^{-1jn\eta d_1 \sin\theta_p}$ and $\boldsymbol{\alpha}_N^n(\theta_p) = e^{-1jn\eta d_2 \sin\theta_p}$ for $\eta = \frac{2\pi}{\lambda}$, d_b denotes $d_1 = N\frac{\lambda}{2}$ or $d_2 = M\frac{\lambda}{2}$ with n representing the position (or the number) of sensor under consideration.

3.2.2 1D DOA Estimation using DECOM with MUSIC Algorithm

To apply MUSIC algorithm, the first step is to compute the covariance matrix of the above two sub-array signals. The covariance matrix of the total received signal for 2D MUSIC is computed as

$$\begin{aligned}\mathbf{R}_{XX_M} &= E[\mathbf{x}_M(t)\mathbf{x}_M^H(t)] = \mathbf{A}_M E[\mathbf{s}(t)\mathbf{s}^H(t)]\mathbf{A}_M^H + E[\mathbf{n}_M(t)\mathbf{n}_M^H(t)] \\ &= \mathbf{A}_M \mathbf{R}_{SSM} \mathbf{A}_M^H \; + \; \sigma_n^2 \mathbf{I}\end{aligned} \tag{3.5a}$$

$$\begin{aligned}\mathbf{R}_{XX_N} &= E[\mathbf{x}_N(t)\mathbf{x}_N^H(t)] = \mathbf{A}_N E[\mathbf{s}(t)\mathbf{s}^H(t)]\mathbf{A}_N^H + E[\mathbf{n}_N(t)\mathbf{n}_N^H(t)] \\ &= \mathbf{A}_N \mathbf{R}_{SSN} \mathbf{A}_N^H \; + \; \sigma_n^2 \mathbf{I}\end{aligned} \tag{3.5b}$$

Where: $\mathbf{R}_{SS} = diag[\sigma_1^2, \sigma_2^2, \ldots, \sigma_P^2]$ represents the received signal power with each individual source represented by σ_p^2 while σ_n^2 is the noise power and $\mathbf{I}$ is an identify matrix. Since the exact covariance matrix cannot be solved, an approximate value is used given as

$$\hat{\mathbf{R}}_{XX_M} = \frac{1}{J}\sum_{t=1}^{J} \mathbf{x}_M(t)\mathbf{x}_M^H(t) \tag{3.6a}$$

$$\hat{\mathbf{R}}_{XX_N} = \frac{1}{J}\sum_{t=1}^{J} \mathbf{x}_N(t)\mathbf{x}_N^H(t) \tag{3.6b}$$

From the expression of the estimated value covariances, if eigenvalue decomposition (EVD) is conducted, the signal and noise subspaces are established respectively as

$$\hat{\mathbf{R}}_{XX_M} = \begin{bmatrix}\hat{\mathbf{U}}_{sM} & \hat{\mathbf{U}}_{nM}\end{bmatrix}\begin{bmatrix}\hat{\mathbf{\Lambda}}_{sM} & 0 \\ 0 & \hat{\mathbf{\Lambda}}_{nM}\end{bmatrix}\begin{bmatrix}\hat{\mathbf{U}}_{sM}^H \\ \hat{\mathbf{U}}_{nM}^H\end{bmatrix} = \hat{\mathbf{U}}_{sM}\hat{\mathbf{\Lambda}}_{sM}\hat{\mathbf{U}}_{sM}^H \; + \hat{\mathbf{U}}_{nM}\hat{\mathbf{\Lambda}}_{nM}\hat{\mathbf{U}}_{nM}^H \tag{3.7a}$$

Where the subspaces are complex matrices of sizes $\hat{\mathbf{U}}_{sM} \in \mathbb{C}^{M\times P}$ and $\hat{\mathbf{U}}_{nM} \in \mathbb{C}^{M\times(M-P)}$ and source and noise powers are also complex matrices of sizes $\hat{\mathbf{\Lambda}}_{sM} \in \mathbb{C}^{P\times P}$ and $\hat{\mathbf{\Lambda}}_n =\in \boldsymbol{C}^{[(M-P)]\times[M-P]}$ respectively, and

$$\hat{\mathbf{R}}_{XX_N} = \begin{bmatrix}\hat{\mathbf{U}}_{sN} & \hat{\mathbf{U}}_{nN}\end{bmatrix}\begin{bmatrix}\hat{\mathbf{\Lambda}}_{sN} & 0 \\ 0 & \hat{\mathbf{\Lambda}}_{nN}\end{bmatrix}\begin{bmatrix}\hat{\mathbf{U}}_{sN}^H \\ \hat{\mathbf{U}}_{nN}^H\end{bmatrix} = \hat{\mathbf{U}}_{sN}\hat{\mathbf{\Lambda}}_{sN}\hat{\mathbf{U}}_{sN}^H \; + \hat{\mathbf{U}}_{nN}\hat{\mathbf{\Lambda}}_{nN}\hat{\mathbf{U}}_{nN}^H \tag{3.7b}$$

Where the subspaces are complex matrices of sizes $\hat{\mathbf{U}}_{sN} \in \mathbb{C}^{N\times P}$ and $\hat{\mathbf{U}}_{nN} \in \mathbb{C}^{N\times(N-P)}$ and source and noise powers are also complex matrices of sizes $\hat{\mathbf{\Lambda}}_{sN} \in \mathbb{C}^{P\times P}$ and $\hat{\mathbf{\Lambda}}_n =\in$

$\mathbf{C}^{[(N-P)]\times[N-P]}$ respectively.

$$F_{MUSIC_M}(\theta) = \frac{1}{\left|\boldsymbol{\alpha}_M^H(\theta)\hat{\mathbf{U}}_{nM}\hat{\mathbf{U}}_{nM}^H\boldsymbol{\alpha}_M(\theta)\right|} \tag{3.8a}$$

$$F_{MUSIC_N}(\theta) = \frac{1}{\left|\boldsymbol{\alpha}_N^H(\theta)\hat{\mathbf{U}}_{nN}\hat{\mathbf{U}}_{nN}^H\boldsymbol{\alpha}_N(\theta)\right|} \tag{3.8b}$$

From the spectra function, a search for the peaks (maximas) is conducted to establish estimated DOAS.

3.3 Unfolded Coprime Linear Array, (UCLA) Method

In this method, a nonuniform coprime linear array is unfolded according to its coprime integer pair to form sub-arrays 1 and 2. As opposed to DECOM, the array is unfolded from the origin where the elements of each sub-array are arranged separately towards the positive and negative side of the axis respectively as shown in Figure. 3.3.

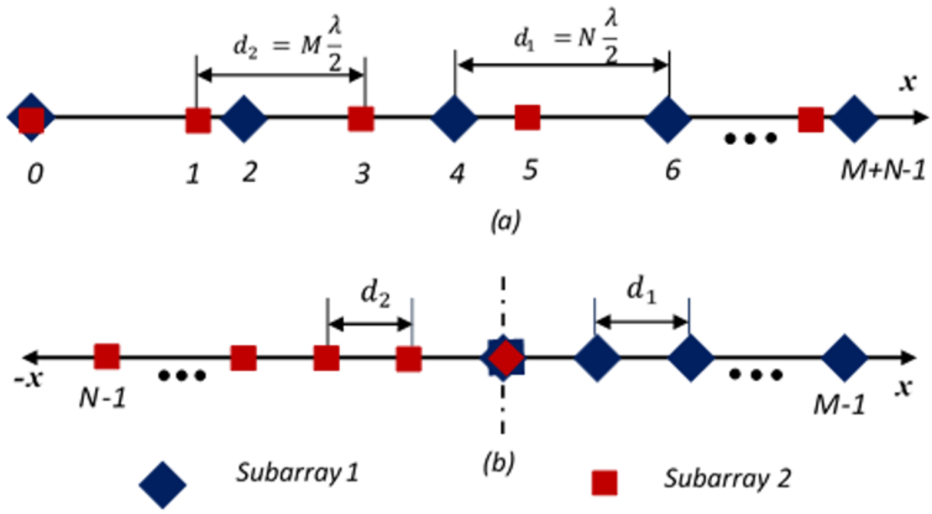

Figure 3.3 (a) Nonuniform coprime linear array (NCLA) (b) Unfolded coprime linear array (UCLA)

This unfolded coprime array geometry, as opposed to uniform linear or DECOM methods, is preferred because of the following advantages (Zhao et al., 2019; He et al., 2020):

- It helps in increasing the number of sensor elements for higher degrees of freedom (DOF) thereby allowing detection of more sources than the number of sensors.
- It ensures retention of the intrinsic mutual information of the arrays thereby an all-array detection may be applied leading to superior performance.
- There is automatic pairing of the estimated DOAs unlike a scenario for DECOM where each sub-array is used separately.

3.3.1 Data Model

The model assumes a total of P uncorrelated far-field narrowband signals $\{s_p(t)\}_{p=1}^{P}$ of wavelength λ impinging on the array such that the pth signal makes an angle of $\{\theta\}_{p=1}^{P}$ where $\theta_p \in (0^0,\ 90^0)$. Besides, if the total signal received by each sub-array in either axis is expressed as $\{x_b\}_{b=1}^{2}$ where b denotes the side of the sub-array considered where 1 denote positive side and 2 negative side respectively, then the received signal of the b^{th} sub-array in x directions for t^{th} snapshot is expressed as

$$\mathbf{x}_b(t) = \mathbf{A}_b\mathbf{s}(t) + \mathbf{n}_b(t) \tag{3.9}$$

Where: $\mathbf{s}(t) = [s_1(t), s_2(t), ..., s_P(t)]^T$ is the signal vector $t = 1, 2, \ldots, J$ is the number of snapshots; $\mathbf{n}_b(t)$ is the additive white Gaussian noise vectors of the form $\mu_n = 0$ and $Var = \sigma_n^2$; $\mathbf{A}_b \in \mathbb{C}^{(N\ or\ M)\times P}$ is the manifold matrix for bth sub-array along x-axis, and is of a Vandermonde matrix which can be further expressed in the form:-

$$\mathbf{A}_b = [\boldsymbol{\alpha}_b(\theta_1), \boldsymbol{\alpha}_b(\theta_2), ..., \boldsymbol{\alpha}_b(\theta_{P-1}), \boldsymbol{\alpha}_b(\theta_P)] \tag{3.10}$$

The corresponding steering vectors of the above matrices for the angle directions along positive and negative x axis respectively is expressed for the range $p = 1, 2, \ldots, P$ as

$$\boldsymbol{\alpha}_1(\theta_1) = [\boldsymbol{\alpha}_1^0(\theta_p), \ldots, \boldsymbol{\alpha}_1^{M-1}(\theta_p)]^T \tag{3.11a}$$

$$\boldsymbol{\alpha}_2(\theta_1) = [\boldsymbol{\alpha}_2^{-(N-1)}(\theta_p), \ldots, \boldsymbol{\alpha}_2^0(\theta_p)]^T \tag{3.11b}$$

Where $\boldsymbol{\alpha}_b^n(\theta_p) = e^{-1j\eta d_b \sin\theta_p}$ for $\eta = \frac{2\pi}{\lambda}$, d_b denotes $d_1 = N\frac{\lambda}{2}$ and $d_2 = M\frac{\lambda}{2}$ with n representing the position (or the number) of sensor under consideration.

3.3.2 1D DOA Estimation with UCLA Method Using MUSIC Algorithm

As established above, the received signals in either sub-arrays are combined to generate the total signal as

$$\mathbf{x}(t) = \begin{bmatrix} \mathbf{x}_1(t) \\ \mathbf{x}_2(t) \end{bmatrix} = \begin{bmatrix} \mathbf{A}_1 \\ \mathbf{A}_2 \end{bmatrix} \mathbf{s}(t) + \begin{bmatrix} \mathbf{n}_1(t) \\ \mathbf{n}_2(t) \end{bmatrix} = \mathbf{A}\mathbf{s}(t) + \mathbf{n}(t) \tag{3.12}$$

Where $\mathbf{A}_x = \left[\mathbf{A}_1^T\ ,\ \mathbf{A}_2^T\ \right]^T = [\boldsymbol{\alpha}(\theta_1), \boldsymbol{\alpha}(\theta_2), \ldots, \boldsymbol{\alpha}(\theta_{P-1}), \boldsymbol{\alpha}(\theta_P)]$. The corresponding steering vector is given by $\boldsymbol{\alpha}\left(\theta_p\right) = \left[\alpha_1^T\left(\theta_p\right),\ \ \alpha_2^T\left(\theta_p\right)\right]^T$. In the same spirit, the total noise is modelled as a collective of the noises in two sub-arrays as $\mathbf{n} = \left[\mathbf{n}_1^T,\ \ \mathbf{n}_2^T\ \right]^T$.

The covariance matrix is then computed as

$$\mathbf{R}_{XX} = E\left[\mathbf{x}(t)\mathbf{x}^H(t)\right] = \mathbf{A}E\left[\mathbf{s}(t)\mathbf{s}^H(t)\right]\mathbf{A}^H + E\left[\mathbf{n}(t)\mathbf{n}^H(t)\right] = \mathbf{A}\mathbf{R}_{ss}\mathbf{A}^H + \sigma_n^2\mathbf{I} \tag{3.13}$$

The approximate covariance matrix is genrated as in Equation 3.14.

$$\hat{\mathbf{R}}_{XX} = \frac{1}{J}\sum_{t=1}^{J}\mathbf{x}(t)\mathbf{x}^H(t) \tag{3.14}$$

Eigenvalue decomposition (EVD) is performed on Equation 3.14 to establish signal and noise subspaces respectively as shown.

$$\hat{\mathbf{R}}_{XX} = \left[\hat{\mathbf{U}}_s\ \ \hat{\mathbf{U}}_n\right] \begin{bmatrix} \hat{\boldsymbol{\Lambda}}_s & \mathbf{0} \\ \mathbf{0} & \hat{\boldsymbol{\Lambda}}_n \end{bmatrix} \begin{bmatrix} \hat{\mathbf{U}}_s^H \\ \hat{\mathbf{U}}_n^H \end{bmatrix} = \hat{\mathbf{U}}_s\hat{\boldsymbol{\Lambda}}_s\hat{\mathbf{U}}_s^H + \hat{\mathbf{U}}_n\hat{\boldsymbol{\Lambda}}_n\hat{\mathbf{U}}_n^H \tag{3.15}$$

Where the subspaces are complex matrixes of sizes $\hat{\mathbf{U}}_s = \in \mathbb{C}^{[N+M]\times P}$ and $\hat{\mathbf{U}}_n = \in \mathbf{C}^{[N+M]\times[(N+M)-P]}$ and source and noise powers are also complex matrices of sizes $\hat{\boldsymbol{\Lambda}}_s = \in \mathbb{C}^{P\times P}$ and $\hat{\boldsymbol{\Lambda}}_n = \in \mathbb{C}^{[(N+M)-P]\times[(N+M)-P]}$ respectively. Finally, the spectral function is expressed as

$$F_{MUSIC}(\theta) = \frac{1}{\left|\boldsymbol{\alpha}^H(\theta)\hat{\mathbf{U}}_n\hat{\mathbf{U}}_n^H\boldsymbol{\alpha}(\theta)\right|} \tag{3.16}$$

3.4 Coprime L-Shaped Antenna Arrays

2D DOA estimation requires a multidimensional array. These arrays include uniform planar like rectangular and circular, nonuniform planar, L-shaped, coprime L-shaped etc. Among them, coprime L-shaped has proved to be simple in implementation and effective in DOA estimating. This has led to many researchers giving it great attention through which algorithms deemed to be computationally efficient being proposed (Dong et al., 2017).

DOA estimation algorithms that work with L-shaped arrays can be classified into two. The first class are those algorithms able to resolve signal sources that are less than the number of sensor elements. Most of these estimate the AoAs corresponding to each uniform linear sub-array (ULA) by application of 1D DOA estimation algorithms to the received data or reconstructed data of each sub-array. The resultant angles needs additional pairing since angle-pairing is not automatic. The second category are those that resolves AoAs with ability of automatic angle pairing. Examples of such algorithms include joint SVD, parallel factor analysis and effective array aperture extension methods. The second class are those that are able to resolve signal sources equal to or greater than the number of sensor elements.

A coprime L-shaped array (CLSA) comprises of two uniform L-shaped sub-arrays 1 and 2 paired along each other in $x-y$ plane for instance, where sub-array 1 and 2 consists of $2M-1$ and $2N-1$ elements respectively for $M < N$ and M and N being a coprime integer pair and the element at the origin being shared for alignments in either direction for either sub-array. (Dong et al., 2017; Yang et al., 2017; Hu et al., 2015). Therefore, the total number of elements for the array then becomes $2M+2N-3$. Letting the wavelength of the signal under consideration to be λ, then the inter-sensor spacing for sub-array 1 and 2 can be expressed as $d_1 = N\frac{\lambda}{2}$ and $d_2 = M\frac{\lambda}{2}$ respectively. The array size is therefore given by total number of sensors per axis times the sensor interspacing distance, $(M-1)N\frac{\lambda}{2} + (N-1)M\frac{\lambda}{2}$. The model geometry is shown in Figure 3.4.

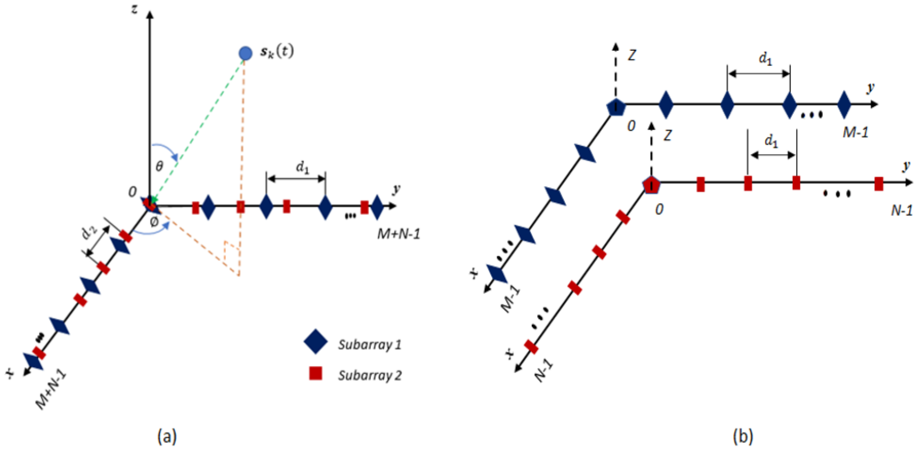

Figure 3.4 (a) Coprime L-shaped array (CLSA) geometry (b) Decomposed sub-arrays 1 and 2

3.4.1 Data Model

Consider K uncorrelated far-field narrowband signals $s_k(t)_{k=1}^{K}$ with same wavelength λ impinging on the L-shaped array above. The elevation and azimuth angles of the signal to the array is $\{\theta_k \ \& \ \phi_k\}_{k=1}^{K}$ respectively where $\theta_k \in (0^0, \ 90^0)$ and $\phi_k \in (0^0, \ 180^0)$ and k is the signal under consideration. The total signal received by the entire array can be analyzed by considering each L-shaped sub-array separately. Firstly, the uniform sub-array with the elements $2M-1$ with $d_1 = N\frac{\lambda}{2}$ is considered

$$\mathbf{x}_M(t) = \mathbf{A}_{Mx}\mathbf{s}(t) + \mathbf{n}_{Mx}(t) \tag{3.17a}$$

$$\mathbf{y}_M(t) = \mathbf{A}_{My}\mathbf{s}(t) + \mathbf{n}_{My}(t) \tag{3.17b}$$

Where: $\mathbf{s}(t) = [s_1(t), \ s_2(t), \ldots, s_K(t)]^T$ is the signal vector $t = 1,2,\ldots,J$ is the number of snapshots; $\mathbf{n}_{Mx}(t)$ and $\mathbf{n}_{My}(t) \in \mathbb{C}^{M\times K}$ are the additive white Gaussian noise vectors with zero mean $(\mu = 0)$ and variance, $Var = \sigma_n^2$ and independent of sources $\mathbf{A}_{Mx}$ and $\mathbf{A}_{My} \in \mathbb{C}^{M\times K}$ are manifold matrices for each sub-array along $x-$ and $y-$ axes respectively and are of the Vandermonde matrices form which is further expressed as

$$\mathbf{A}_{Mx} = [\boldsymbol{\alpha}_{Mx}(\theta_1,\phi_1), \boldsymbol{\alpha}_{Mx}(\theta_2,\phi_2), \ldots, \boldsymbol{\alpha}_{Mx}(\theta_{K-1},\phi_{k-1}), \boldsymbol{\alpha}_{Mx}(\theta_K,\phi_K)] \tag{3.18a}$$

$$\mathbf{A}_{My} = [\boldsymbol{\alpha}_{My}(\theta_1,\phi_1), \boldsymbol{\alpha}_{My}(\theta_2,\phi_2), \ldots, \boldsymbol{\alpha}_{My}(\theta_{K-1},\phi_{K-1}), \boldsymbol{\alpha}_{My}(\theta_K,\phi_K)] \tag{3.18b}$$

The corresponding steering vectors of the above matrices for the angle directions along positive $x-$ and $y-$ axes respectively is expressed for the range $k = 1,2,\ldots,K$ as

$$\mathbf{A}_{Mx} = \left[\boldsymbol{\alpha}^{0}_{Mx}(\theta_1,\phi_1),\boldsymbol{\alpha}^{1}_{Mx}(\theta_2,\phi_2),\ldots,\boldsymbol{\alpha}^{M-2}_{Mx}(\theta_{K-1},\phi_{K-1}),\boldsymbol{\alpha}^{M-1}_{Mx}(\theta_K,\phi_K)\right]^T \tag{3.19a}$$

$$\mathbf{A}_{My} = \left[\boldsymbol{\alpha}^{0}_{My}(\theta_1,\phi_1),\mathbf{a}^{1}_{My}(\theta_2,\phi_2),\ldots,\boldsymbol{\alpha}^{M-2}_{My}(\theta_{K-1},\phi_{K-1}),\boldsymbol{\alpha}^{M-1}_{My}(\theta_K,\phi_K)\right]^T \tag{3.19b}$$

where $\boldsymbol{\alpha}^{n}_{Mx}(\theta_k,\phi_k) = e^{j\eta n d_b \sin\theta_k \cos\phi_k}$ and $\boldsymbol{\alpha}^{n}_{My}(\theta_k,\phi_k) = e^{j\eta n d_b \sin\theta_k \sin\phi_k}$ for $\eta = \frac{2\pi}{\lambda}$, d_b denoting $d_1 = N\frac{\lambda}{2}$ for sub-array 1 and $d_2 = M\frac{\lambda}{2}$ for sub-array 2 respectively and n is the position (the number) of the sensor under consideration. Consequently, sub-array 2 contains N elements in both x and y directions and can be modelled in the same manner as above leading to received signal given by

$$\mathbf{x}_N(t) = \mathbf{A}_{Nx}\mathbf{s}(t) + \mathbf{n}_{Nx}(t) \tag{3.20a}$$

$$\mathbf{y}_N(t) = \mathbf{A}_{Ny}\mathbf{s}(t) + \mathbf{n}_{Ny}(t) \tag{3.20b}$$

3.4.2 MUSIC Algorithm for 2D DOA Estimation with CLSA

To apply MUSIC algorithm for the spectral peak searching, the sub-arrays are considered separately, and the final spectra merged for automatic pairing of the estimated angles. This eliminates ambiguity in the spectrum and the paired angles considered true DOAs. Consider Equation3.17a and Equation3.17b, the total received signal for sub-array 1 is expressed as

$$\mathbf{z}_M(t) = \begin{bmatrix}\mathbf{A}_{Mx}\\ \mathbf{A}_{My}\end{bmatrix}\mathbf{s}(t) + \begin{bmatrix}\mathbf{n}_{Mx}(t)\\ \mathbf{n}_{My}(t)\end{bmatrix} = \mathbf{A}_M\mathbf{s}(t) + \mathbf{n}_M \tag{3.21}$$

Where $\mathbf{A}_M = \left[\mathbf{A}^T_{Mx},\ \mathbf{A}^T_{My}\right]^T = [\boldsymbol{\alpha}_M(\theta_1,\phi_1),\ldots,\boldsymbol{\alpha}_M(\theta_k,\phi_k)] \in \mathbb{C}^{2M\times K}$ and $\boldsymbol{\alpha}_M(\theta_k,\phi_k) = \left[\boldsymbol{\alpha}^T_{Mx}(\theta_k,\phi_k),\ \boldsymbol{\alpha}^T_{My}(\theta_k,\phi_k)\right]^T$. Similarly, the total noise is modelled as $\mathbf{n}_M = \left[\mathbf{n}^T_{Mx},\ \mathbf{n}^T_{My}\right]^T$. The covariance matrix of the total received signal for 2D MUSIC is given as

$$\begin{aligned}\mathbf{R}_{\mathbf{ZZ}_M} &= E\left[\mathbf{z}_M(t)\mathbf{z}^H_M(t)\right] = \mathbf{A}_M E\left[\mathbf{s}(t)\mathbf{s}^H(t)\right]\mathbf{A}^H_M + E\left[\mathbf{n}_M(t)\mathbf{n}^H_M(t)\right]\\ &= \mathbf{A}_M\mathbf{R}_{ss}\mathbf{A}^H_M + \sigma^2_n\mathbf{I}\end{aligned} \tag{3.22}$$

Approximation of the covariance matrix is applied due to complexity in determination of the actual covariance matrix. This approximate value is described by

$$\hat{\mathbf{R}}_{ZZ_M} = \frac{1}{J}\sum_{t=1}^{J}\mathbf{z}_M(t)\mathbf{z}_M^H(t) \tag{3.23}$$

Lastly, eigenvalue decomposition (EVD) is conducted to establish signal and noise subspaces respectively as shown.

$$\hat{\mathbf{R}}_{ZZ_M} = \begin{bmatrix}\hat{\mathbf{U}}_{sM} & \hat{\mathbf{U}}_{nM}\end{bmatrix}\begin{bmatrix}\hat{\mathbf{\Lambda}}_{sM} & \mathbf{0} \\ \mathbf{0} & \hat{\mathbf{\Lambda}}_{nM}\end{bmatrix}\begin{bmatrix}\hat{\mathbf{U}}_s^H \\ \hat{\mathbf{U}}_n^H\end{bmatrix} = \hat{\mathbf{U}}_{sM}\hat{\mathbf{\Lambda}}_{sM}\hat{\mathbf{U}}_{sM}^H + \hat{\mathbf{U}}_{nM}\hat{\mathbf{\Lambda}}_{nM}\hat{\mathbf{U}}_{nM}^H \tag{3.24}$$

Where the subspaces are complex matrixes of sizes $\hat{\mathbf{U}}_{sM} =\in \mathbb{C}^{M\times K}$ and $\hat{\mathbf{U}}_{nM} =\in \mathbb{C}^{[2M\times[2M-K]}$ and source and noise powers are also complex matrices of sizes $\hat{\mathbf{\Lambda}}_{sM} =\in \mathbb{C}^{K\times K}$ and $\hat{\mathbf{\Lambda}}_n =\in \mathbb{C}^{[2M-K]\times[2M-K]}$ respectively. MUSIC power spectral function can then be expressed as

$$P_{MUSIC_M}(\theta,\phi) = \frac{1}{\left|\boldsymbol{\alpha}_M^H(\theta,\phi)\hat{\mathbf{U}}_{nM}\hat{\mathbf{U}}_{nM}^H\boldsymbol{\alpha}_M(\theta,\phi)\right|} \tag{3.25}$$

Consequently, considering the second sub-array, from Equation(3.20a) and Equation(3.20b) it will as well yield

$$P_{MUSIC_N}(\theta,\phi) = \frac{1}{\left|\boldsymbol{\alpha}_N^H(\theta,\phi)\hat{\mathbf{U}}_{nN}\hat{\mathbf{U}}_{nN}^H\boldsymbol{\alpha}_N(\theta,\phi)\right|} \tag{3.26}$$

Merging the two spectra above, true DOAs automatically pair up leaving the ambiguous DOAs which in most cases are represented with weaker power maxima values in the spectrum.

3.4.3 MUSIC-Like Low Complexity Method

A low complexity method (Zhang et al., 2019; Gong et al., 2018) is used to estimate DOA where the 2D problem is reduced to 1D spectral peak searching through a transformation defined by two factors given by

$$\begin{cases}\gamma_k = \sin\theta_k\cos\phi_k & \text{for} \quad \gamma_k \in (-1,1) \\ \beta_k = \sin\theta_k\sin\phi_k & \text{for} \quad \beta_k \in (0,1)\end{cases} \tag{3.27}$$

Using the above transformation, the manifold matrices represented in Equation (3.18a) and Equation (3.18b) can be rewritten as

$$\mathbf{A}_{xM} = [\boldsymbol{\alpha}_{xM}(\gamma_1), \boldsymbol{\alpha}_{xM}(\gamma_2), ..., \boldsymbol{\alpha}_{xM}(\gamma_{K-1}), \boldsymbol{\alpha}_{xM}(\gamma_K)] \tag{3.28a}$$

$$\mathbf{A}_{yM} = [\boldsymbol{\alpha}_{yM}(\beta_1), \boldsymbol{\alpha}_{yM}(\beta_2), ..., \boldsymbol{\alpha}_{yM}(\beta_{K-1}), \boldsymbol{\alpha}_{yM}(\beta_K)] \tag{3.28b}$$

With their respective steering vectors becoming

$$\boldsymbol{\alpha}_{xM}^{(\gamma_k)} = [\boldsymbol{\alpha}_{x1}^{0}(\gamma_k), ..., \boldsymbol{\alpha}_{x1}^{M-1}(\gamma_k)]^T \tag{3.29a}$$

$$\boldsymbol{\alpha}_{yM}^{(\beta_k)} = [\boldsymbol{\alpha}_{y1}^{0}(\beta_k), ..., \boldsymbol{\alpha}_{y1}^{M-1}(\beta_k)]^T \tag{3.29b}$$

Consequently, the respective elements in either vectors transform to $\boldsymbol{\alpha}_{xM}^{n}(\gamma_k) = e^{j\eta n d_1 \gamma_k}$ and $\boldsymbol{\alpha}_{yM}^{n}(\beta_k) = e^{j\eta n d_1 \beta_k}$ respectively. With the above transformation, the two items to be searched, are independent of each other and therefore, as suggested by Zhang et al. (2019); Tayem & Kwon (2005); Zhang et al. (2017), 1D spectral peak searching algorithms can be applied. For 2D MUSIC, the covariance matrix of the received signal is expressed as

$$\begin{aligned} \mathbf{R}_{ZZ_M} &= E\left[\mathbf{z}_M(t)\mathbf{z}_M^H(t)\right] = \mathbf{A}E\left[\mathbf{s}(t)\mathbf{s}^H(t)\right]\mathbf{A}^H + E\left[\mathbf{n}_M(t)\mathbf{n}_M^H(t)\right] \\ &= \mathbf{A}\mathbf{R}_{ss}\mathbf{A}^H + \sigma_n^2\mathbf{I} \end{aligned} \tag{3.30}$$

Since the exact covariance matrix cannot be solved, an approximation of the same is used as

$$\hat{\mathbf{R}}_{ZZ_M} = \frac{1}{J}\sum_{t=1}^{J}\mathbf{z}_M(t)\mathbf{z}_M^H(t) \tag{3.31}$$

From the expression of the estimated value covariances, if eigenvalue decomposition (EVD) is conducted, then the signal and noise subspaces are established respectively as.

$$\hat{\mathbf{R}}_{ZZ_M} = \begin{bmatrix}\hat{\mathbf{U}}_s & \hat{\mathbf{U}}_{nM}\end{bmatrix}\begin{bmatrix}\hat{\boldsymbol{\Lambda}}_s & \mathbf{0} \\ \mathbf{0} & \hat{\boldsymbol{\Lambda}}_{nM}\end{bmatrix}\begin{bmatrix}\hat{\mathbf{U}}_s^H \\ \hat{\mathbf{U}}_{nM}^H\end{bmatrix} = \hat{\mathbf{U}}_s\hat{\boldsymbol{\Lambda}}_s\hat{\mathbf{U}}_s^H + \hat{\mathbf{U}}_{nM}\hat{\boldsymbol{\Lambda}}_{nM}\hat{\mathbf{U}}_{nM}^H \tag{3.32}$$

To estimate $\gamma_k \in (-1, 1)$ and $\beta_k \in (0, 1)$, first the covariance matrix is redefined as

$$\hat{\mathbf{R}}_{ZZ_M} = \frac{1}{J}\sum_{t=1}^{J}\begin{bmatrix}\mathbf{x}_M(\mathbf{t}) \\ \mathbf{y}_M(\mathbf{t})\end{bmatrix}\begin{bmatrix}\mathbf{x}_M^H(t) & \mathbf{y}_M^H(t)\end{bmatrix} = \begin{bmatrix}\hat{\mathbf{R}}_{XX_M} & \hat{\mathbf{R}}_{XY_M} \\ \hat{\mathbf{R}}_{YX_M} & \hat{\mathbf{R}}_{YY_M}\end{bmatrix} \tag{3.33}$$

Where J is the number of snapshots and $\hat{\mathbf{R}}_{XX_M} = \frac{1}{J}\sum_{t=1}^{J}\mathbf{x}_M(t)\mathbf{x}_M^H(t) \in \mathbb{C}^{M\times M}$, $\hat{\mathbf{R}}_{YY_M} = \frac{1}{J}\sum_{t=1}^{J}y_M(t)\mathbf{y}_M^H(\mathbf{t}) \in \mathbb{C}^{M\times M}$, $\hat{\mathbf{R}}_{XY_M} = \frac{1}{J}\sum_{t=1}^{J}\mathbf{x}_M(t)\mathbf{y}_M^H(t) \in \mathbb{C}^{M\times M}$

and $\hat{\mathbf{R}}_{YX_M} = \frac{1}{J}\sum_{t=1}^{J}\mathbf{y}_M(t)\mathbf{x}_M^H(t) \in \mathbb{C}^{M\times M}$ are covariance matrices of received signals in the directions of the subscripts indicated. It is possible to find the eigenvalue decomposition (EVD) for $\hat{\mathbf{R}}_{XX}$.

$$\begin{aligned}\hat{\mathbf{R}}_{XX_M} &= \begin{bmatrix}\hat{\mathbf{U}}_{sx_M} & \hat{\mathbf{U}}_{nx_M}\end{bmatrix}\begin{bmatrix}\hat{\mathbf{\Lambda}}_{sx_M} & \mathbf{0} \\ \mathbf{0} & \hat{\mathbf{\Lambda}}_{nx_M}\end{bmatrix}\begin{bmatrix}\hat{\mathbf{U}}_{sx_M}^H \\ \hat{\mathbf{U}}_{nx_M}^H\end{bmatrix} \\ &= \hat{\mathbf{U}}_{sx_M}\hat{\mathbf{\Lambda}}_{sx_M}\hat{\mathbf{U}}_{sx_M}^H + \hat{\mathbf{U}}_{nxM}\hat{\mathbf{\Lambda}}_{nx_M}\hat{\mathbf{U}}_{nx_M}^H\end{aligned} \tag{3.34}$$

Where the signal and noise subspaces are complex matrixes of sizes $\hat{\mathbf{U}}_{sx} =\in \mathbf{C}^{M\times K}$ and $\hat{\mathbf{U}}_{nx} = \in C^{M\times[M-K]}$. It is noted that the steering vector is identical with the signal subspace and orthogonal to the noise subspace $\hat{\mathbf{U}}_{nx}$. Therefore, the peak search function, $\gamma_k, (k = 1, 2 \ldots, K)$ is modelled as

$$P_M(\gamma) = \frac{1}{\left\|\hat{\mathbf{U}}_{nx_M}^H \boldsymbol{\alpha}_x(\gamma)\right\|^2}, \gamma \in (-1, 1) \tag{3.35}$$

The $\hat{\gamma}_k$ which corresponds to K peaks is assumed to be the estimation of γ. With the value of $\hat{\gamma}_k$, it is possible to estimate β_k as follows.

$$P_M(\beta) = \frac{1}{\left\|\hat{\mathbf{U}}_{n_M}^H \begin{bmatrix}\boldsymbol{\alpha}_{x_M}(\hat{\gamma}_k) \\ \boldsymbol{\alpha}_{y_M}(\beta)\end{bmatrix}\right\|^2}, \beta \in (0, 1) \tag{3.36}$$

In the second function, $\mathbf{a}_x(\hat{\gamma}_k)$ is a constraint to the spectrum calculation. This constraint enables an automatic matching of the azimuth to its corresponding elevation angle pairs (Zhang et al., 2019). The final angle pairs are expressed as

$$\hat{\theta}_{k_M} = sin^{-1}\left(\sqrt{\hat{\gamma}_k + \hat{\beta}_k}\right) \tag{3.37}$$

$$\hat{\phi}_{k_M} = tan^{-1}\left(\frac{\hat{\beta}_k}{\hat{\gamma}_k}\right) \tag{3.38}$$

To get the true DOAs, the estimated AoAs are computed with respect to sub-array 2. Finally, the estimated DOAs are generated by combining and pairing the two spectra DOAs.

3.5 Unfolded Coprime L-shaped Array (UCLSA)

An unfolded coprime L-shaped array (UCLSA) geometry is composed of two L-shaped uniform linear arrays arranged in a manner that the coprime elements form two sub-arrays 1 and 2 respectively which are aligned orthogonal to each other on the plane considered (Zhang et al., 2019; Gong et al., 2018). The number of elements for each sub-array are chosen according to coprime integer pair say M and N where $M < N$. The structure can be imagined as four uniform linear arrays (ULAs) or two L-shaped arrays stretching from the origin with the element at the origin being the reference element and therefore shared by all the sub-arrays.

Assuming the sub-arrays to be two L-shaped, then, sub-array 1 can be viewed to be made up of elements aligned in positive x and y directions with a total number of elements of $2M-1$. Consequently sub-array 2 has its elements aligned in negative x and y directions with a total number of elements of $2N-1$. It then follows that the total number of elements in the array is $2M+2N-3$.

If the wavelength of the signal under consideration is λ, then the inter-sensor spacing can be expressed as $d_1 = N\frac{\lambda}{2}$ and $d_2 = M\frac{\lambda}{2}$ for sub-array 1 and 2 respectively. The array size is therefore given by total number of sensors per axis times the sensor inter-spacing distance, $(M-1)N\frac{\lambda}{2} + (N-1)M\frac{\lambda}{2}$, (Zhang et al., 2019; Pal & Vaidyanathan, 2011; Li & Zhang, 2017; Vaidyanathan & Pal, 2010; Zhang et al., 2018; Wang et al., 2017). A generalized UCLSA structure is shown in Figure 3.5.

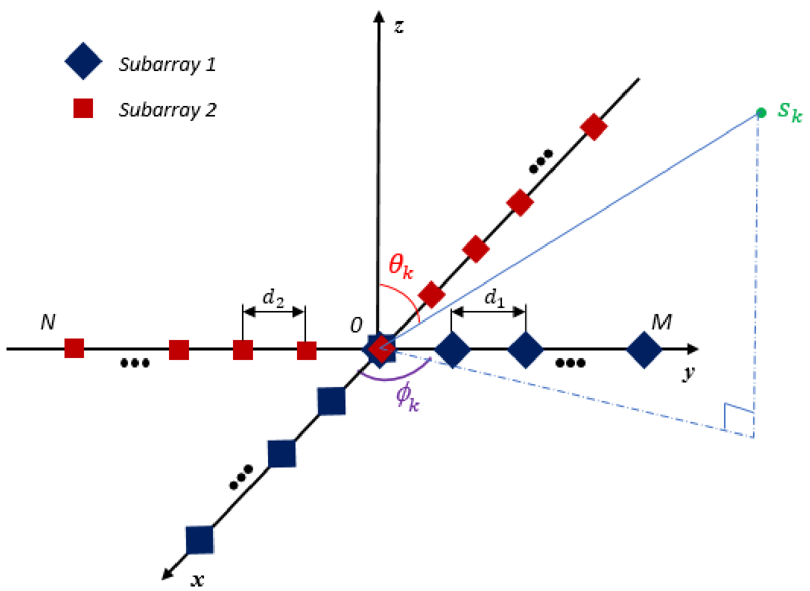

Figure 3.5 Unfolded coprime L-shaped array (UCLSA) geometry

3.5.1 Data Model

Suppose K uncorrelated far-field narrowband signals $\{s_k(t)\}_{k=1}^{K}$ of wavelength λ impinge on the array in a manner that kth signal makes an elevation and azimuth angle of $\{\theta_k \text{ and } \phi_k\}_{k=1}^{K}$ where $\theta_k \in (0^0,\ 90^0)$ and $\phi_k \in (0^0,\ 180^0)$ respectively. Further, suppose the base-band total signal received by each sub-array in either axis is expressed as $\{x_b \text{ and } y_b\}_{b=1}^{2}$ where b denotes the side of the sub-array considered. Letting 1 denote positive side and 2 negative side respectively. The received signal of the b^{th} sub-array in x directions for t^{th} snapshot is expressed as

$$\mathbf{x}_1(t) = \mathbf{A}_{x1}\mathbf{s}(t) + \mathbf{n}_{x1}(t) \tag{3.39a}$$

$$\mathbf{x}_2(t) = \mathbf{A}_{x2}\mathbf{s}(t) + \mathbf{n}_{x2}(t) \tag{3.39b}$$

Where $\mathbf{s}(t) = [s_1(t),\ s_2(t), \ldots, s_K(t)]^T$ is the signal vector $t = 1, 2, \ldots, J$ is the number of snapshots $\mathbf{n}_{x1}(t)$ and $\mathbf{n}_{x2}(t)$ are the additive white Gaussian noise vectors assumed to have zero mean, and variance σ_n^2 and independent of sources and $\mathbf{A}_{xb} \in \mathbb{C}^{(N\ or\ M)\times K}$ is the manifold matrix for bth sub-array along x-axis, is a Vandermonde matrix and can be individually expressed as

$$\mathbf{A_{x1}} = [\boldsymbol{\alpha}_{x1}(\theta_1, \phi_1),\ \boldsymbol{\alpha}_{x1}(\theta_2, \phi_2), ..., \boldsymbol{\alpha}_{x1}(\theta_{K-1}, \phi_{K-1}),\ \boldsymbol{\alpha}_{x1}(\theta_K, \phi_K)] \tag{3.40a}$$

$$\mathbf{A_{x}}_2 = [\boldsymbol{\alpha}_{x2}(\theta_1, \phi_1),\ \boldsymbol{\alpha}_{x2}(\theta_2, \phi_2), ...,\ \boldsymbol{\alpha}_{x2}(\theta_{K-1}, \phi_{K-1}),\ \boldsymbol{\alpha}_{x2}(\theta_K, \phi_K)] \tag{3.40b}$$

The corresponding steering vectors of the above matrices for the angle directions along positive and negative x axis respectively is expressed for the range $k = 1, 2, ..., K$ as

$$\boldsymbol{\alpha}_{x1}(\theta_1, \phi_1) = \left[\alpha_{x1}^{0}(\theta_k, \phi_k),\ ..., \alpha_{x1}^{M-1}(\theta_k, \phi_k)\right]^T \tag{3.41a}$$

$$\boldsymbol{\alpha}_{x2}(\theta_1, \phi_1) = \left[\alpha_{x2}^{-(N-1)}(\theta_k, \phi_k),\ ..., \alpha_{x2}^{0}(\theta_k, \phi_k)\right]^T \tag{3.41b}$$

where $\alpha_{xb}^{n}(\theta_k,\ \phi_k) = exp[j\,\eta\, n\, d_b \sin\theta_k \cos\phi_k]$ for $\eta = \frac{2\pi}{\lambda}, d_b$ denotes $d_1 = N\frac{\lambda}{2}$ or $d_2 = M\frac{\lambda}{2}$ and n is the position (the number) of sensor under consideration. Similarly, received signal of the bth sub-array in y directions for tth snapshot is expressed as

$$\mathbf{y}_1(t) = \mathbf{A}_{y1}\mathbf{s}(t) + \mathbf{n}_{y1}(t) \tag{3.42a}$$

$$\mathbf{y}_2(t) = \mathbf{A}_{y2}\mathbf{s}(t) + \mathbf{n}_{y2}(t) \tag{3.42b}$$

Where $\mathbf{s}(t) = [s_1(t),\ s_2(t), \ldots, s_K(t)]^T$ is the signal vector $t = 1, 2, \ldots, J$ is the number of snapshots $\mathbf{n}_{y1}(t)$ and $\mathbf{n}_{y2}(t)$ are the additive white Gaussian noise vectors assumed to have zero mean, and variance σ_n^2 and independent of sources and $\mathbf{A}_{yb} \in \mathbb{C}^{(N\ or\ M)\times K}$ is the manifold matrix for bth sub-array along y-axis, is a Vandermonde matrix and can be individually expressed as

$$\mathbf{A}_{y1} = [\boldsymbol{\alpha}_{y1}(\theta_1,\phi_1),\ \boldsymbol{\alpha}_{y1}(\theta_2,\phi_2), ..., \boldsymbol{\alpha}_{y2}(\theta_{K-1},\phi_{K-1}),\ \boldsymbol{\alpha}_{y1}(\theta_K,\phi_k)] \tag{3.43a}$$

$$\mathbf{A}_{\mathbf{y}2} = [\boldsymbol{\alpha}_{y2}(\theta_1,\phi_1),\ \boldsymbol{\alpha}_{y2}(\theta_2,\phi_2), ...,\ \boldsymbol{\alpha}_{y2}(\theta_{K-1},\phi_{K-1}),\ \boldsymbol{\alpha}_{y2}(\theta_K,\phi_K)] \tag{3.43b}$$

The corresponding steering vectors of the above matrices for the angle directions along positive and negative y axis respectively is expressed for the range $k = 1, 2, \ldots, K$ as

$$\boldsymbol{\alpha}_{y1}(\theta_1,\phi_1) = \left[\alpha_{y1}^{0}(\theta_k,\phi_k), \ldots, \alpha_{y1}^{M-1}(\theta_k,\phi_k)\right]^T \tag{3.44a}$$

$$\boldsymbol{\alpha}_{y2}(\theta_1,\phi_1) = \left[\alpha_{y2}^{-(N-1)}(\theta_k,\phi_k), \ldots, \alpha_{y2}^{0}(\theta_k,\phi_k)\right]^T \tag{3.44b}$$

where $\alpha_{yb}^{n}(\theta_k,\phi_k) = exp[j\,\eta\,n\,d_b\,\sin\theta_k\,\sin\phi_k]$ for $\eta = \frac{2\pi}{\lambda}$, d_b denotes $d_1 = N\frac{\lambda}{2}$ or $d_2 = M\frac{\lambda}{2}$ and n is the position of sensor under consideration.

3.5.2 2D DOA Estimation with UCLSA using MUSIC Algorithm

The total received data is leveraged in estimation of DOA using MUSIC algorithm. Therefore, first the received signal is combined to yield total received signal $\mathbf{z}(t)$. Pairing shall then be applied and removal of phase ambiguity. From the all array MUSIC analysis stated by Gong et al. (2018), signals from x-axis and y-axis are combined to create the resultant total received signal $\mathbf{z}(t)$.

$$\mathbf{x}(t) = \begin{bmatrix}\mathbf{x}_1(t)\\ \mathbf{x}_2(t)\end{bmatrix} = \begin{bmatrix}\mathbf{A}_{x1}\\ \mathbf{A}_{x2}\end{bmatrix}\mathbf{s}(t) + \begin{bmatrix}\mathbf{n}_{x1}(t)\\ \mathbf{n}_{x2}(t)\end{bmatrix} = \mathbf{A}_x\mathbf{s}(t) + \mathbf{n}_x(t) \tag{3.45a}$$

$$\mathbf{y}(t) = \begin{bmatrix}\mathbf{y}_1(t)\\ \mathbf{y}_2(t)\end{bmatrix} = \begin{bmatrix}\mathbf{A}_{y1}\\ \mathbf{A}_{y2}\end{bmatrix}\mathbf{s}(t) + \begin{bmatrix}\mathbf{n}_{y1}(t)\\ \mathbf{n}_{y2}(t)\end{bmatrix} = \mathbf{A}_y\mathbf{s}(t) + \mathbf{n}_y(t) \tag{3.45b}$$

Where:
$\mathbf{A}_x = \left[\mathbf{A}_{x1}^T,\ \mathbf{A}_{x2}^T\right]^T = [\boldsymbol{\alpha}_x(\theta_1,\phi_1),\ \boldsymbol{\alpha}_x(\theta_2,\phi_2), \ldots, \boldsymbol{\alpha}_x(\theta_{K-1},\phi_{K-1}),\ \boldsymbol{\alpha}_x(\theta_K,\phi_K)]$ and
$\mathbf{A}_y = \left[\mathbf{A}_{y1}^T,\ \mathbf{A}_{y2}^T\right]^T = [\boldsymbol{\alpha}_y(\theta_1,\phi_1),\ \boldsymbol{\alpha}_y(\theta_2,\phi_2), \ldots, \boldsymbol{\alpha}_y(\theta_{K-1},\phi_{K-1}), \boldsymbol{\alpha}_y(\theta_K,\phi_K)]$, with their

respective steering vectors given as
$\boldsymbol{\alpha}_x(\theta_k,\phi_k) = \left[\boldsymbol{\alpha}_{x1}^T(\theta_k,\phi_k),\ \ \boldsymbol{\alpha}_{x2}^T(\theta_k,\phi_k)\right]^T$ and $\boldsymbol{\alpha}_y(\theta_k,\phi_k) = \left[\boldsymbol{\alpha}_{y1}^T(\theta_k,\phi_k),\ \ \boldsymbol{\alpha}_{y2}^T(\theta_k,\phi_k)\right]^T$.
The total amalgamated signal therefore becomes

$$\mathbf{z}(t) = \begin{bmatrix}\mathbf{x}(t)\\ \mathbf{y}(t)\end{bmatrix} = \begin{bmatrix}\mathbf{A}_x\\ \mathbf{A}_y\end{bmatrix}\mathbf{s}(t) + \begin{bmatrix}\mathbf{n}_x(t)\\ \mathbf{n}_y(t)\end{bmatrix} = \mathbf{A}\mathbf{s}(t) + \mathbf{n}(t) \tag{3.46}$$

Where $\mathbf{A} = \left[\mathbf{A}_x^T,\ \mathbf{A}_y^T\right]^T = [\boldsymbol{\alpha}(\theta_1,\phi_1),\ldots,\ \boldsymbol{\alpha}(\theta_K,\phi_K)] \in \mathbb{C}^{2(N+M)\times K}$ and $\boldsymbol{\alpha}(\theta_k,\phi_k) = \left[\boldsymbol{\alpha}_x^T(\theta_k,\phi_k),\ \boldsymbol{\alpha}_y^T(\theta_k,\phi_k)\right]^T$. Similarly, the total noise is modelled as a collective of the noises in four directions of the array where both the positive and negative $x-$ axis noises and positive and negative $y-$ axis noise are summed separately as $\mathbf{n}_x = \left[\mathbf{n}_{x1}^T,\ \mathbf{n}_{x2}^T\right]^T$ and $\mathbf{n}_y = \left[\mathbf{n}_{y1}^T,\ \mathbf{n}_{y2}^T\right]^T$ to yield total noise as $\mathbf{n} = \left[\mathbf{n}_x^T,\ \mathbf{n}_y^T\right]^T$. The covariance matrix of the total received signal for 2D MUSIC algorithm is modelled as

$$\mathbf{R}_{ZZ} = E\left[\mathbf{z}(t)\mathbf{z}^H(t)\right] = \mathbf{A}E\left[s(t)\,s^H(t)\right]\mathbf{A}^H + E\left[\mathbf{n}(t)\mathbf{n}^H(t)\right] = \mathbf{A}\mathbf{R}_{ss}\mathbf{A}^H + \sigma_n^2\mathbf{I} \tag{3.47}$$

Since the exact covariance matrix cannot be solved, an approximation of the same is used as

$$\hat{\mathbf{R}}_{ZZ} = \frac{1}{J}\sum_{t=1}^{J}\mathbf{z}(t)\mathbf{z}^H(t) \tag{3.48}$$

From the expression of the estimated value covariances, if eigenvalue decomposition (EVD) is conducted, signal and noise subspaces are established respectively as shown

$$\hat{\mathbf{R}}_{ZZ} = \begin{bmatrix}\hat{\mathbf{U}}_s & \hat{\mathbf{U}}_n\end{bmatrix}\begin{bmatrix}\hat{\boldsymbol{\Lambda}}_s & \mathbf{0}\\ \mathbf{0} & \hat{\boldsymbol{\Lambda}}_n\end{bmatrix}\begin{bmatrix}\hat{\mathbf{U}}_s^H\\ \hat{\mathbf{U}}_n^H\end{bmatrix} = \hat{\mathbf{U}}_s\hat{\boldsymbol{\Lambda}}_s\hat{\mathbf{U}}_s^H + \hat{\mathbf{U}}_n\hat{\boldsymbol{\Lambda}}_n\hat{\mathbf{U}}_n^H \tag{3.49}$$

Where the signal and noise subspaces are complex matrices of sizes $\hat{\mathbf{U}}_s = \in \mathbb{C}^{2(N+M)\times K}$ and $\hat{\mathbf{U}}_n = \in \mathbb{C}^{[2(N+M)]\times[2(N+M)-K]}$ respectively. Consequently the signal and noise powers are also complex matrices of sizes $\hat{\boldsymbol{\Lambda}}_s = \in \mathbb{C}^{K\times K}$ and $\hat{\boldsymbol{\Lambda}}_n = \in \mathbb{C}^{[2(N+M)-K]\times[2(N+M)-K]}$. Finally, the spectral function is expressed as

$$P_{MUSIC}(\theta,\phi) = \frac{1}{\left|\boldsymbol{\alpha}^H(\theta,\phi)\hat{\mathbf{U}}_n\hat{\mathbf{U}}_n^H\boldsymbol{\alpha}(\theta,\phi)\right|} \tag{3.50}$$

From the spectrum function, the true DOAs are the one represented by the greater maximas.

3.5.3 MUSIC-Like Low Complexity Method for UCLSA

As proposed by Zhang et al. (2019) and Gong et al. (2018), a low computational complexity method for estimating 2D DOA using UCLSA is possible. This method employs all the sub-arrays in the search algorithm and uses a transformation that helps in reducing the estimation complexity and thereby reducing the total implementation cost. The method entails reducing the 2D problem to 1D which is less complex to perform spectral peak searching. Consider a transformation defined by $\gamma_k = \sin\theta_k \cos\phi_k$ and $\beta_k = \sin\theta_k \sin\phi_k$ for $\gamma_k \in (-1, 1)$ and $\beta_k \in (0, 1)$ respectively. The steering vectors defined by Eq. 3.41 and Eq. 3.44 becomes.

$$\boldsymbol{\alpha}_{x1}(\gamma_k) = \left[\alpha_{x1}^{0}(\gamma_k), ..., \alpha_{x1}^{M-1}(\gamma_k)\right]^T \tag{3.51a}$$

$$\boldsymbol{\alpha}_{x2}(\gamma_k) = \left[\alpha_{x2}^{-(N-1)}(\gamma_k), ..., \alpha_{x2}^{0}(\gamma_k)\right]^T \tag{3.51b}$$

$$\boldsymbol{\alpha}_{y1}(\beta_k) = \left[\alpha_{y1}^{0}(\beta_k), ..., \alpha_{y1}^{M-1}(\beta_k)\right]^T \tag{3.51c}$$

$$\boldsymbol{\alpha}_{y2}(\beta_k) = \left[\alpha_{y2}^{-(N-1)}(\beta_k), ..., \alpha_{y2}^{0}(\beta_k)\right]^T \tag{3.51d}$$

Consequently, the respective elements in either vectors transform to $\boldsymbol{\alpha}_{xb}^{n}(\gamma_k) = e^{j\eta n d_b \gamma_k}$ and $\boldsymbol{\alpha}_{yb}^{n}(\beta_k) = e^{j\eta n d_b \beta_k}$ respectively. With the above transformation, the two items to be searched, are independent of each other and therefore, as suggested by Zhang et al. (2019); Tayem & Kwon (2005) and Zhang et al. (2017), 1D spectral peak searching algorithms can be applied. For 2D MUSIC, the covariance matrix of the received signal is expressed as

$$\mathbf{R}_{ZZ} = E\left[\mathbf{z}(t)\mathbf{z}^H(t)\right] = \mathbf{A}E\left[\mathbf{s}(t)\mathbf{s}^H(t)\right]\mathbf{A}^H + E\left[\mathbf{n}(t)\mathbf{n}^H(t)\right] = \mathbf{A}\mathbf{R}_{ss}\mathbf{A}^H + \sigma_n^2\mathbf{I} \tag{3.52}$$

Since the exact covariance matrix cannot be solved, an approximation of the same is used as

$$\hat{\mathbf{R}}_{ZZ} = \frac{1}{J}\sum_{t=1}^{J}\mathbf{z}(t)\mathbf{z}^H(t) \tag{3.53}$$

From the expression of the estimated value covariances, if eigenvalue decomposition (EVD) is conducted, signal and noise subspaces are established respectively as

$$\hat{\mathbf{R}}_{ZZ} = \begin{bmatrix}\hat{\mathbf{U}}_s & \hat{\mathbf{U}}_n\end{bmatrix}\begin{bmatrix}\hat{\mathbf{\Lambda}}_s & \mathbf{0} \\ \mathbf{0} & \hat{\mathbf{\Lambda}}_n\end{bmatrix}\begin{bmatrix}\hat{\mathbf{U}}_s^H \\ \hat{\mathbf{U}}_n^H\end{bmatrix} = \hat{\mathbf{U}}_s\hat{\mathbf{\Lambda}}_s\hat{\mathbf{U}}_s^H + \hat{\mathbf{U}}_n\hat{\mathbf{\Lambda}}_n\hat{\mathbf{U}}_n^H \tag{3.54}$$

To estimate $\gamma_k \in (-1, 1)$ and $\beta_k \in (0, 1)$, firstly, the covariance matrix is redefined as

$$\hat{\mathbf{R}}_{ZZ} = \frac{1}{J}\sum_{t=1}^{J}\begin{bmatrix}\mathbf{x}(\mathbf{t})\\ \mathbf{y}(\mathbf{t})\end{bmatrix}\begin{bmatrix}\mathbf{x}^H(t) & \mathbf{y}^H(t)\end{bmatrix} = \begin{bmatrix}\hat{\mathbf{R}}_{XX} & \hat{\mathbf{R}}_{XY}\\ \hat{\mathbf{R}}_{YX} & \hat{\mathbf{R}}_{YY}\end{bmatrix} \tag{3.55}$$

Where: $\hat{\mathbf{R}}_{XX} = \frac{1}{J}\sum_{t=1}^{J}\mathbf{x}(t)\mathbf{x}^H(t) \in \mathbb{C}^{(M+N)\times(M+N)}$, $\hat{\mathbf{R}}_{YY} = \frac{1}{J}\sum_{t=1}^{J}\mathbf{y}(t)\mathbf{y}^H(t) \in \mathbb{C}^{(M+N)\times(M+N)}$, $\hat{\mathbf{R}}_{XY} = \frac{1}{J}\sum_{t=1}^{J}\mathbf{x}(t)\mathbf{y}^H(t) \in \mathbb{C}^{(M+N)\times(M+N)}$ and $\hat{\mathbf{R}}_{YX} = \frac{1}{J}\sum_{t=1}^{J}\mathbf{y}(t)\mathbf{x}^H(t) \in \mathbb{C}^{(M+N)\times(M+N)}$ are covariance matrices of received signals in the directions of the subscripts indicated and J is the number of snapshots. It is possible to find the eigenvalue decomposition (EVD) for $\hat{\mathbf{R}}_{XX}$.

$$\hat{\mathbf{R}}_{XX} = \begin{bmatrix}\hat{\mathbf{U}}_{sx} & \hat{\mathbf{U}}_{nx}\end{bmatrix}\begin{bmatrix}\hat{\mathbf{\Lambda}}_{sx} & \mathbf{0}\\ \mathbf{0} & \hat{\mathbf{\Lambda}}_{nx}\end{bmatrix}\begin{bmatrix}\hat{\mathbf{U}}_{sx}^H\\ \hat{\mathbf{U}}_{nx}^H\end{bmatrix} = \hat{\mathbf{U}}_{sx}\hat{\mathbf{\Lambda}}_{sx}\hat{\mathbf{U}}_{sx}^H + \hat{\mathbf{U}}_{nx}\hat{\mathbf{\Lambda}}_{nx}\hat{\mathbf{U}}_{nx}^H \tag{3.56}$$

Where the signal and noise subspaces are complex matrixes of sizes $\hat{\mathbf{U}}_{sx} = \in \mathbb{C}^{(N+M)\times K}$ and $\hat{\mathbf{U}}_{nx} = \in \mathbb{C}^{[(N+M)]\times[(N+M)-K]}$. Since the steering vector is identical with eh signal subspace and orthogonal to the noise subspace $\hat{\mathbf{U}}_{nx}$,the peak search function, γ_k ($k = 1, 2\ldots, K$) can be defined as

$$P(\gamma) = \frac{1}{\left\|\hat{\mathbf{U}}_{nx}^H\boldsymbol{\alpha}_x(\gamma)\right\|^2}\ ,\ \gamma \in (-1, 1) \tag{3.57}$$

It is then assumed that the $\hat{\gamma}_k$ corresponding to the K peaks is the estimation of γ. With the value of $\hat{\gamma}_k$, it is possible to estimate β_k as follows.

$$P(\beta) = \frac{1}{\left\|\hat{\mathbf{U}}_n^H\begin{bmatrix}\boldsymbol{\alpha}_x(\hat{\gamma}_k)\\ \boldsymbol{\alpha}_y(\beta)\end{bmatrix}\right\|^2}\ ,\ \beta \in (0, 1) \tag{3.58}$$

In the second function, $\boldsymbol{\alpha}_x(\hat{\gamma}_k)$ is a constraint to the spectrum calculation thereby enabling automatic pair matching of the azimuth and elevation angles (Zhang et al., 2019). The final angle pairs are expressed as

$$\hat{\theta}_k = sin^{-1}\left(\sqrt{\hat{\gamma}_k + \hat{\beta}_k}\right) \tag{3.59}$$

$$\hat{\phi}_k = tan^{-1}\left(\frac{\hat{\beta}_k}{\hat{\gamma}_k}\right) \tag{3.60}$$

3.6 Virtual Array Interpolation Method

Array interpolation is a signal processing technique that maps arbitrary antenna structure to a uniform array (Li et al., 2014). In practical applications like DOA estimation, line spectrum estimation, super resolution, beamforming and coprime spatial filter bank design (Liu et al., 2016), sparse array structures like nested and coprime arrays which are unions of two uniform ULAs with different inter-element spacing are preferred to normal ULAs because of their ability to identify more sources due to their increased DOF (Guo et al., 2018). However, the co-array of these sparse arrays normally have holes which prevents the conventional algorithms from estimating DOAs. To fill the holes, virtual array interpolation technique is necessary.

3.6.1 Coprime co-array Interpolation

This is a method of DOA estimation using augmented coprime array with a sole objective of increasing the aperture and DOF of the conventional coprime array to ensure increased number of resolvable sources. A ULA of M number of elements can resolve up to $M-1$ sources only using the conventional DOA estimation algorithms. Sparse arrays like coprime, however; have the ability to resolve signal sources of up to $O(MN)$ using only $O(M+N)$ sensor elements for which M & N are coprime integer pairs and $M < N$ (Chen et al., 2020; Liu et al., 2016; Hassan et al., 2018; Liu et al., 2017; Hosseini & Sebt, 2017). However, the coprime arrays as described and used in the previous sections fails to reach this target. This is because, the virtual coprime co-array produces a contiguos ULA at the near centre and nonuniform linear array with holes at either ends, which is symmetric on either directions. Furthermore, algorithms like MUSIC only utilises data from the contagious ULA co-array section but discarding the far end elements characterised by holes.

The principle of array interpolation enables the filling of the holes in the co-array to increase the DOF beyond that captured in the contiguous ULA section of the array and thereby transforming a virtual symmetric nonuniform linear array (VSNLA) to a filled uniform linear array (ULA) Liu et al. (2017).

Interpolation techniques like SS-MUSIC, positive definite Toeplitz completion, array interpolation, ℓ_1 minimization or LASSO can be used for interpolating the sensors for the holes in the co-array. The only drawback in using them is that they will require additional tuning parameters like matrix vectorisation, reshaping, spatial smoothing or discretization of parameter space into a dense grid respectively resulting in computational complexity.

Nuclear norm minimization technique which is preferred because it is computationally tractable, free from predefined dense grids, positive definite requirements, and requires no additional tuning parameters will be adopted for interpolating holes of the difference co-array (Hosseini & Sebt, 2017; Liu et al., 2016; Hassan et al., 2018).

3.6.2 Signal Model

Assume a coprime array consisting of sensor elements described by a coprime integer pair M and N for $M < N; M, N \in N^+$. In this description, each coprime integer subsets $\mathbb{S}_{2M} = \{0,\ M,\ 2M, \ldots,\ (2M-1)N\}$ and $\mathbb{S}_{\mathbb{N}} = \{0,\ N,\ 2N, \ldots,\ (N-1)M\}$ can be viewed as independent ULA sub-arrays with $2M$ & N element respectively. The location of the sensors can be represented by $p \times d$ where $d = \lambda/2$ and λ being the wavelength of the impinging signal and p belongs to the set

$$\mathbb{S} = \{0,\ M,\ 2M, \ldots,\ (2M-1)N\} \cup \{0,\ N,\ 2N, \ldots, (N-1)M\} \tag{3.61}$$

The total physical elements in a coprime set is therefore $2M + N - 1$.

A unique set called a difference array, $\mathbb{D}$ needs to be defined to enable full exploitation of the coprime array DOF. From the above coprime integer set $\mathbb{S}$, $\mathbb{D}$ is generated as

$$\mathbb{D} = \{p_1 - p_2 \mid p_1, p_2 \in \mathbb{S}\} \tag{3.62}$$

The sensor location for the difference set $\mathbb{D}$ is given by $\mathbb{D} \times d$. $\mathbb{D}$ is a viewed as a virtual symmetric nonuniform linear array (VSNLA) with holes. The holes in this set limits the utilisation of the full DOF of the array and at the same time hinders the application of conventional DOA estimation algorithms that only performs on ULA matrix data.

A central contiguous ULA segment can be extracted from the difference array $\mathbb{D}$ which is given by

$$\mathbb{U} = \{m \mid \{-|m|, \ldots, -3, -2-1, 0, 1, 2, 3, \ldots, |m|\} \subseteq \mathbb{D}\} \tag{3.63}$$

This ULA is a subset of the difference array $\mathbb{D}$, which means, if used for DOA estimation, it has less DOF, which will limit the resolvable sources. The aim is to achieve maximum DOF and restructure the co-array in a way that subspace algorithms can be applied. This then means that the difference array has to be exploited since it contains the maximum achievable DOF for the sparse array. Therefore the ULA containing maximum $\mathbb{D}$ is the integer set given by

$$\mathbb{V} = \{m \mid min(\mathbb{D}) \leq m \leq max(\mathbb{D})\} \tag{3.64}$$

Figure 3.6 (a) represents the coprime array for $M = 2$ and $N = 5$. Its corresponding co-array is represented in (b) and its augmented array in (c) where p_1 and p_2 represents the number of sensors at level 1 and level 2 respectively as described by Vaidyanathan & Pal (2011).

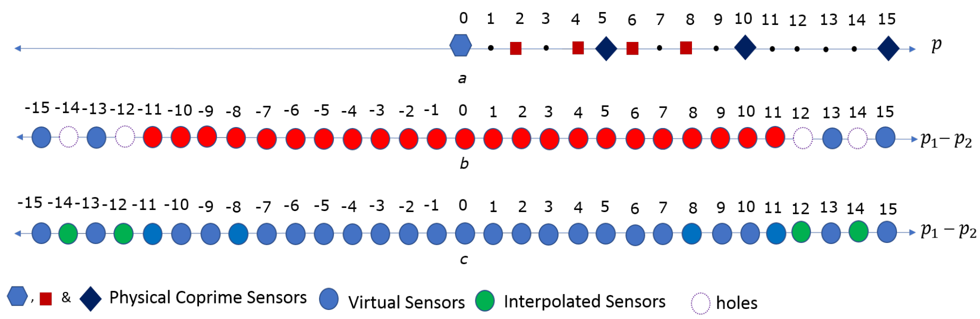

Figure 3.6 (a) Coprime Array Configuration; (b) Difference co-array with contagious ULA cenrally placed (marked in red); (c) Augmented coprime array with filled "holes"

From the definitions and descriptions above, the cardinalities of $\mathbb{S}$, $\mathbb{D}$, $\mathbb{U}$, and $\mathbb{V}$ can be summarised as Equation 3.65.

$$|\mathbb{S}| = 2M + N - 1 \tag{3.65a}$$

$$|\mathbb{D}| = 3MN + M - N \tag{3.65b}$$

$$|\mathbb{U}| = 2MN + 2M - 1 \tag{3.65c}$$

$$|\mathbb{V}| = 4MN - 2N + 1 \tag{3.65d}$$

Assume that K far-field narrowband uncorrelated signals $s_k(t)_{k=1}^{K}$ with the same wavelength λ impinge on the array at an elevation angle of $\{\theta_k\}_{k=1}^{K}$ where $\theta_k \in (-90^0, 90^0)$. The total received signal in the coprime array can be modelled as

$$\mathbf{x}_{\mathbb{S}}(t) = \mathbf{A}\mathbf{s}_k(t) + \mathbf{n}(t) \tag{3.66}$$

where all the used symbols having the same meaning as in data models of the previously described sections. The covariance matrix of the above received signal is given as

$$\mathbf{R}_{XX} = E\left[\boldsymbol{x}_{\mathbb{S}}(t)\boldsymbol{x}_{\mathbb{S}}^{H}(t)\right] = \mathbf{A}E\left[\mathbf{s}(t)\mathbf{s}^{H}(t)\right]\mathbf{A}^{H} + E\left[\mathbf{n}(t)\mathbf{n}^{H}(t)\right] = \mathbf{A}\mathbf{R}_{SS}\mathbf{A}^{H} + \sigma_n^2\mathbf{I} \tag{3.67}$$

Where: $\mathbf{A}$ is the manifold matrix with its corresponding steering vector given as $\mathbf{A} = [\boldsymbol{\alpha}_{\mathbb{S}}(\theta_1), \boldsymbol{\alpha}_{\mathbb{S}}(\theta_2), ..., \boldsymbol{\alpha}_{\mathbb{S}}(\theta_{K-1}), \boldsymbol{\alpha}_{\mathbb{S}}(\theta_K)]$ and $\boldsymbol{\alpha}_{\mathbb{S}}(\theta_k) = [\alpha^0(\theta_k), \ldots, \alpha^{M+N-1}(\theta_k)]^T$ and

$\alpha^{\mathbb{S}}(\theta_k) = e^{-1j\eta p d \sin\theta_k}$ for $\eta = \frac{2\pi}{\lambda}$; $\mathbf{R}_{SS} = diag[\sigma_1^2, \sigma_2^2, \ldots, \sigma_K^2]$ represents the received signal power with each individual source represented by σ_k^2 and σ_n^2 being the noise power.

Normally, it is not possible to calculate the exact covariance, therefore an estimated value given by $\hat{\mathbf{R}}_{XX} = \frac{1}{J}\sum_{t=1}^{J} \mathbf{x}_{\mathbb{S}}(t)\mathbf{x}_{\mathbb{S}}^H(t)$ where J is the total number of snapshots is used.

The auto-correlations of sensor output signal evaluated at lags defined by $\mathbb{D}$, $\mathbb{U}$ and $\mathbb{V}$ can be denoted by $\boldsymbol{R}_{\mathbb{D}\mathbb{D}}$, $\boldsymbol{R}_{\mathbb{U}\mathbb{U}}$ and $\boldsymbol{R}_{\mathbb{V}\mathbb{V}}$ respectively.

The objective then becomes to interpolate the VSNLA provided by set $\mathbb{D}$ to the virtual uniform linear array (VULA) set $\mathbb{V}$. This then allows application of co-array MUSIC algorithm while utilising the full DOF provided by the difference co-array set $\mathbb{D}$.

3.6.3 Array Interpolation using Nuclear Norm Minimization

Nuclear norm minimization is a low complexity interpolation method that does not require either vectorization or spatial smoothing operations as a way of reducing computational complexity. The process of retrieving covariance matrix $\boldsymbol{R}_{\mathbb{V}\mathbb{V}}$ from the received signal data covariance $\boldsymbol{R}_{\mathbb{S}\mathbb{S}}$ is a convex case problem of nuclear norm minimisation (Hosseini & Sebt, 2017; Liu et al., 2016; Hassan et al., 2018). This can be achieved through semidefinite programming using the CVX programming developed by Grant et al. (2009).

$$\widetilde{\mathbf{R}}_{\mathbb{V}\mathbb{V}}^{NN} = \underset{\widetilde{\mathbf{R}}_{\mathbb{V}\mathbb{V}} \in C^{|\mathbb{V}^+|\times|\mathbb{V}^+|}}{arg\ min} \ ||\widetilde{\mathbf{R}}_{\mathbb{V}\mathbb{V}}||_* \tag{3.68a}$$

$$\text{Subject to} \quad \widetilde{\mathbf{R}}_{\mathbb{V}\mathbb{V}} = \widetilde{\mathbf{R}}_{\mathbb{V}\mathbb{V}}^H; \tag{3.68b}$$

$$\langle\widetilde{\mathbf{R}}_{\mathbb{V}\mathbb{V}}\rangle_{p1,p2} = \langle\widetilde{\mathbf{R}}_{\mathbb{V}\mathbb{V}}\rangle_{p1-p2} \tag{3.68c}$$

Where: $||\cdot||_*$ represents the nuclear norm of a given matrix. Further, for $p \in \mathbb{S}$, the triangular bracket notation $\langle\mathbf{R}_{\mathbb{S}\mathbb{S}}\rangle_p$ is used to denote the value of the signal at the support location p; $p_1, p_2 \in \mathbb{V}^+ = \{p \mid p \in \mathbb{V}, \quad p \geq 0\}$ and $\langle \mathbf{R}_{\mathbb{V}\mathbb{V}} \rangle_{p1,p2} = E[\langle \mathbf{R}_{\mathbb{V}\mathbb{V}} \rangle_{p1} \langle \mathbf{R}_{\mathbb{V}\mathbb{V}} \rangle^*_{p2}]$.

Consequently, nuclear norm minimization is applied where the number of resolvable signal sources is equivalent to the number of positive lags in the virtual array $\mathbb{V}$ and is given by

$$L = \frac{(|\mathbb{V}| - 1)}{2} = \frac{[(4MN - 2N + 1) - 1]}{2} = 2MN - N \tag{3.69}$$

The optimal solution of the above equation contains Hermitian Toeplitz matrix $\mathbf{R}_{\mathbb{V}\mathbb{V}}$. This covariance matrix can be directly applied in the co-array MUSIC algorithm for DOA estimation through following the conventional MUSIC algorithm procedure of first performing eigen value decomposition (EVD) to obtain the signal and noise subspaces, $\boldsymbol{U}_S$ and $\boldsymbol{U}_N$ respectively followed by searching the steering matrices in the specified angle range and finally computing the Co-array MUSIC spectral function.

CHAPTER FOUR
SIMULATIONS AND DISCUSSIONS

MATLAB simulations, performance analysis and comparisons of different geometries described in Chapter 3 are conducted. For purposes of uniformity and ease of analysis, the narrow band far field signals are considered in all cases. Practical case signals for wireless fidelity (Wi-Fi) operating at a frequency of 2.4 GHz: 802.11b/g/n, a service platform which has greatest demand especially for internet of things (IoT) is considered. The elevation and azimuth angles are taken in the range of, $\theta_k \in (0^0, 90^0)$ and $\theta_k \in (0^0, 180^0)$ respectively.

The simulations are subdivided into three parts. The first is 1D DOA estimations featuring DECOM and CLSA geometries and the second is 2D DOA estimations featuring CLSA and UCLSA geometries all of which MUSIC algorithm was applied. Lastly, virtual array interpolation for coprime nonuniform linear array for which co-array MUSIC algorithm was used for estimation the DOAs was considered.

In each scenario, the approach taken followed the parameter sequence as enumerated below

- Variation of signal to noise ratio (SNR)
- Variation of the number of snapshots
- Variation of the number of sensor elements
- Variation of signal arrival angles for specific scenarios.
- Estimating the DOAs with contagious ULA data as well as for interpolated co-array data using co-array MUSIC for interpolation case.
- RMSE for each case was determined as a performance metric.

4.1 MUSIC Algorithm Implementation Procedure in MATLAB

The steps for implementation of MUSIC algorithm in MATLAB program are highlighted as in flow diagram Figure 4.1.

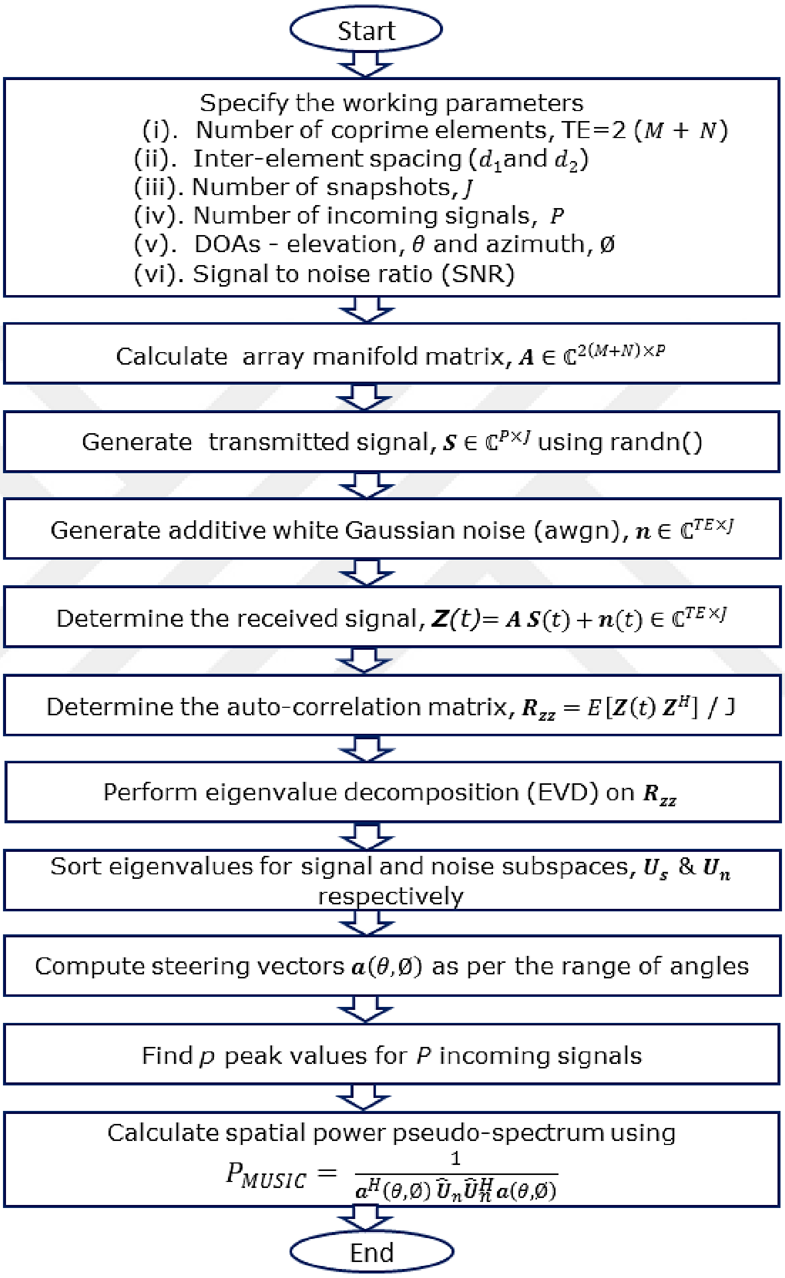

Figure 4.1 Implementation of MUSIC algorithm in MATLAB program

4.2 Simulation Results for DECOM Method for Nonuniform Linear Array

Simulations were carried out to evaluate the performance of DECOM using MUSIC algorithm with respect to varying environmental and array structural parameters. The 1D power pseudo-spectra maxima plots are used as pointers for the estimated DOAs and further RMSE evaluated between estimated and the actual DOA values.

4.2.1 Simulation 1: Variation of SNR

In this Simulation, DECOM(4,5) is used to estimate the direction of arrival with respect to the SNR. Firstly, a single DOA is estimated in two different environments where SNR values of -5 and 20 were used for actual DOA of 60^0. Consequently, multiple source were estimated using DECOM(5,7), still with with respect to the SNR of -5 and 20 values with actual DOAs of 60^0 and 68^0. In these two case scenarios, the number of snapshots was held constant at $J = 200$.

Figures 4.2 & 4.3 represents MATLAB plots for estimating DOA with SNR of -5 and 20 respectively from which it was observed that the latter figure with the higher SNR gave a higher resolution DOA estimates than the former. The same simulation was repeated for multiple signal sources as shown in plots of Figures 4.4 & 4.5 respectively.

It was observed that when estimating multiple DOAs with DECOM method, higher SNR values gives distinctive DOAs as opposed to when estimating with lower SNR values. A point to note was ambiguous DOAs that characterised the power pseudo-spectrum. To identify the true DOAs, the automatically paired DOAs are selected form the isolated ones which represents the ambiguous AoAs.

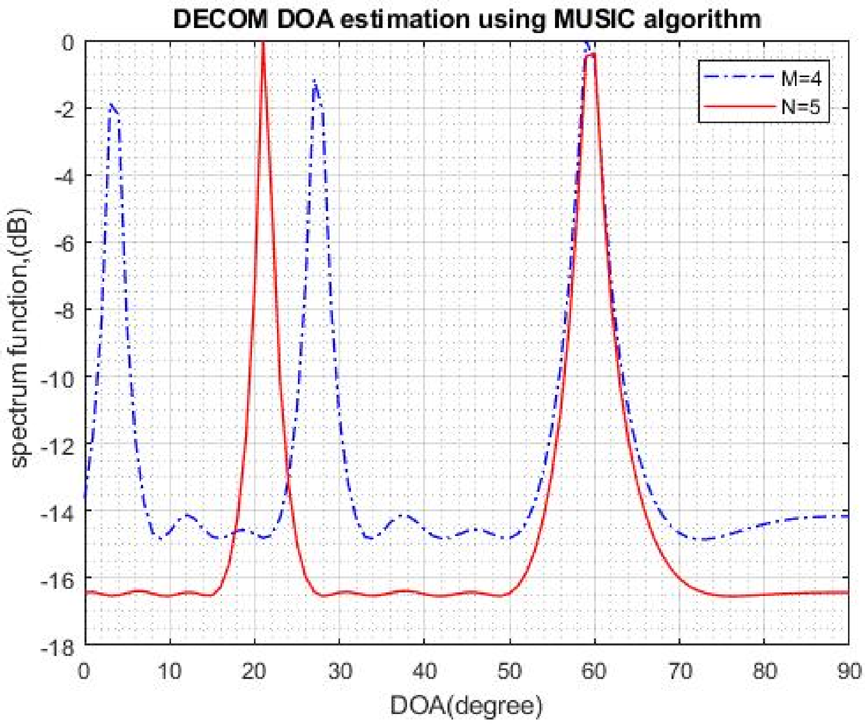

Figure 4.2 DECOM (4,5) DOA estimation for 60^0 for SNR=-5

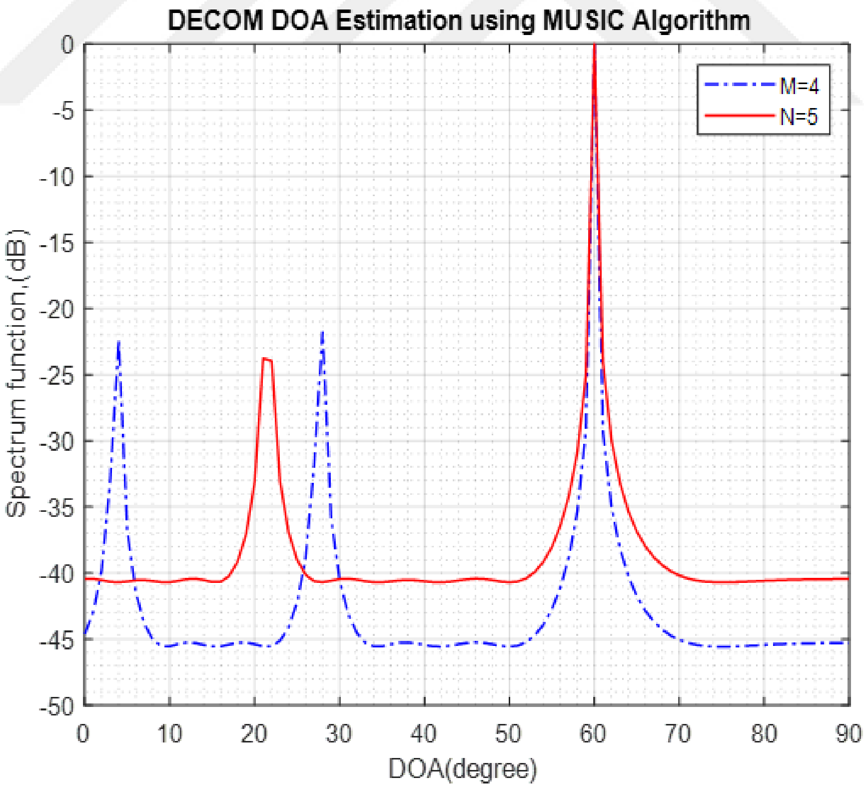

Figure 4.3 DECOM (4,5) DOA estimation for 60^0 for SNR=20

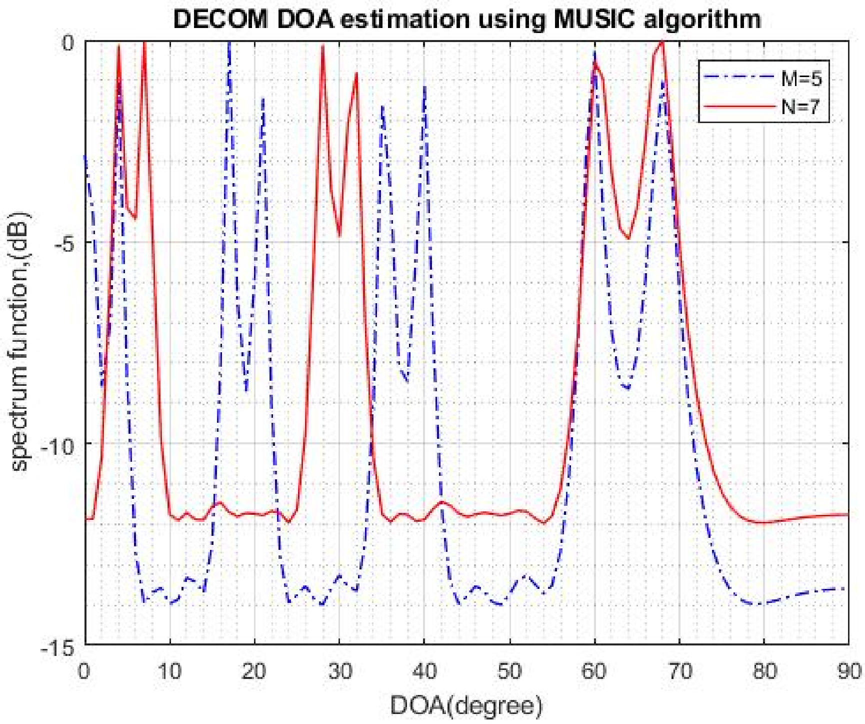

Figure 4.4 DECOM(5,7) DOA estimation for 60^0 & 68^0 for SNR=-5

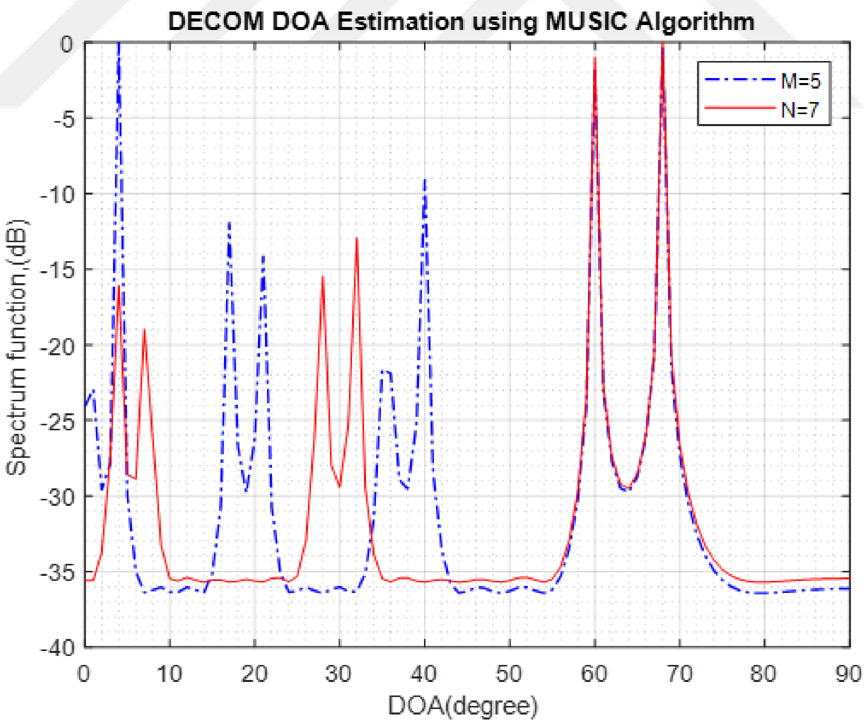

Figure 4.5 DECOM(5,7) DOA estimation for 60^0 & 68^0 for for SNR=20

4.2.2 Simulation 2: Variation of Number of Snapshots

The performance of DECOM geometry is in this Simulation investigated for varying number of snapshots with a constant $SNR = 5$. As in Simulation 1, the first pair of Simulations investigates the performance of one source and the second pair investigates multiple sources. actual DOAs used were 60^0 for DECOM (4,5) and 60^0 68^0 for DECOM (5,7) respectively.

Figures 4.6 & 4.7 shows the curves for number of snapshots 100 and 1000 respectively. When the number of snapshots is 100, the resolution is low and there are several ambiguous DOA maximas. When snapshots is increased to 1000, the resolution improves and the estimator also tends to perform with fewer ambiguous DOAs.

Figures 4.8 & 4.9 represents multiple sources estimation with snapshots of 100 and 1000 respectively. It can be seen that the latter curves with higher snapshots gave better resolution as opposed to the former. When the snapshots are lower, it is not easier to distinguish sources when the distance of separation is very small. This improves by increasing the number of snapshots.

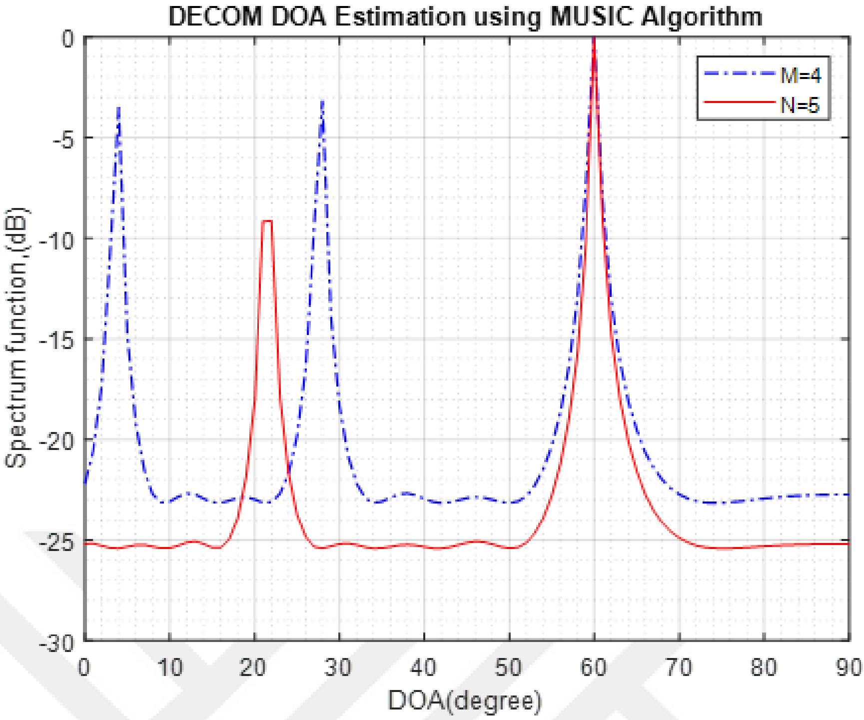

Figure 4.6 DECOM (4,5) DOA estimation for 60^0 for snapshots=100

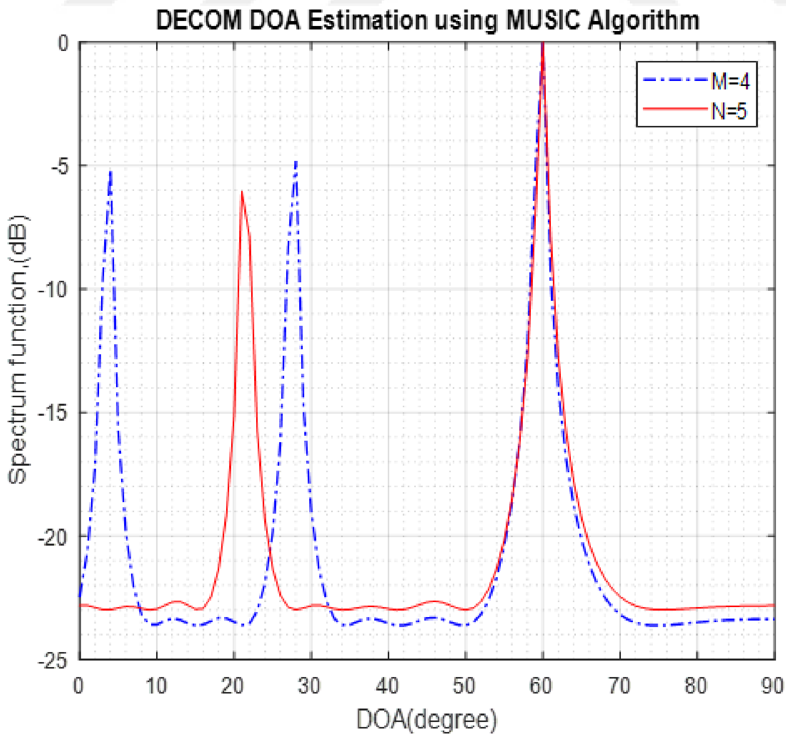

Figure 4.7 DECOM (4,5) DOA estimation for 60^0 for snapshots=1000

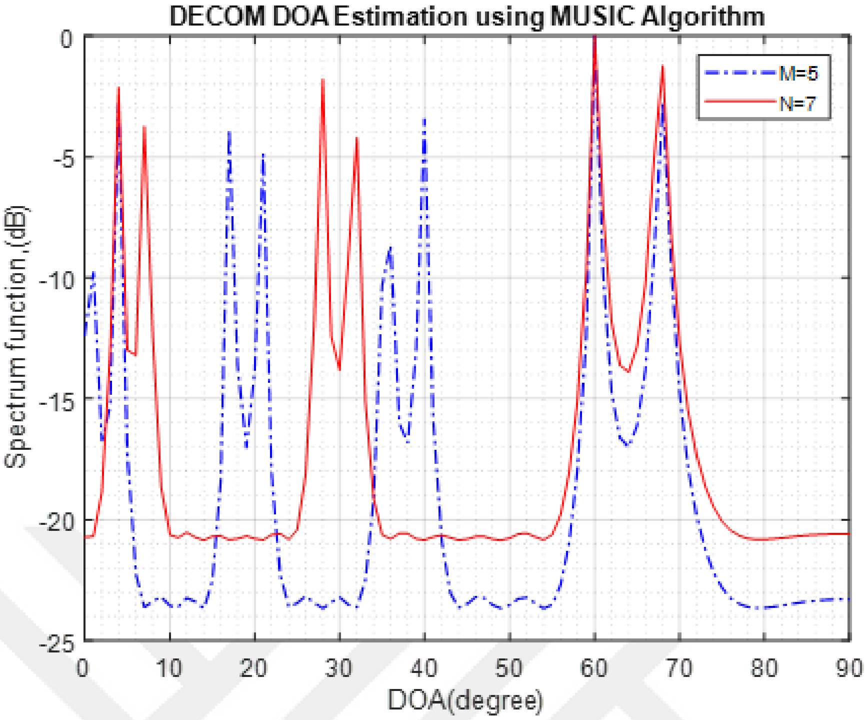

Figure 4.8 DECOM (5,7) DOA estimation for 60^0 & 68^0 for snapshots=100

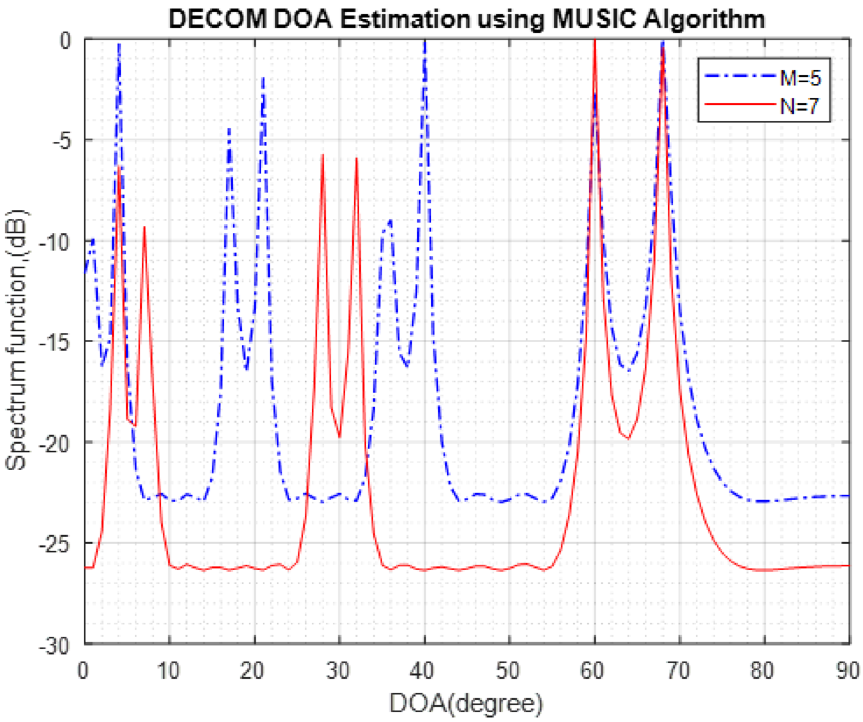

Figure 4.9 DECOM (5,7) DOA estimation for 60^0 & 68^0 for snapshots=1000

4.2.3 Simulation 3: Error Analysis for DECOM

The root mean square error (RMSE) was calculated as the performance metric for the estimation method. As expressed in (Zhou et al., 2013; Bhuiya et al., 2012; Li & Zhang, 2017), for one dimensional angle estimation methods, RMSE is expressed as

$$RMSE = \frac{1}{L}\left(\frac{1}{K}\sum_{l=1}^{L}\sum_{k=1}^{K}(\hat{\theta}_k^{(l)} - \theta_k)^2\right)^{1/2} \tag{4.1}$$

Where L is the Monte Carlo number of trials conducted, $\hat{\theta}$ is the approximated angle and θ is the actual DOA and K represents the number of signals. DECOM geometry with varying number of sensors were compared while varying SNR and number of snapshots in the first and second instances respectively.

In Figure 4.10, the number of snapshots were held constant at 200 and for Figure 4.11, SNR was constant at 5. In each instance 1000 Monte-Carlo trials were performed. It was established that in both cases, increasing the number of sensors reduces the errors in estimation.

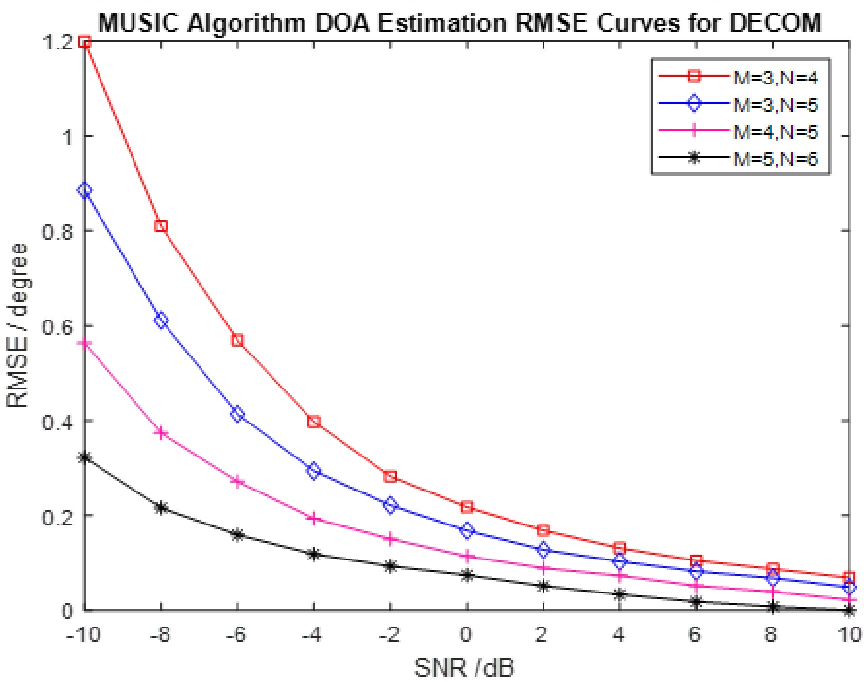

Figure 4.10 Performance of DECOM geometries with varying SNR

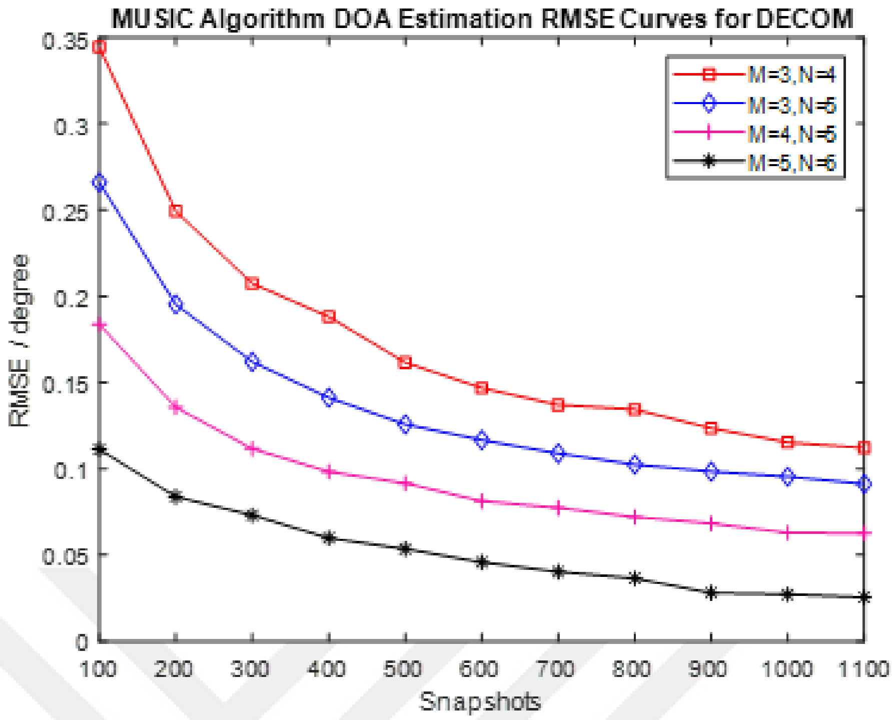

Figure 4.11 Performance of DECOM geometries with varying Snapshots

4.3 Simulation Results for 1D UCLA with MUSIC Algorithm

4.3.1 Simulation 1: Variation of SNR

Simulations for UCLA geometry using MUSIC algorithm was conducted while varying the values performance parameters. Figures 4.12 & 4.13 represents power pseudo-spectra for UCLA geometries of (3,4), (4,5), (5,7) and (9,7) plotted with SNR values of -5 and 20 respectively for actual DOA of 60^0 at a constant number of snapshots of $J = 200$. In both scenarios, there were no ambiguous DOAs. However, the plots generated with higher value of SNR produced higher resolutions and better estimations.

In a repeat simulation, two distinct incoherent sources were used with actual DOAs at 60^0 & 68^0 while holding the other parameters constant. Figure 4.14 represents shows the DOA maximas for SNR=-5 and Figure 4.15 represents that of SNR=20. Again, it was observed that the estimator with higher SNR had higher resolution.

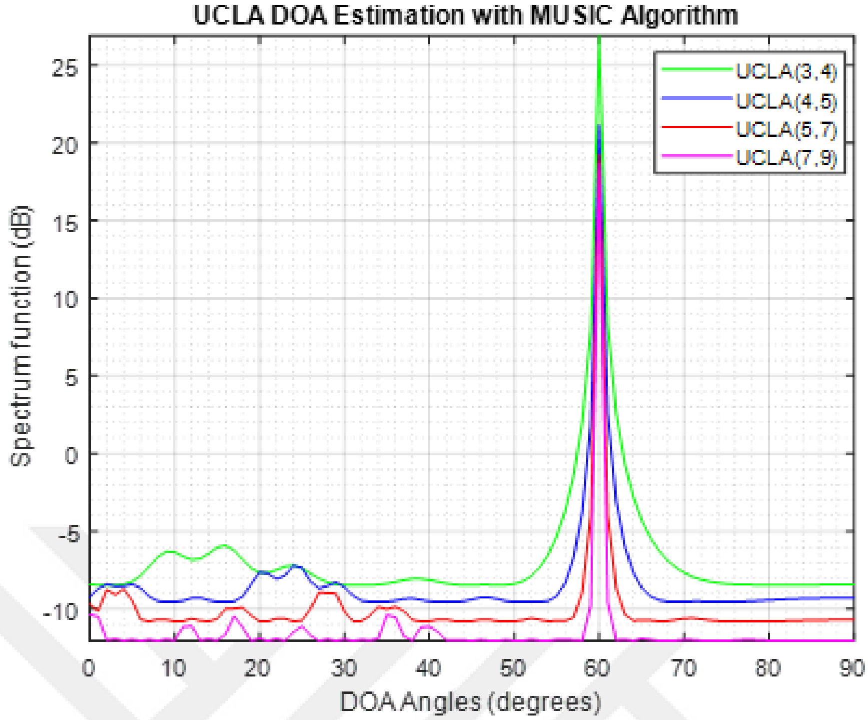

Figure 4.12 Performance of UCLA geometries for 60^0 for $SNR = -5$

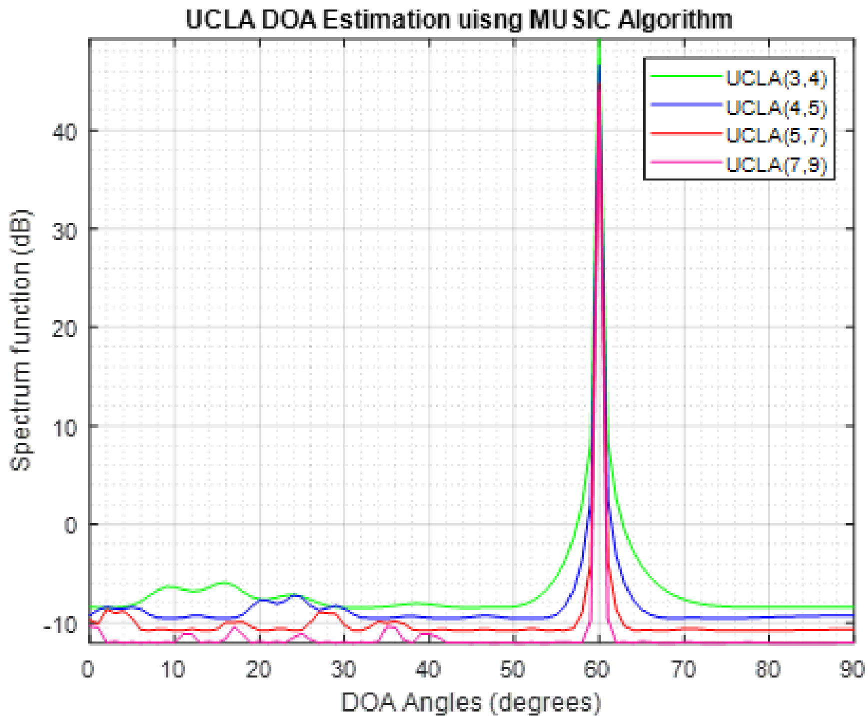

Figure 4.13 Performance of UCLA geometries for 60^0 for $SNR = 20$

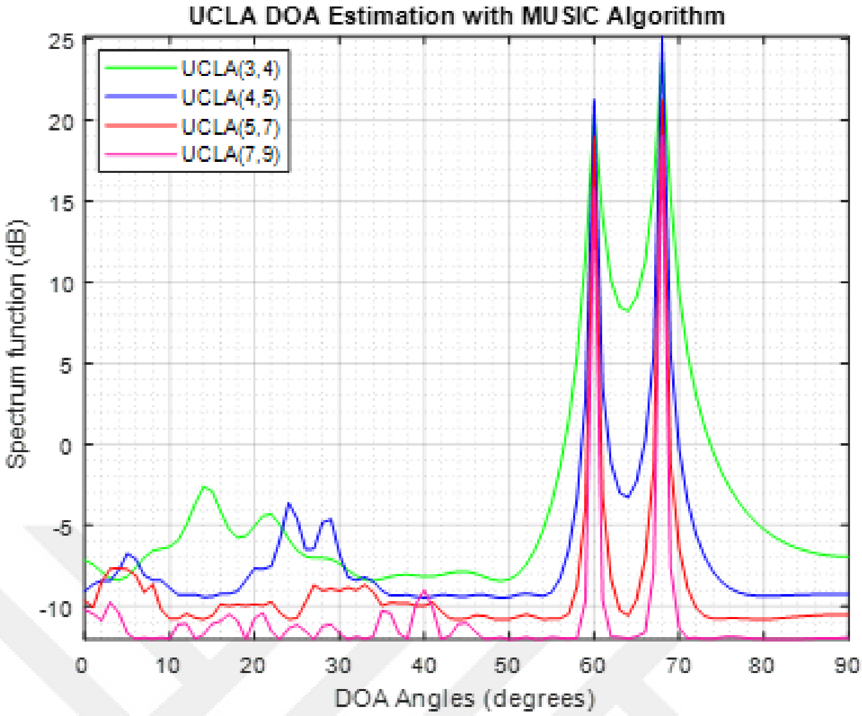

Figure 4.14 Performance of UCLA geometries for 60^0 & 68^0 for $SNR = -5$

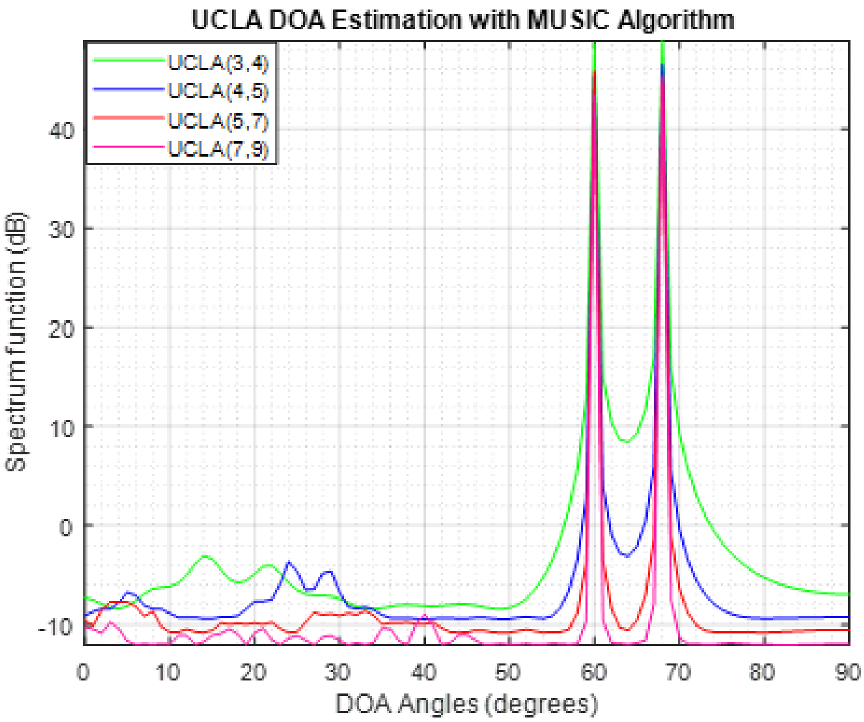

Figure 4.15 Performance of UCLA geometries for 60^0 & 68^0 for $SNR = 20$

4.3.2 *Simulation 2: Varying the Number of Snapshots*

This Simulation intended to investigate the performance of different UCLA geometries with varying number of snapshots. Figure 4.16 & 4.17 represents curves for estimating a single actual DOA of 60^0 with number of snapshots of 100 and 1000 respectively for constant SNR of -5. It was observed that when the number of snapshots is small and the number of sensors are also few, the estimator produces inconspicuous spectral peaks. By increasing number of snapshots as well as numbers of sensors results to conspicuous peaks with almost no errors.

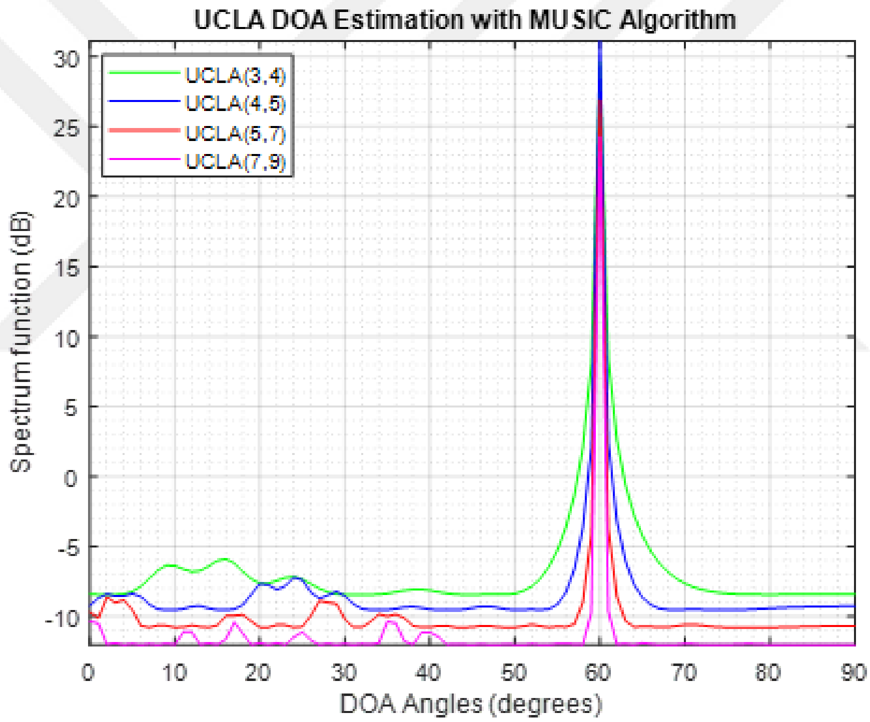

Figure 4.16 UCLA(4,5) DOA estimation for 60^0 for snapshots=100

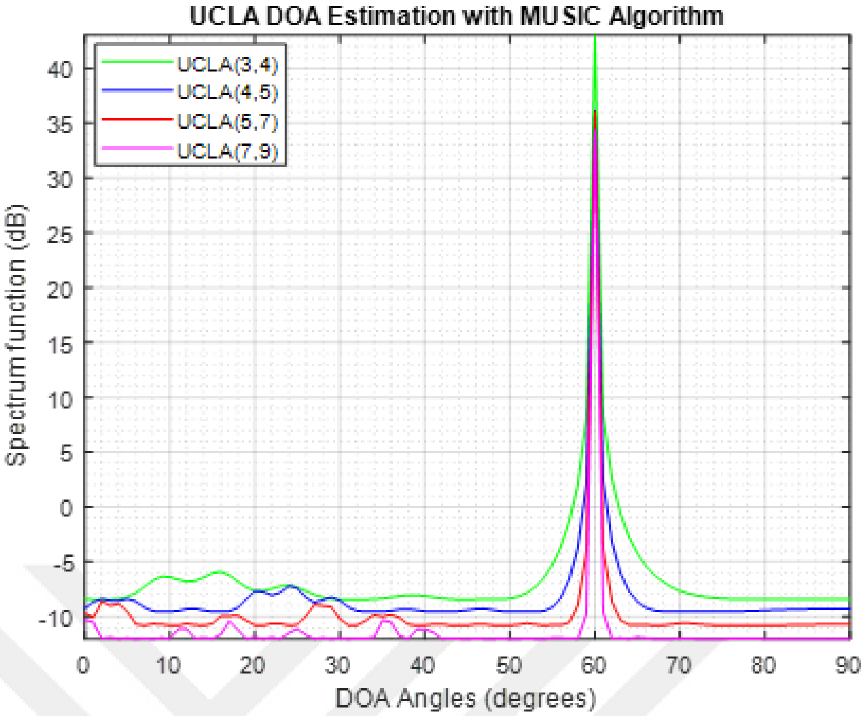

Figure 4.17 UCLA(4,5) DOA estimation for 60^0 for snapshots=1000

A repeat of the aforementioned Simulation was performed for multiple sources of actual DOAs of 60^0 & 68^0. Figures 4.18 & 4.19 represents estimation for number of snapshots of 100 and 100 respectively where it was observed that higher number of snapshots presented better resolution with less prominent ambiguous DOAs in the spectrum.

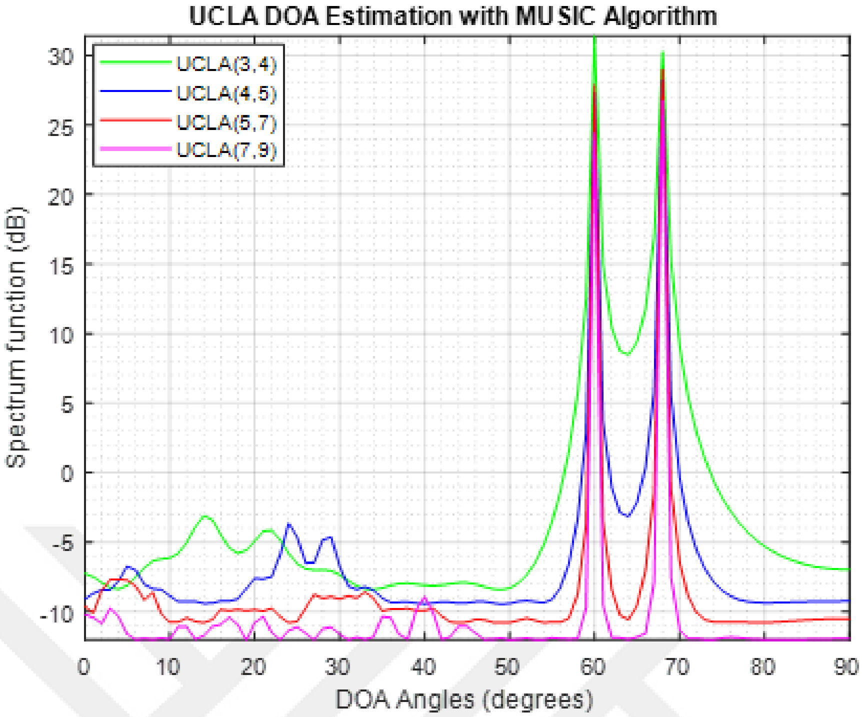

Figure 4.18 UCLA(5,7) DOA estimation for 60^0 & 68^0 for *snapshots* = 100

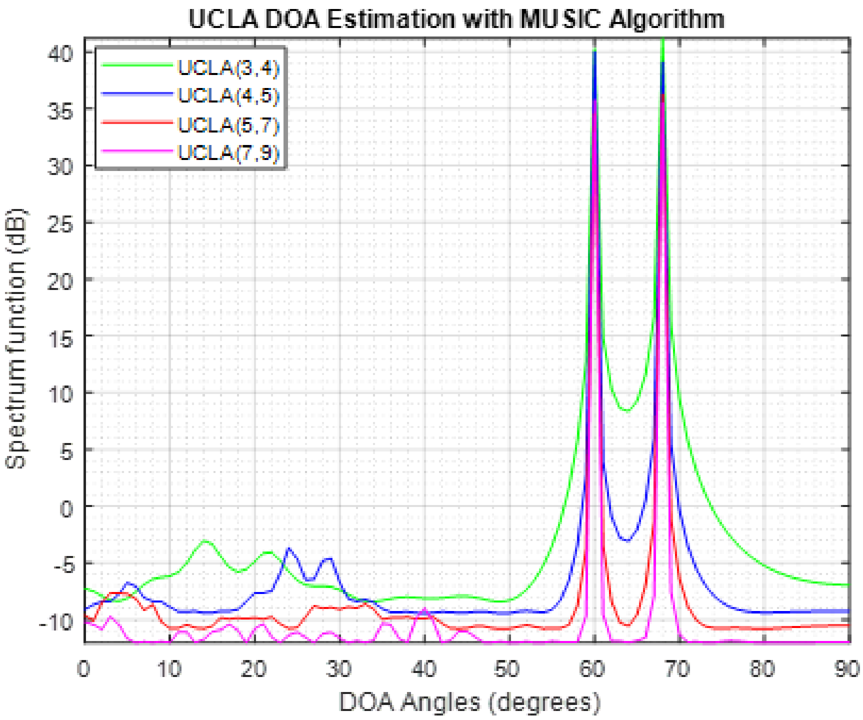

Figure 4.19 UCLA(5,7) DOA estimation for 60^0 & 68^0 for snapshots = 1000

4.3.3 Simulation 3: Error Analysis for UCLA

UCLA performance analysis using root mean square error (RMSE) as the performance metric is considered. As suggested in subsec. 4.2.3, the following formula is adopted for error analysis.

$$RMSE = \frac{1}{L}\left(\frac{1}{K}\sum_{l=1}^{L}\sum_{k=1}^{K}(\hat{\theta}_k^{(l)} - \theta_k)^2\right)^{1/2} \tag{4.2}$$

Where L is the Monte Carlo number of trials conducted, $\hat{\theta}$ is the approximated angle and θ is the actual DOA and K is the number of sources.

RMSE for different UCLA geometries were computed for varying SNR and number of snapshots and their respective graphs plotted as in Figure 4.20 and Figure 4.21 respectively with the former having the number of snapshots held constant at 200, and the latter, SNR was constant at 5. In each instance 1000 Monte-Carlo trials were performed with actual DOA of 60^0. It was established that in both cases, UCLA geometries with higher sensors gave lower errors.

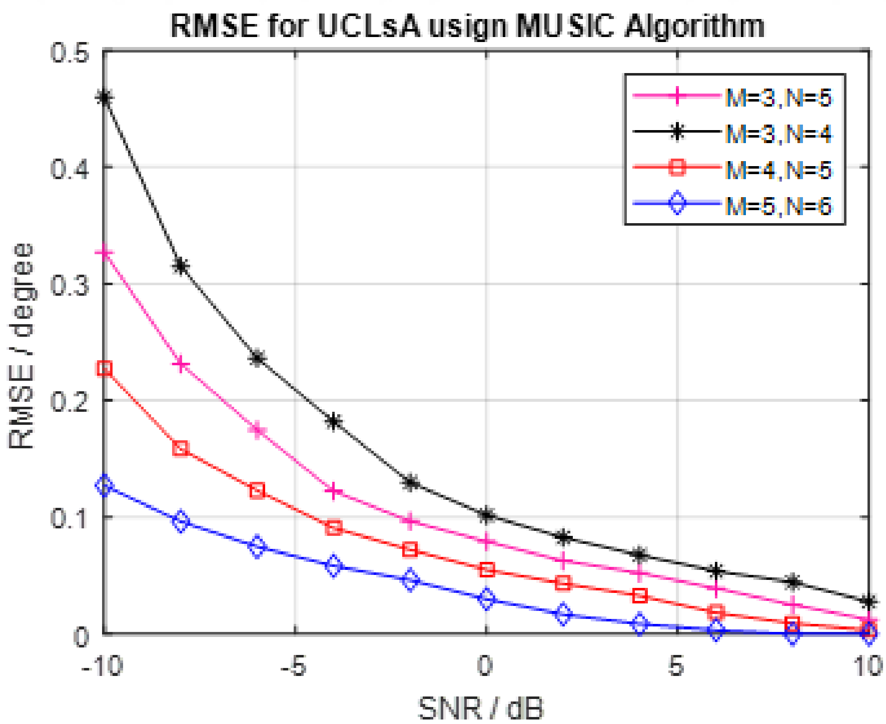

Figure 4.20 Performance of UCLA geometries with varying SNR

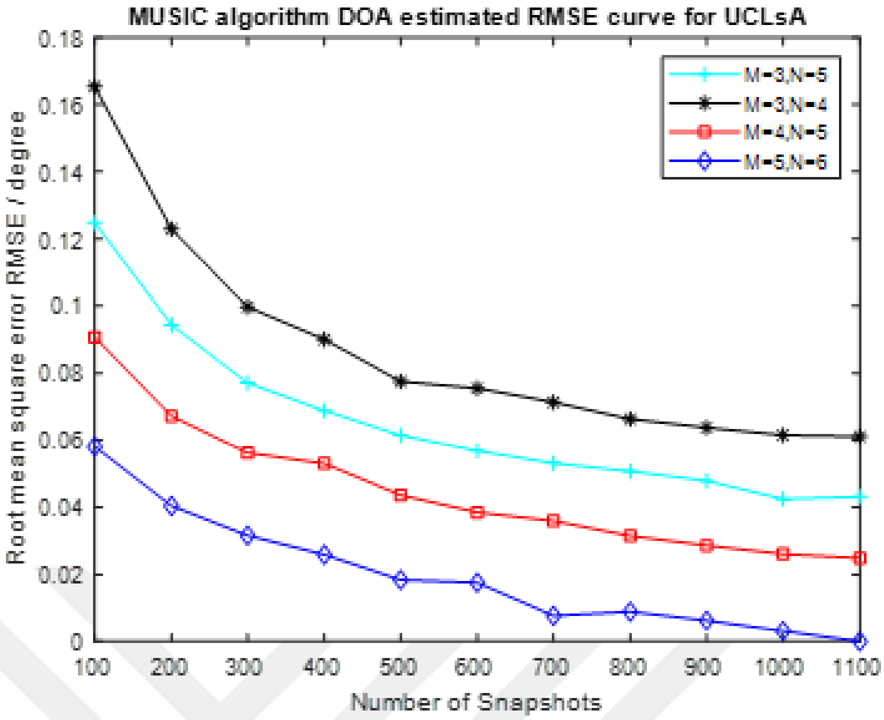

Figure 4.21 Performance of UCLA geometries with varying Snapshots

Additionally, RMSE analysis was conducted for different arrival angles for UCLA geometries at a constant SNR=5 and J = 1024 with 1000 Monte Carlo trials. In Figure 4.22, UCLAs (3,5),(3,4),(4,5) and (5,6) were considered for arrival angle of a span of $(0^0 - 90^0)$ where it was observed that generally, estimating lower angles have low errors and using many sensors also reduces the errors.

4.4 Simulation 4: Performance Comparison between DECOM and UCLA

Performance comparison was conducted using the RMSE as the performance metric for different geometries of DECOM and UCLA which are all 1D methods. In all instances, 1000 Monte-Carlo trials were considered. Figure 4.23 considered varying SNR from $-10 - 10$ in steps of 2 with a constant number of snapshots of $J = 1024$ for actual DOA of 60^0. It was observed that for both DECOM and UCLA, the errors exponentially reduce with increase in SNR. In the same spirit, if the same number of

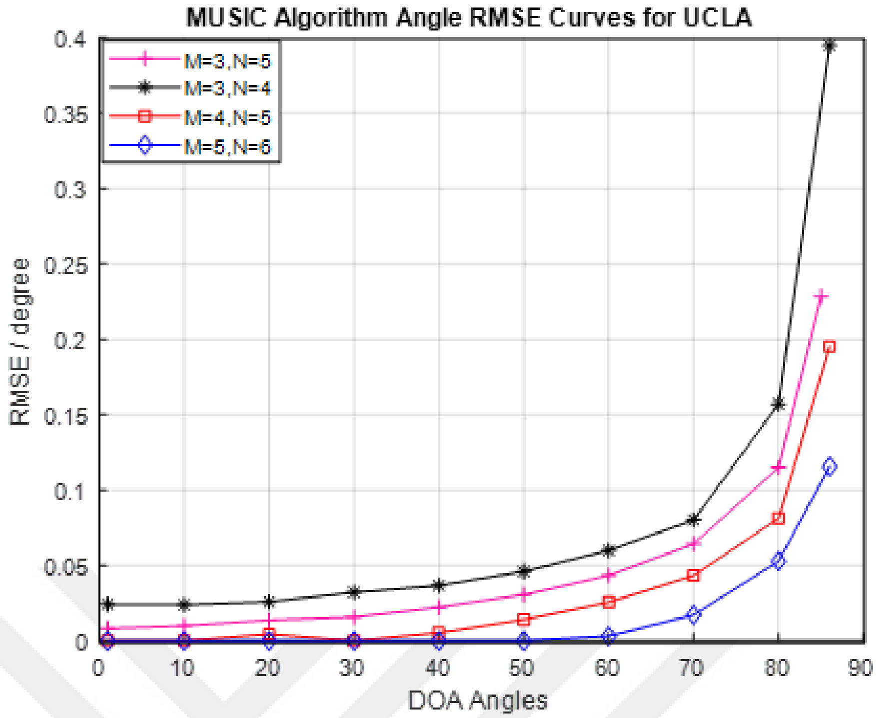

Figure 4.22 Performance analysis for varying arrival angles for UCLA

sensors is considered for both DECOM and UCLA geometries, the latter registered lower errors as opposed to former.

Figure 4.24 shows a repeat of the previous Simulation, this time holding SNR constant at 5 and varying number of snapshots from 100 – 1100 in steps of 100. The results were again observed to favor UCLA as opposed to DECOM. A common observation to both the geometries was that the errors reduce exponentially with increase in number of snapshots but at a slower rate as opposed to varying SNR in the former Simulation.

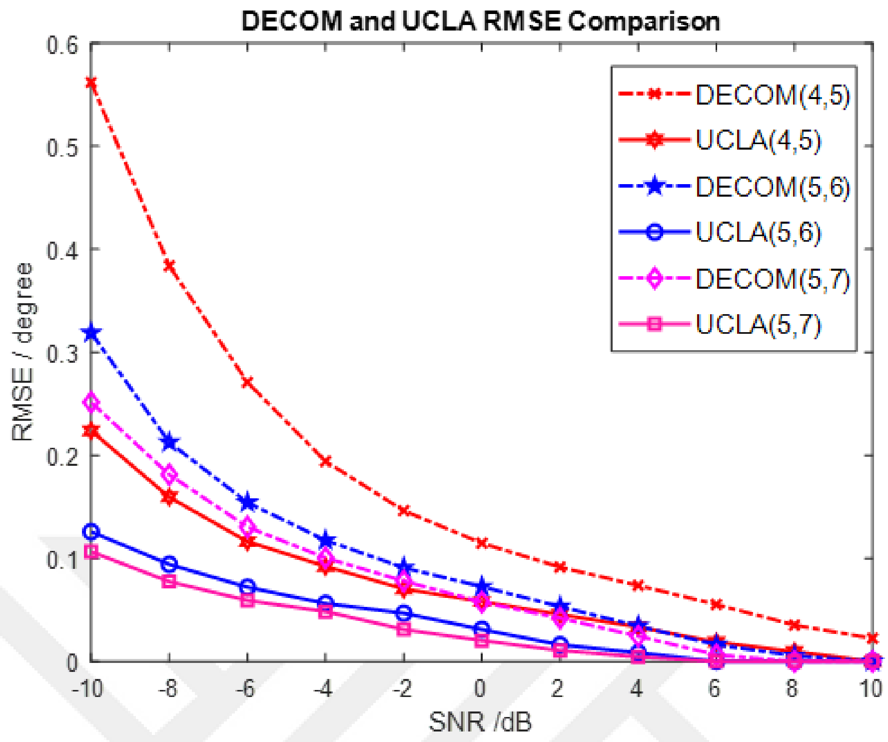

Figure 4.23 Performance comparison for DECOM and UCLA by varying SNR

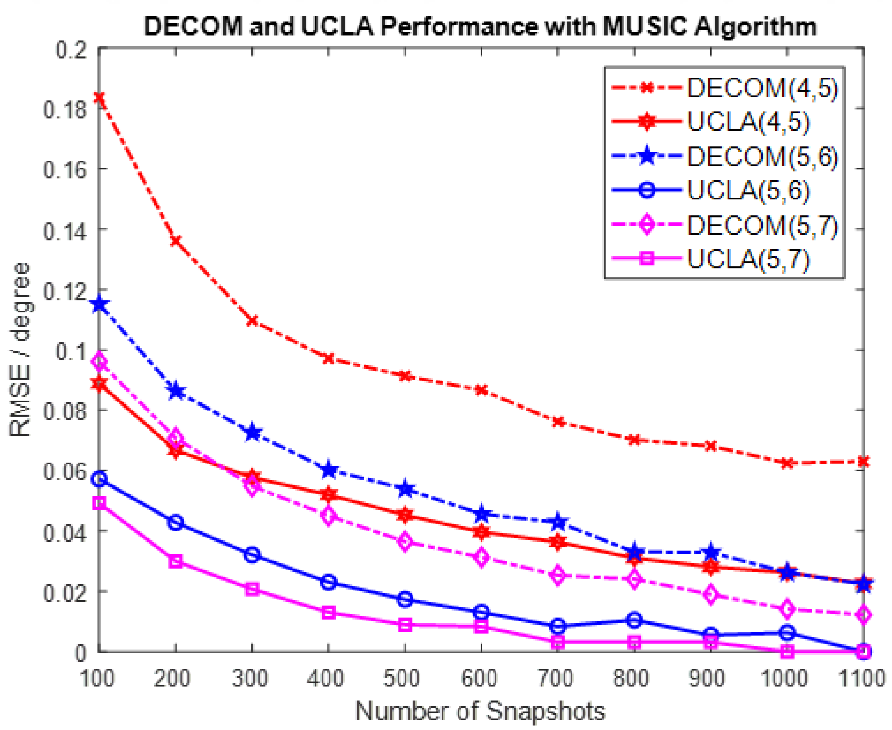

Figure 4.24 Performance comparison between DECOM and UCLA by varying snapshots

It was observed that UCLA geometry registered lower RMSE as opposed to DECOM for all the parameters investigated. It emerged that both the structures' performances increase with increase in number of snapshots and SNR. Furthermore, it was established that in either scenario, a structure with larger number of elements performs better than when the elements are less. In practical scenarios, it is normally a trade-off between the cost and performance function. For instance, although array with many elements would have better performance, it is normally a trade-off between the cost of implementation and the operational complexity that would in return affect the speed.

The performance comparison for the 1D DOA estimation methods using MUSIC algorithm with DECOM and UCLA is summarized in Table 4.1.

Table 4.1 Performance comparison of DECOM and UCLA methods

Parameter	**DECOM**	**UCLA**
Operation	Operates on each sub-array separately thereby losing the intrinsic mutual information of the array.	Utilizes signals from two sub-arrays simultaneously therefore preserving the intrinsic mutual information of the array
Computation Complexity	Computationally intensive since each sub-array is analyzed separately	Less computations involved since the analysis is done simultaneously for all sub-arrays
Angle Pairing	Achieved by combination DOAs of two sub-arrays	Automatic angle-pairing
RMSE	DOAs estimation performed with each sub-array separately. This means lesser elements (half) used in each case leading to higher errors	Very low since two sub-arrays are considered simultaneously leading to estimation with higher number of sensors.
Performance	Associated with ambiguous DOAs due to the inter-sensor spacing of greater than half-wavelength	Achieves very high resolution with suppressed ambiguous DOAs
Signal detection	Can detect sources of $K \leq \frac{1}{2}MN$ with only $M+N-1$ sensor elements	Can detect sources of $K \leq \frac{1}{2}MN$ with only $M+N-1$ sensor elements

4.5 Simulations Results for CLSA Using MUSIC Algorithm

Simulations were carried out to evaluate the performance of CLSA using both MUSIC and MUISC-like low complexity algorithms with respect to varying environmental and array structural parameters. The power pseudo-spectra maxima plots are used as pointers for the estimated DOAs and further RMSE evaluated between estimated and the actual DOA values.

4.5.1 Simulation 1: Estimation of Single DOA with CLSA

In this Simulation CLSA(4,5) is considered for SNR=5 and number of snapshots of J=200. actual DOA under consideration is $(\theta,\phi) = (60^0,60^0)$. Figure 4.25 shows the spectral peak for sub-array 1 of M elements which shows a successful 2D DOA estimation with no ambiguous angles.

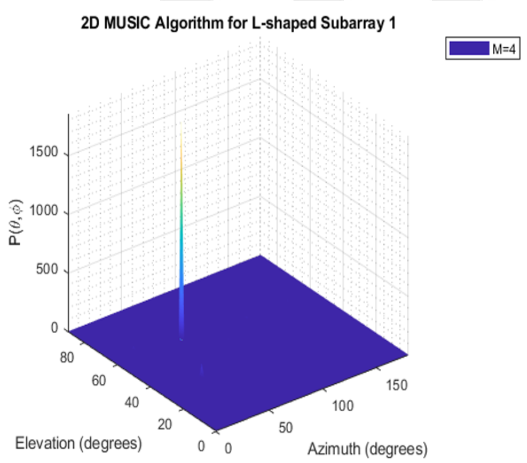

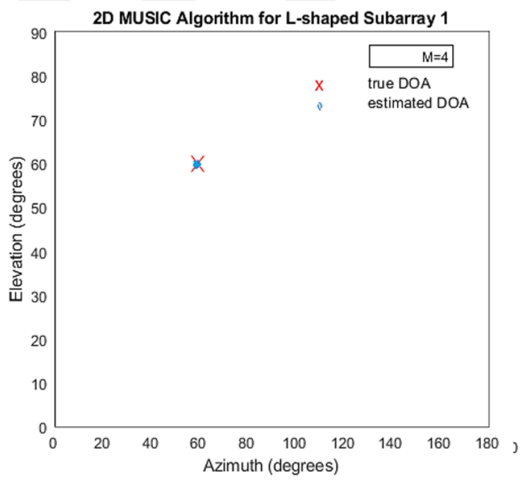

Figure 4.25 CLSA(4,5) sub-array 1 spectral peak for $(\theta,\phi) = (60^0,60^0)$

Consequently, Figure 4.26 shows the plot for the second sub-array representing the number of elements $N = 5$. It is again observed that the sub-array ia able to estimate the DOA, with no ambiguities just as the first sub-array.

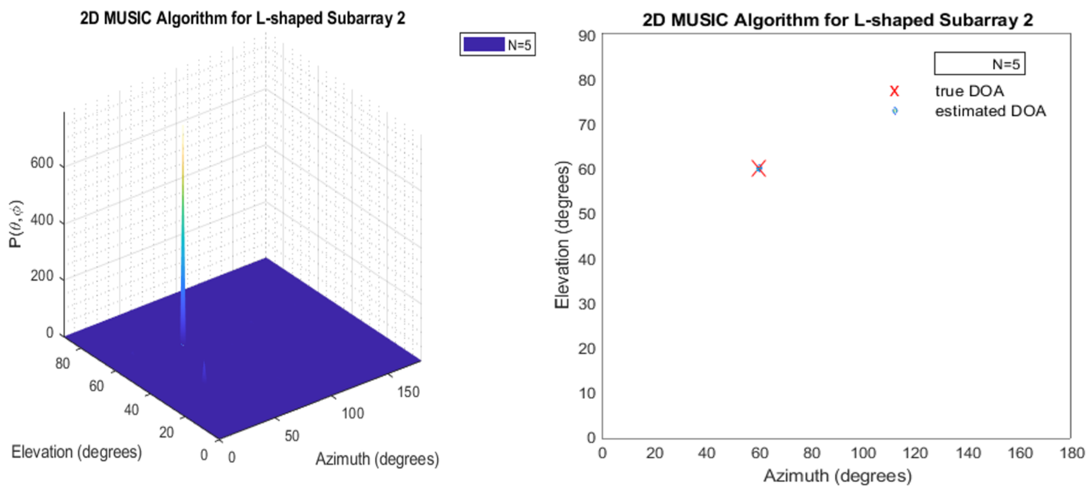

Figure 4.26 CLSA(4,5) sub-array 2 spectral peak for $(\theta,\phi) = (60^0, 60^0)$

4.5.2 *Simulation 2: Estimation of Multiple DOAs with CLSA*

Three close sources of elevation angles, $\theta = [60^0,\ 64^0,\ 68^0]$ and azimuth angles, $\phi = [60^0,\ 64^0,\ 68^0]$ were estimated using CLSA(4,5) with the snapshot number of $J = 200$ and $SNR = 5$. Figure 4.27 (a) & (b) represents the spectral peaks for sub-arrays 1 and 2 respectively. It was observed that in estimation of multiple DOAs, there were emergent of ambiguous angles. Sub-array 1 which estimates with lesser number of elements is seen to have very prominent ambiguous DOAs than sub-array 2 which has higher elements than the former by 1.

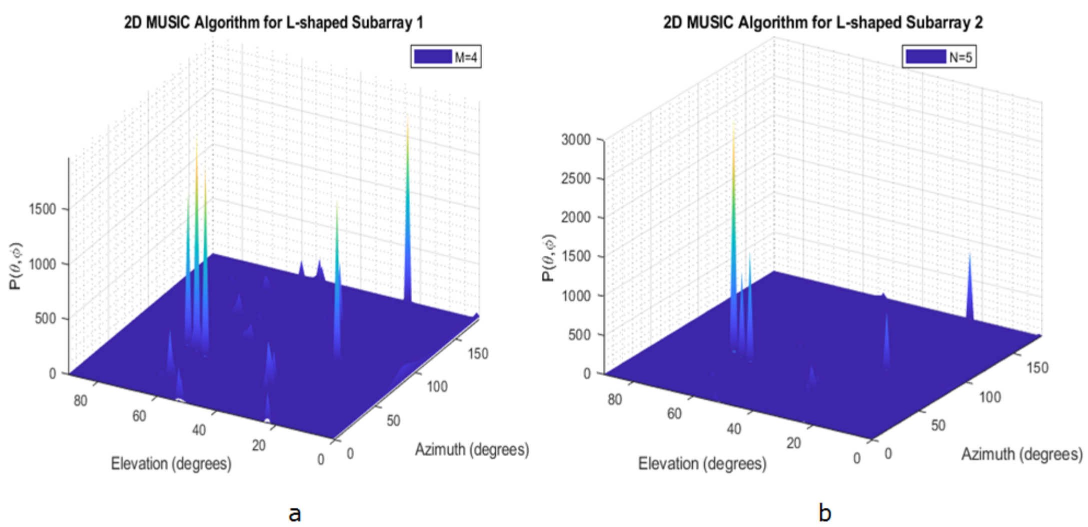

Figure 4.27 Multiple DOA estimation with CLSA(4,5)

Further, CLSA(9,11) is used to estimate 11 sources as shown in Figure 4.28. It was established that in both scenarios, all the sources were estimated correctly, however; the estimation resolution when the sensors are less than sources was seen to be lower and with many ambiguous DOAs as in (a) as opposed to when the number of sensors is equal to sources as in (b).

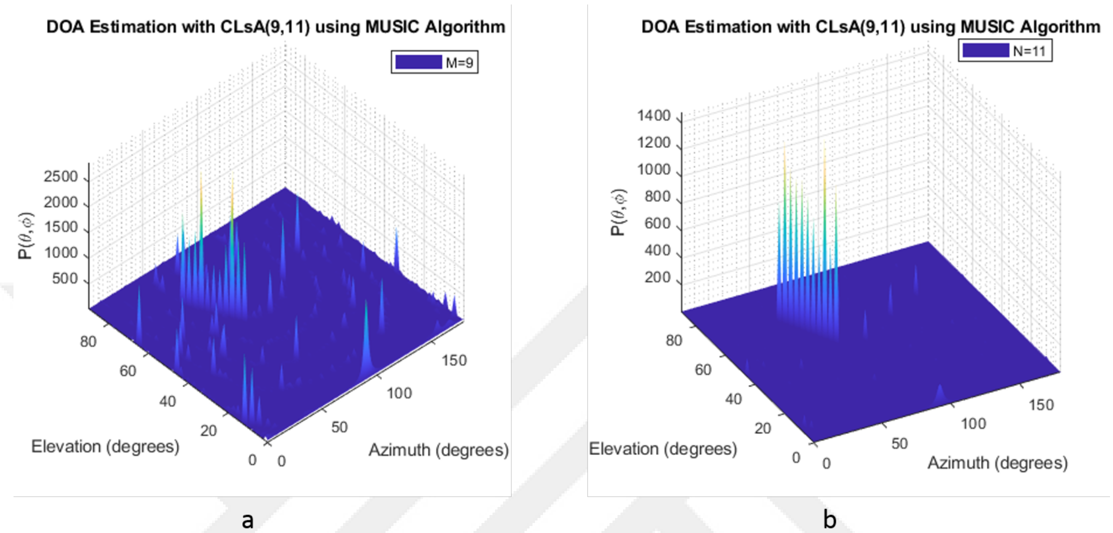

Figure 4.28 Multiple DOA estimation with CLSA(9,11)

4.5.3 Simulation 3: CLSA Performance Analysis

For the performance analysis of 2D CLSA method using MUSIC algorithm, RMSE is used as the performance metric. Further, since the conventional 2D method is computationally complex, a MUSIC-like low complexity method is adopted which transforms the 2D problem to 1D.

A single DOA is considered in CLSA(4,5) with $SNR = 5$ and snapshots, $J = 200$. The actual DOA chosen was $(\theta, \phi) = (60^0, 60^0)$. Figure 4.29 & 4.30 represents gamma and beta peak searches respectively. It was observed that in each plots there emerged several unpaired ambiguous peaks but with only one paired peak for the two plots in each graph respectively. The matching peak values are the ones considered since they are the ones that represent the actual DOAs under estimation.

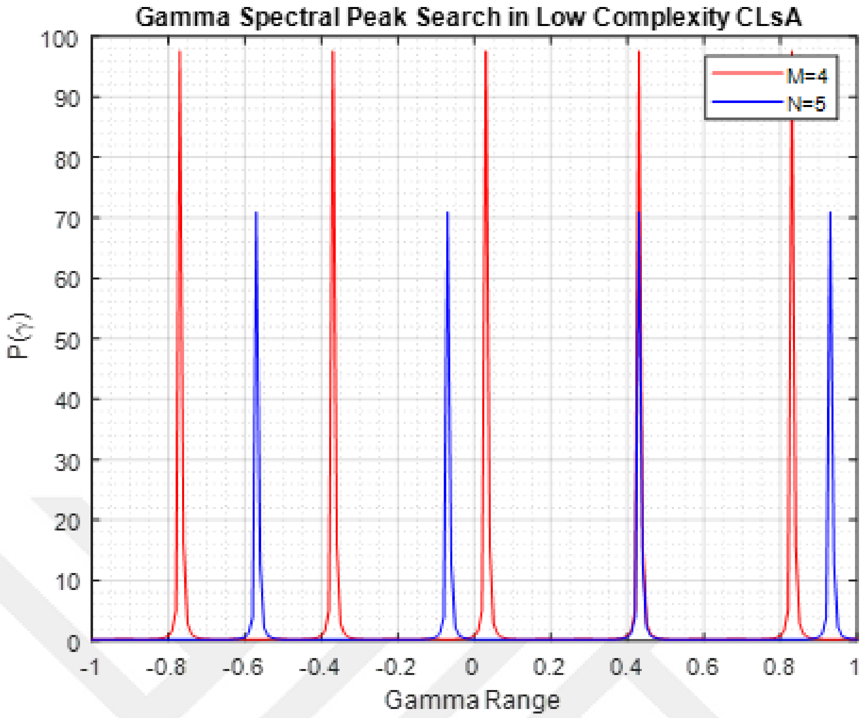

Figure 4.29 Estimation of transformation parameters gamma and beta

The values of gamma and beta was then used to calculate the estimated elevation and azimuth angles for which RMSE was calculated using the formula

$$RMSE = \left(\frac{1}{L} \sum_{l=1}^{L} \frac{1}{K} \sum_{k=1}^{K} [(\hat{\theta}_k^{(l)} - \theta_k)^2 + (\hat{\phi}_k^{(l)} - \phi_k)^2] \right)^{1/2} \quad (4.3)$$

Where K represents the number of sources, L represents the number of independent Monte-Carlo trials and $\hat{\theta}_k^{(l)}$ and $\hat{\emptyset}_k^{(l)}$ are the estimated elevation, θ_k and azimuth, $\emptyset_k$ angles respectively in the lth Monte-Carlo Simulation.

For the above single trial, the RMSE for each sub-array may be calculated as

$$\text{sub-array 1: Est. theta}, \hat{\theta} = 60.7459 \text{ \& Est.phi}, \hat{\phi} = 60.3203 \quad RMSE_M = 0.8117 \quad (4.4a)$$

$$\text{sub-array 2: Est. theta}, \hat{\theta} = 60.1410 \text{ \& Est.phi}, \hat{\phi} = 60.1240 \quad RMSE_N = 0.1878 \quad (4.4b)$$

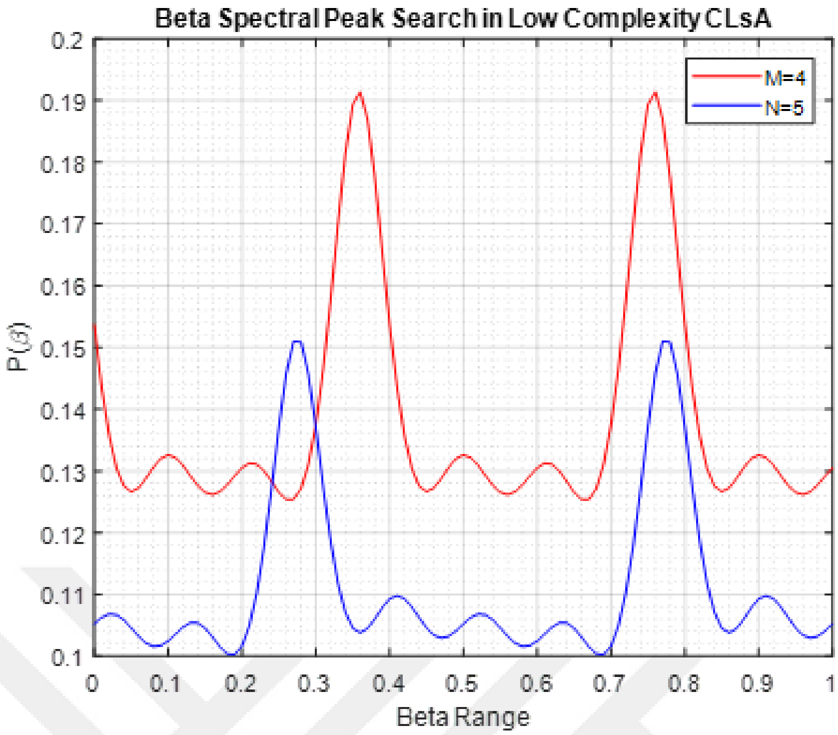

Figure 4.30 Estimation of transformation parameters gamma and beta

4.6 Simulation Results for 2D DOA Estimation Using UCLSA

Simulations were carried out to evaluate the performance of CLSA using both MUSIC and MUISC-like low complexity algorithms with respect to varying environmental and array structural parameters. The power pseudo-spectra maxima plots are used as pointers for the estimated DOAs and further RMSE evaluated between estimated and the actual DOA values.

4.6.1 Simulation 1: Single DOA Estimation with UCLSA

A single DOA estimation was performed for UCLSA(4,5) for actual DOA of elevation and azimuth angles, $(\theta,\phi) = (60^0, 60^0)$ respectively where the number of snapshots was chosen as, $J = 200$, and $SNR = 5$. In Figure 4.31, it was observed that UCLSA with MUSIC algorithm managed to estimate with high accuracy a single DOA with totally no ambiguous peaks.

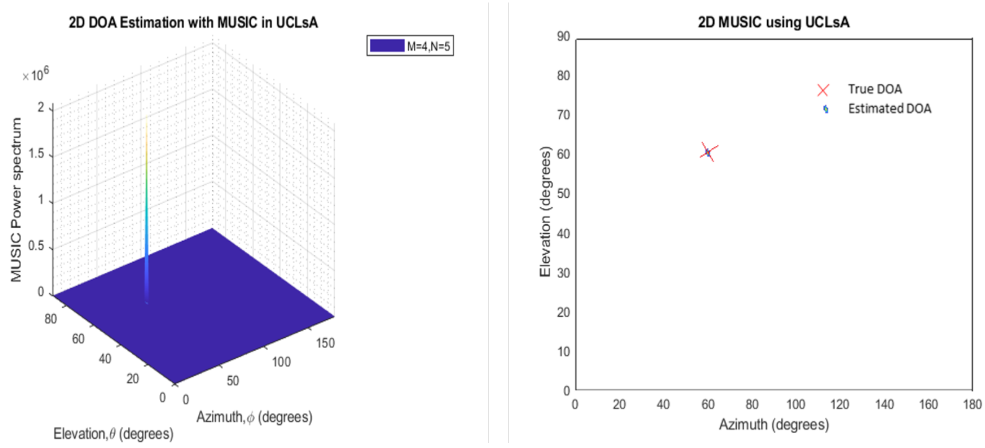

Figure 4.31 UCLSA(4,5) estimation of a single DOA

Further, the above Simulation was repeated for different number of sensors and Figure 4.32 (a) and (b) was generated which showed that if the elements are very few, there is a conspicuous ambiguous DOA which disappears with increase in number of sensors.

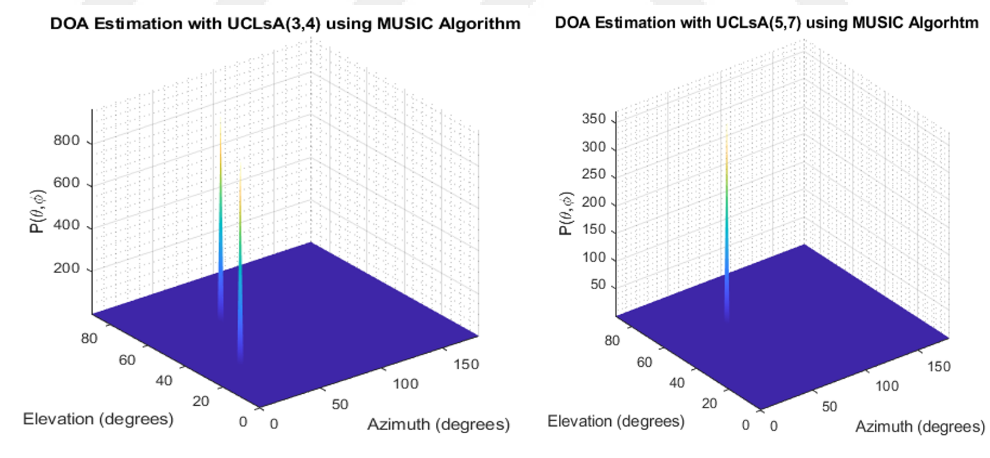

a b

Figure 4.32 Signle DOAs estimation using UCLSA

4.6.2 *Simulation 2: Multiple Sources Estimation with UCLSA(4,5)*

Figure 4.33 shows the spectral peaks when UCLSA(4,5) was used for estimating five sources having a separation angles of less than 3^0. the elevations and azimuth angles were set at $(\theta, \phi) = \{[60^0;\ 62^0;\ 65^0;\ 67^0;\ 70^0], [60^0;\ 62^0;\ 65^0;\ 67^0;\ 70^0]\}$ for $J = 200$ and $SNR = 5$. It was observed that all the five sources were estimated with high accuracy and no ambiguous DOAs appearing.

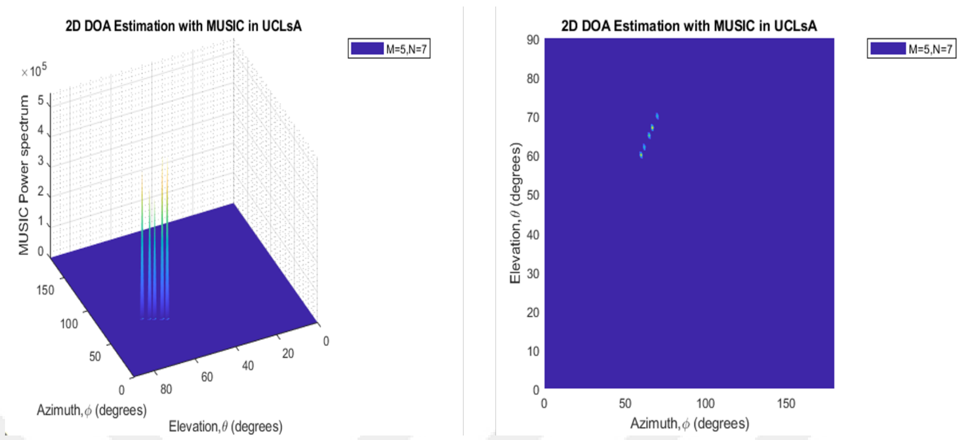

Figure 4.33 Multiple Sources estimation using UCLSA

In the same spirit, the above Simulation was repeated for 11 sources and varying the number of sensors from 9 to 16. Figure 4.34 (a) and (b) showed that in both cases, the sources were successfully identified, however; when the number of sensors are less than that of the sources, the resolution is very low as in Figure 4.34 (a). Increasing the number of sensors to surpass that of the sources increases resolution and reduces the estimation errors as evident in Figure 4.34 (b).

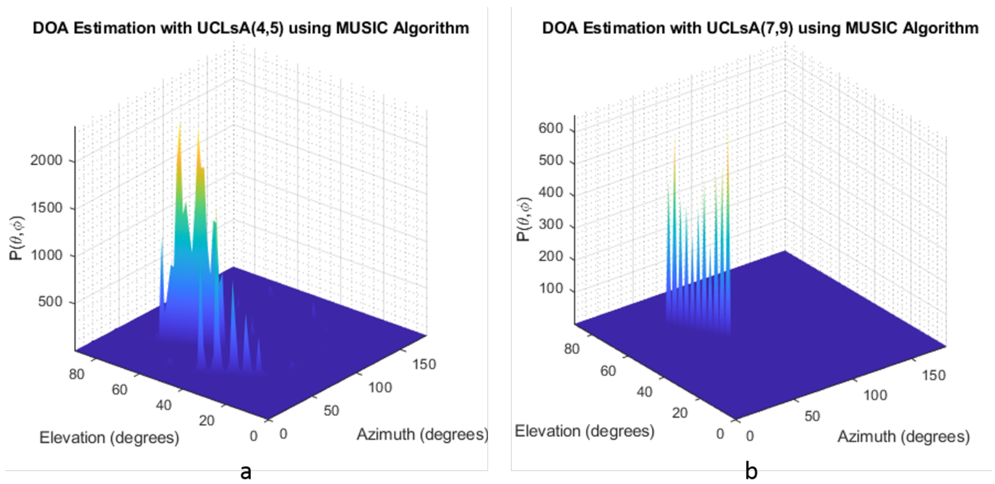

Figure 4.34 Estimation of multiple DOAs using UCLSA

4.6.3 Simulation 3: UCLSA Performance Analysis

As previously indicated in the CLSA geometry performance analysis, UCLSA performance analysis followed the same method as described for CLSA, where the RMSE was used as performance metric where the low computational complexity MUSIC-like method was employed that transforms the 2D problem to 1D.

A single DOA was considered for UCLSA(4,5) choosing the other parameters as; $SNR = 5$ and snapshots, $J = 200$ and actual DOA, $(\theta, \phi) = (60^0, 60^0)$. Figure 4.35 & 4.36 represents gamma and beta peak spectra respectively. It was observed that the gamma was estimated with very sharp single peak and no any other ambiguous peaks appearing while for beta, it was also estimated with a fairly sharp peak.

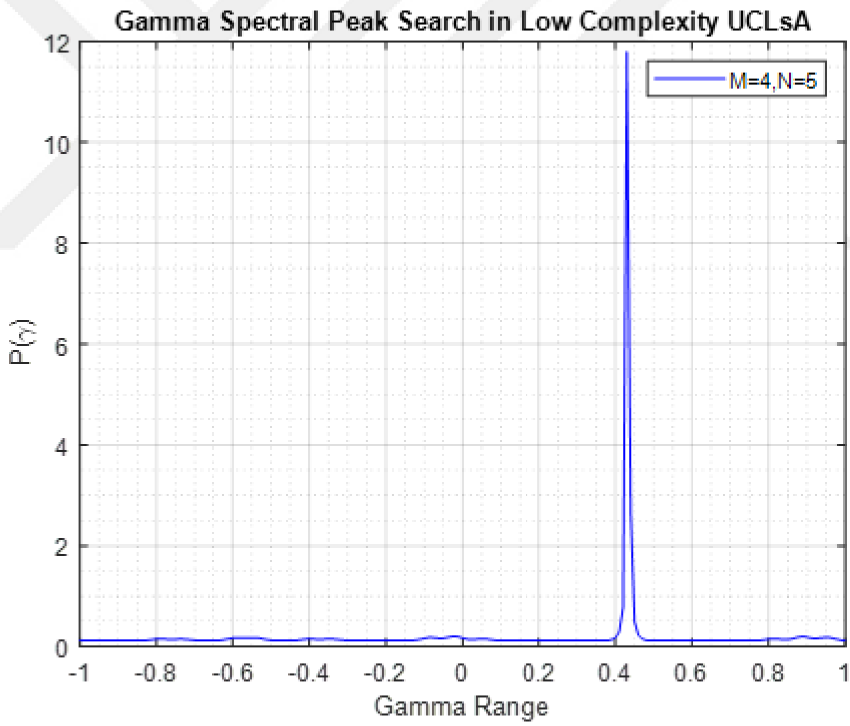

Figure 4.35 Gamma spectral search plot for UCLSA(4,5)

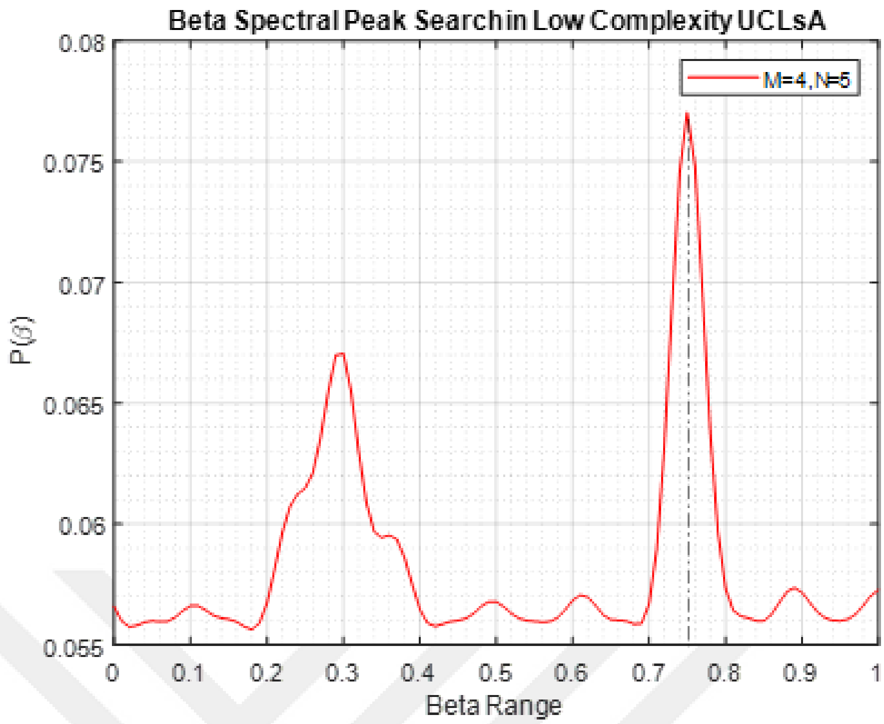

Figure 4.36 Beta spectral search plot for UCLSA(4,5)

4.7 Simulation 4: Performance Comparison between CLSA and UCLSA

RMSE was used as a performance metric for the 2D DOA estimations. The low complexity MUSIC-like method together with the 2D RMSE formula in Equation (4.3) was applied for 50 Monte-Carlo trials in two scenarios: First for varying SNR value from -10 to 10 in steps of 5 while holding all other parameters constant for number of snapshots of 200 and sensor elements of 9. In the second simulation, all other parameters were held constant as in the previous simulation but varying number of snapshots from 100 to 600 in steps of 100 with SNR of 5.

Figures 4.37 and 4.38 shows the plots for varying SNR and number of snapshots respectively where it is observed that generally, increase in SNR and number of snapshots leads to reduction in errors. Moreover, UCLSA has lower angle errors compared to CLSA.

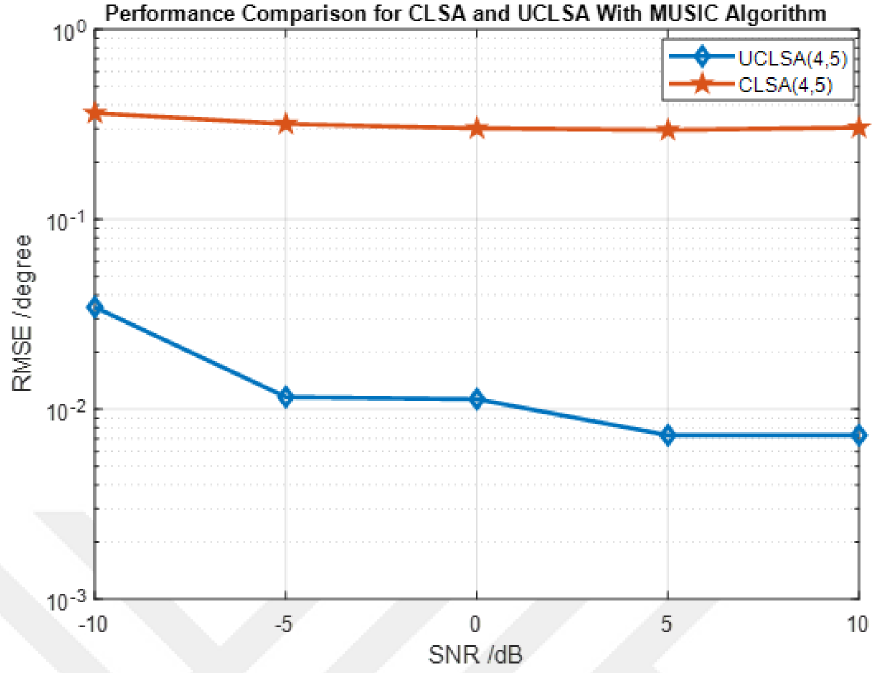

Figure 4.37 RMSE for varying SNR in CLSA(4,5) and UCLSA(4,5)

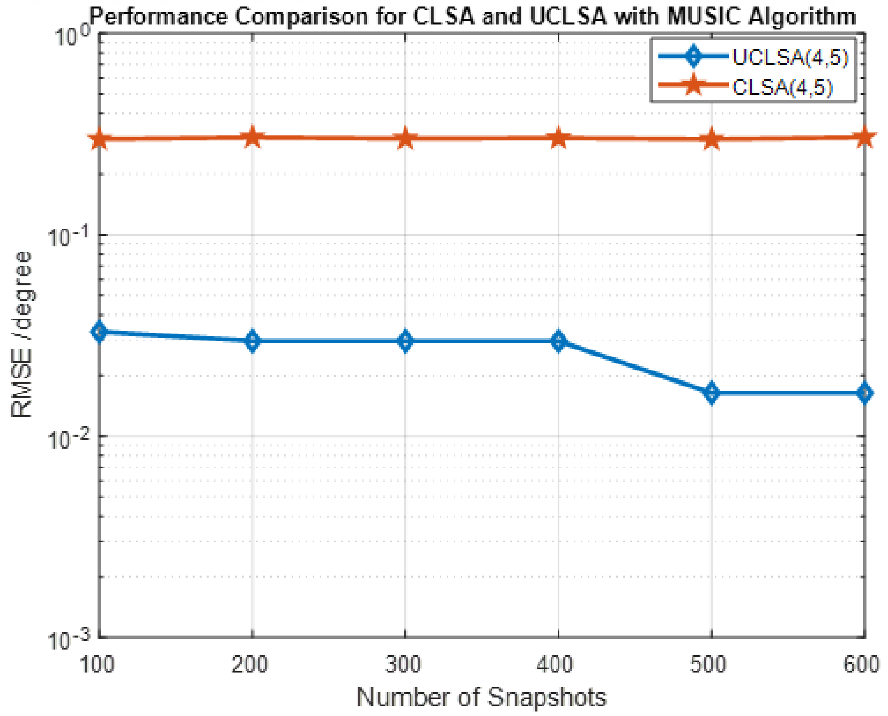

Figure 4.38 RMSE for Varying Number of Snapshots in CLSA(4,5) & UCLSA(4,5)

The performance of the 2D DOA estimation methods is summarized in Table 4.2.

Table 4.2 Performance comparison of CLSA and UCLSA

Parameter	**CLSA**	**UCLSA**
Realization	Operates on each sub-array separately leading to lose of intrinsic mutual information of the array.	Utilizes the signals from all the sub-arrays simultaneously thereby preserving the intrinsic mutual information of the array
Computation Complexity	Computationally intensive since each sub-array is analyzed separately	Lesser computations involved since total signals from all sub-arrays is used simultaneously
Angles Pairing	Achieved by manually combining DOAs of two sub-arrays	Actualised automatically
RMSE	Higher errors since each sub-array is analyzed separately thus the estimator 'sees' less number of sensors	Low errors since all the sensors are considered simultaneously.
Performance	Associated with ambiguous DOAs due to the inter-sensor spacing being greater than half-wavelength	Higher resolution possible with suppressed ambiguous DOAs
Signal detection	Detects sources of $K \leq \frac{1}{2}MN$ with only $2M+2N-3$ sensors	Detects sources of $K \leq \frac{1}{2}MN$ with only $2M+2N-3$ sensors

4.8 Simulation Results for Virtual Array Interpolation Method

Simulations were carried out to evaluate the performance of arrays with interpolated elements using both co-array MUSIC algorithm with respect to varying environmental and array structural parameters. The power pseudo-spectra maxima plots are used as pointers for the estimated DOAs and further RMSE evaluated between estimated and the actual DOA values.

4.8.1 Simulation 1: Comparison of Non-augmented & Augmented co-arrays

Coprime array with elements ($M = 2; N = 5$), alternatively known as Coprime(2,5), was used for this Simulation. First, the contiguous ULA of the difference co-array was used to generate the covariance matrix $\boldsymbol{R}_{\mathbb{UU}}$ and in another instance, the interpolation of virtual array performed to fill the holes in the original difference co-array as a way of utilizing the entire DOF of the array and used to generate covariannce matrix $\boldsymbol{R}_{\mathbb{VV}}$. The 10 actual DOAs to be resolved were equally spaced between the linespace $-0.45to0.45$ in the normalised scale of $\sin(\theta)$. Further, the number of snapshots was chosen as, $J = 200$, and $SNR = 5$. As show in Figure 4.39 and Figure 4.40, it was observed that in both the instances, all the sources were resolved successfully.

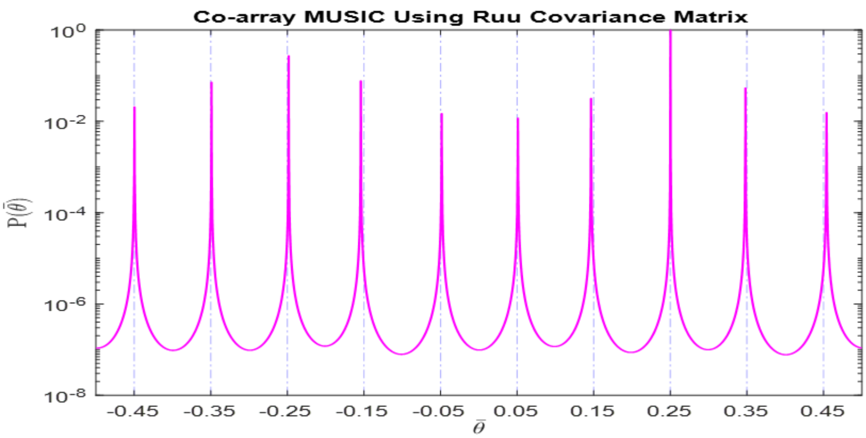

Figure 4.39 DOA Estimation with $\boldsymbol{R}_{\mathbb{UU}}$ co-array MUSIC for 10 sources

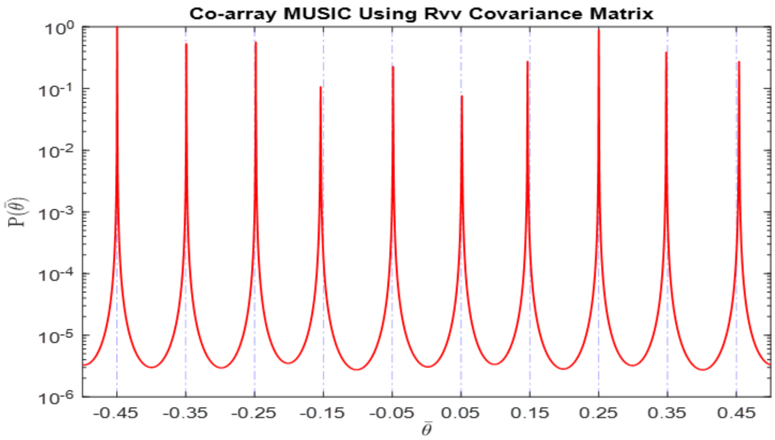

Figure 4.40 DOA Estimation with $\boldsymbol{R}_{\mathbb{VV}}$ co-array MUSIC for 10 sources

The above Simulation was repeated by increasing the number of sources to $2MN - N = 15$ which is the maximum number that can be resolved by the cardinal set $\mathbb{V}$.

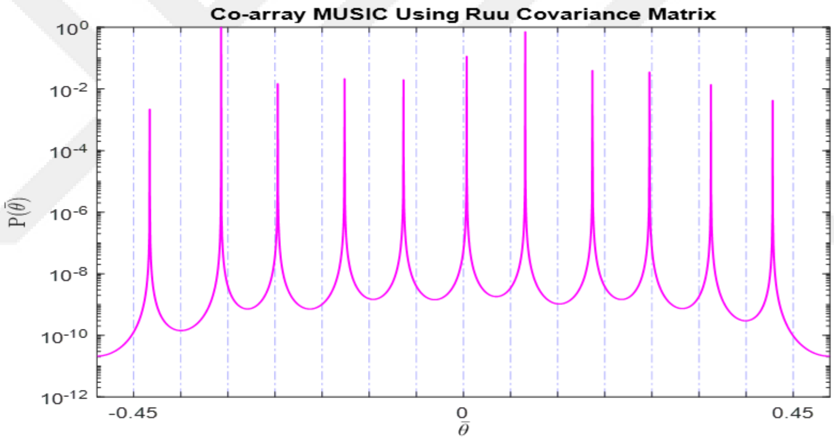

Figure 4.41 DOA Estimation with $\boldsymbol{R}_{\mathbb{UU}}$ co-array MUSIC for 15 sources

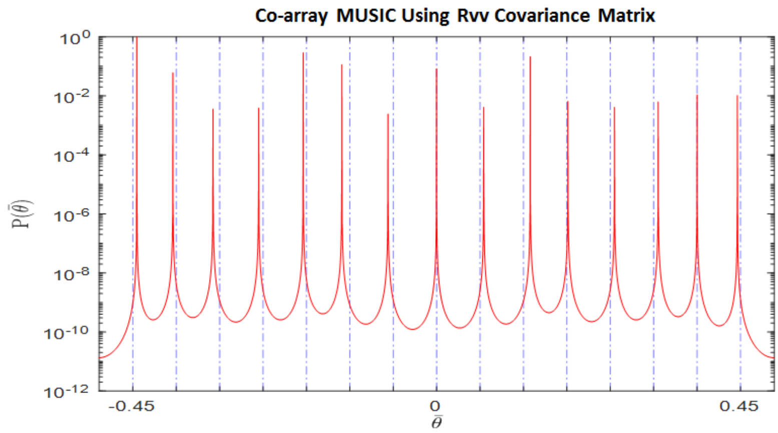

Figure 4.42 DOA Estimation with $\boldsymbol{R}_{\mathbb{VV}}$ co-array MUSIC for 15 sources

As illustrated in Figure 4.41 and Figure 4.42 respectively, the contiguous ULA covariance matrix data represented by $\boldsymbol{R}_{\mathbb{UU}}$ was only able to resolve 11 sources whereas the filled (interpolated) virtual difference co-array covariance matrix data $\boldsymbol{R}_{\mathbb{VV}}$ resolved all the 15 sources successfully.

In another instance, 10 sources were placed with an asymmetric distances of separation. Coprime(4,5) was used to resolve the sources for number of snapshots and SNR of 200 and 5 respectively. Figure 4.43 and 4.44 represents the outputs for the contiguous ULA and interpolated co-array matrix data respectively. In both cases, the sources were resolved successfully.

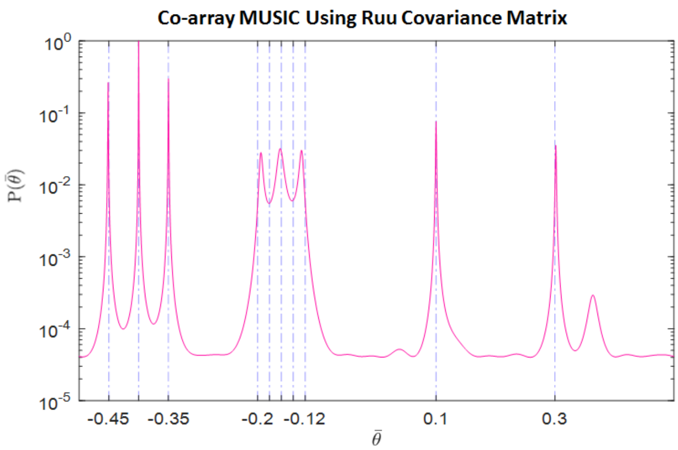

Figure 4.43 DOA Estimation of Asymmetrically placed Sources for Coprime(4,5) Using $\boldsymbol{R}_{\mathbb{UU}}$ co-array

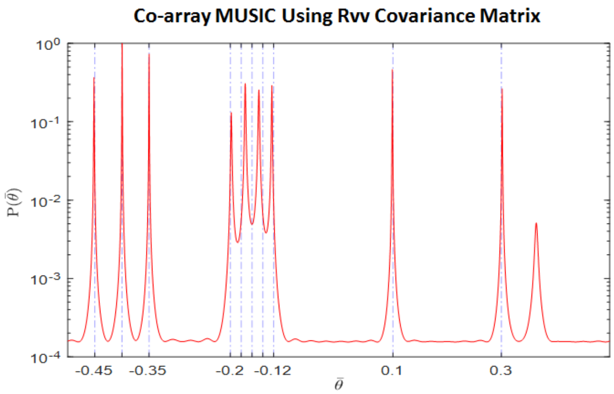

Figure 4.44 DOA Estimation of Asymmetrically placed Sources for Coprime(4,5) Using $\boldsymbol{R}_{\mathbb{VV}}$ co-array

4.8.2 Simulation 2: DOA Estimation with Selected Interpolated Arrays

For the first part of this Simulation, sensor elements of the coprime array were set as M = 3 and N = 5 and sources = 15 while keeping the other parameters constant as in Simulation 1 above. Figure 4.45 shows the output where it is observed that the estimator resolved all the 15 sources successfully.

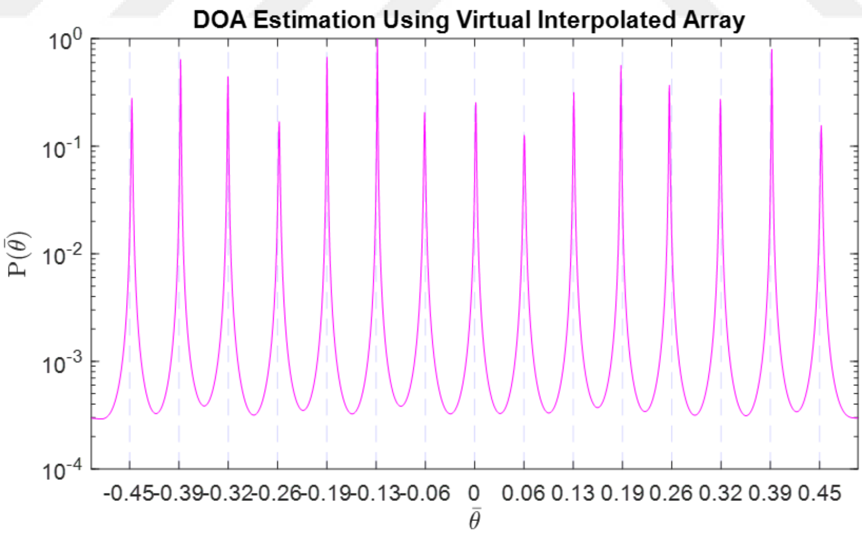

Figure 4.45 DOA Estimation with Coprime(3,5) $\boldsymbol{R}_{\mathbb{VV}}$ co-array MUSIC for 15 sources

Consequently, in the second part of the Simulation, the coprime elements were set as M = 4 and N = 5 and sources = 20 with the other parameters remaining constant. Figure 4.46 shows the output where it was observed that the estimator resolved all the

20 sources successfully.

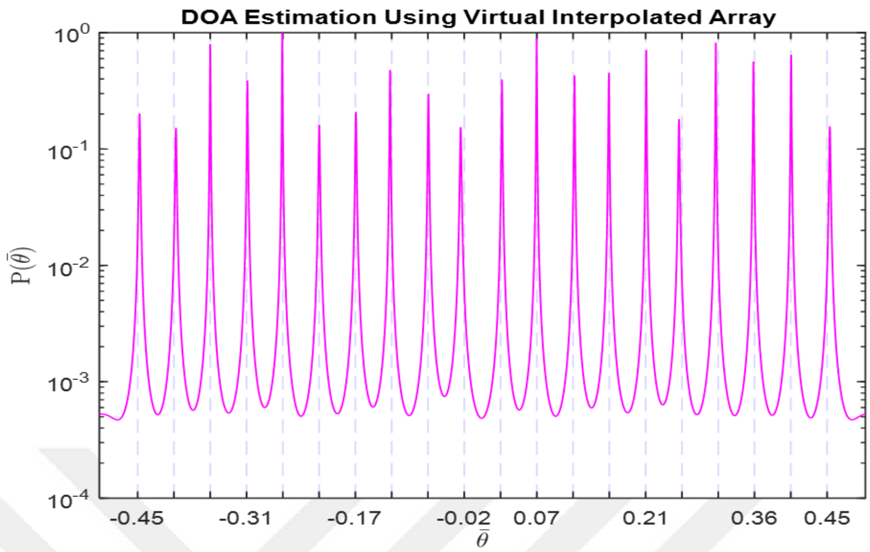

Figure 4.46 DOA Estimation with Coprime(4,5) $\boldsymbol{R}_{\mathbb{VV}}$ co-array MUSIC for 20 sources

4.9 Simulation 3: Performance Evaluation of Interpolated Coprime Arrays

RMSE was calculated as the performance metric for the virtual interpolated array. In the first instance, the number of snapshots were held constant at 200 and SNR varied from -5 to 15 in steps of 5. The two sparse array geometries taken as a representation were coprime(2,5) and coprime(4,5). The sources were set to 10 and 20 for Coprime(2,5) and Coprime(4,5) respectively.

Tables 4.3 & 4.4 show the RMSE values for 10 Monte Carlo runs for each geometry respectively.

Table 4.3 RMSE vs SNR for Interpolated Co-array MUSIC Algorithm Using Coprime(2,5)

	SNR				
Trial	-5	0	5	10	15
1	0.0027395	0.0030299	0.0014785	0.0015638	0.0018356
2	0.0030653	0.0027353	0.0007943	0.0018452	0.0014103
3	0.0030717	0.0020172	0.0025201	0.0018939	0.0019134
4	0.0028915	0.0021420	0.0020907	0.0019924	0.0009914
5	0.0031855	0.0027389	0.0024767	0.0019022	0.0014484
6	0.0029133	0.0024731	0.0015091	0.0019821	0.0015883
7	0.0032205	0.0017158	0.0021594	0.0022299	0.0015482
8	0.0026893	0.0024716	0.0024954	0.0026428	0.0012206
9	0.0031252	0.0030156	0.0016349	0.0009521	0.0018446
10	0.0029449	0.0016085	0.0020388	0.001312	0.0015937
Avg.	0.0029847	0.0023948	0.00191979	0.0018316	0.0015395

Table 4.4 RMSE vs SNR for Interpolated Co-array MUSIC Algorithm Using Coprime(4,5)

	SNR				
Trial	-5	0	5	10	15
1	0.0017773	0.0016619	0.0011668	0.0014724	0.0014753
2	0.0014627	0.0016785	0.0015005	0.0016766	0.0014103
3	0.0021342	0.0015729	0.001408	0.0015418	0.0014923
4	0.0018558	0.0017105	0.0015645	0.001684	0.0011956
5	0.0023968	0.0016255	0.0016359	0.0014352	0.0013147
6	0.0023854	0.0015698	0.0016619	0.0013715	0.0014415
7	0.0020491	0.0012843	0.0013831	0.0011483	0.0013795
8	0.0019083	0.0018868	0.0016006	0.001421	0.001598
9	0.0016101	0.0017974	0.0015887	0.0016738	0.0011234
10	0.0018008	0.001738	0.0017118	0.0014529	0.0012285
Avg.	0.0019381	0.001653	0.0015222	0.0014878	0.0013659

Different RMSE curves for DECOM, UCLA and interpolated array were plotted in the same plane at same operating parameters for performance comparison as shown in Figure 4.47.

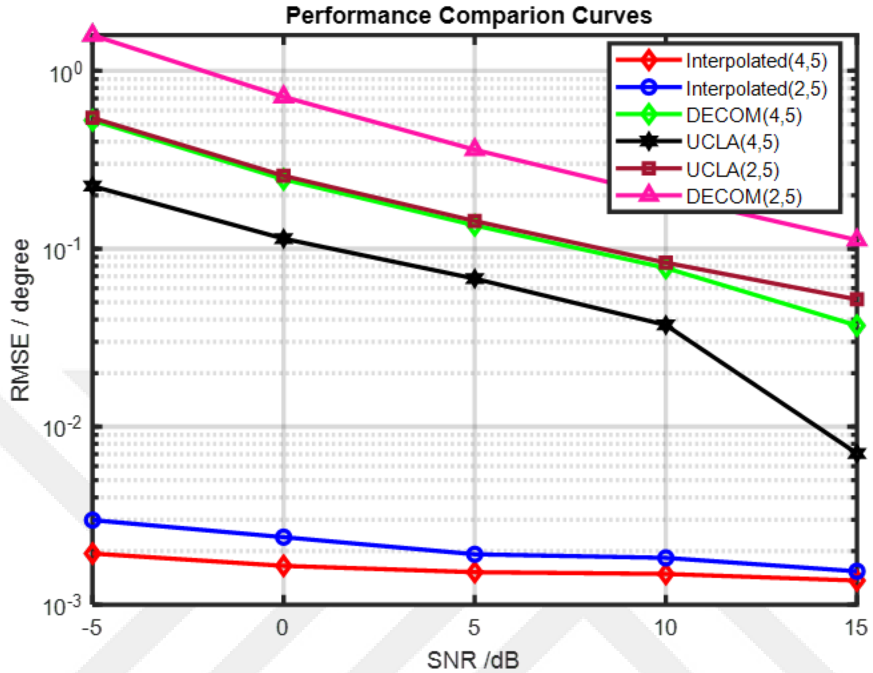

Figure 4.47 RMSE for varying SNR in DOA Estimation Using DECOM, UCLA & Interpolated Arrays

The following observations and inferences were made:

a. Increase in SNR reduces the RMSE.

b. Increasing the number of sensors increases the number of resolvable sources and at the same time improves the overall performance.

c. Interpolated array registered the lowest RMSE followed by UCLA and lastly DECOM that registered the highest RMSE values.

Consequently, the number of snapshots was varied from 100 to 600 in steps of 100 while keeping SNR constant at 5 and all the other parameters unchanged as in the case for varying SNR. Tables 4.5 & 4.6 shows the generated RMSE for Coprime(2,5) and Coprime(4,5) respectively for 10 Monte-Carlo trails.

Table 4.5 RMSE vs Snapshots for Interpolated Co-array MUSIC Algorithm Using Coprime(2,5)

	Number of Snapshots					
Trial	100	200	300	400	500	600
1	0.003419	0.001479	0.001914	0.001131	0.001063	0.001176
2	0.003023	0.0007943	0.001472	0.00141	0.001227	0.0007542
3	0.003328	0.002520	0.002167	0.001383	0.001264	0.001279
4	0.002621	0.002091	0.001416	0.001214	0.001091	0.0005663
5	0.002662	0.002477	0.0008064	0.001278	0.001418	0.0005875
6	0.002479	0.001509	0.001906	0.001153	0.001497	0.001163
7	0.002788	0.002159	0.001318	0.001468	0.001055	0.0007306
8	0.002081	0.002495	0.001613	0.0009972	0.0008209	0.001100
9	0.002509	0.001635	0.001275	0.00158	0.000813	0.0006992
10	0.002411	0.002039	0.001537	0.00150	0.001207	0.001142
Avg.	0.0027321	0.001920	0.001542	0.001311	0.0011456	0.000920

Table 4.6 RMSE vs Snapshots for Interpolated Co-array MUSIC Algorithm Using Coprime(4,5)

	Number of Snapshots					
Trial	100	200	300	400	500	600
1	0.002059	0.001167	0.001123	0.001262	0.0008807	0.0007587
2	0.002141	0.001501	0.001304	0.000793	0.000755	0.0008367
3	0.002002	0.00141	0.001370	0.001095	0.0007824	0.0007936
4	0.001584	0.001565	0.001165	0.001063	0.00097	0.000654
5	0.001973	0.001636	0.0009861	0.0009058	0.001045	0.0009786
6	0.001516	0.001662	0.0006826	0.001033	0.001004	0.000875
7	0.001901	0.001383	0.001218	0.001097	0.000812	0.0008402
8	0.002117	0.001601	0.001335	0.001116	0.0008575	0.000749
9	0.002160	0.001589	0.001424	0.0009348	0.0009045	0.0008356
10	0.002188	0.001712	0.001090	0.001330	0.0009674	0.000837
Avg.	0.00196	0.00152	0.001170	0.001063	0.00090	0.000816

The tabulated data for varying snapshots was represented in a plot of Figure 4.48 for which DECOM and UCLA coprime arrays were also plotted for a better comparison with the interpolated array in the same figure. It was observed that an increase in the number of snapshots as well as the number of sensors reduces the errors recorded but in general, interpolated array recorded the least RMSE followed by UCLA and DECOM in that order.

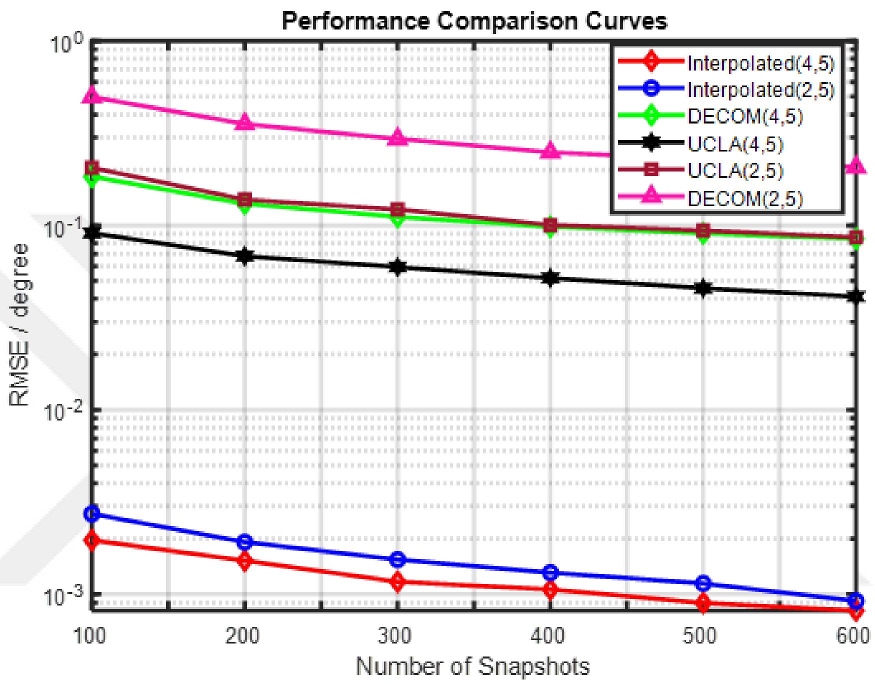

Figure 4.48 RMSE for varying Number of Snapshots in DOA Estimation Using DECOM, UCLA & Interpolated Arrays

CHAPTER FIVE
CONCLUSION AND FUTURE WORK

5.1 Conclusion

5.1.1 1D DOA Estimation Methods

In 1D scenario, both DECOM and UCLA structures can be considered as high-resolution arrays structures especially if implemented with MUSIC algorithm. However, different performance indicators throughout this analysis have emerged to favour UCLA geometry. For instance, It was found out that when the SNR is lower and sources are closer, the resolution of estimation reduces. Increasing the sensor elements number as well as SNR improves the estimation resolution and detection of the individual sources.

DECOM operates decomposes the signals in each sub-array and processes this data separately thereby losing the intrinsic mutual information of the array whereas for UCLA the the signal information from all the sub-arrays are processed simultaneously therefore preserving the intrinsic mutual information of the array leading to automatic pairing, reduction in ambiguous maximas and reduced RMSEs. On the same note, DECOM method is viewed as a computationally intensive and time consuming method since each sub-array data follows the whole procedure to estimate the DOAs independently, a case that is avoided in UCLA since it amalgamates all the signals from both sub-arrays before processing.

5.1.2 2D DOA Estimation Methods

In 2D DOA estimation methods, the two geometries analyzed are seen to be providing high resolutions with less errors. A point to note is that UCLSA , unlike CLSA, has the ability to suppress ambiguous DOAs and automatically pair the elevation angles with the azimuths.

The CLSA method operates on each sub-array separately thereby losing the intrinsic mutual information of the array leading to ambiguous DOAs on the the spectrum. This method also requires physical pairing of the DOAs estimated by the separate sub-arrays and at the same time it is seen as a computationally complex method as the sub-array data is processed separately. In the contrary, UCLSA method processes the total signal simultaneously thereby preserving the intrinsic mutual information of the array leading to automatically paired DOAs, very limited ambiguous DOAs in the spectrum as well as low RMSEs as opposed to CLSA

5.1.3 DOA Estimation Using Virtual Array Interpolation

Application of virtual array interpolation for sparse arrays increases the DOF of the array thereby enabling the array to resolve more sources. This is important especially for practical applications since it helps in increasing the aperture arbitrarily without adding physical sensors which reduces the computational complexity and hence increases the overall array response time. More specifically, nuclear norm minimization method does not require matrix vectorisation, spatial smoothing or discretization of parameter space into a dense grid respectively all which when applied leads to computational complexity.

5.2 Future Work

Coprime array, one of the sparse array geometries has provided a platform for computationally less complex 2D DOA estimation. Virtual interpolated co-array is proving productive in resolution of more sources than sensors. Focus should therefore be on finding an interpolating algorithm with much lesser complexity than the one applied here. Further, interpolation of arrays in multidimensional with automatic angle pairing is an area of future focus. Coprime L-shaped array (CLSA) can as well be considered for different orientations like cross-shaped for purposes of determining an optimal orientation.

REFERENCES

Al-Sarawi, S., Anbar, M., Abdullah, R., & Al Hawari, A. B. (2020). Internet of things market analysis forecasts, 2020–2030. In *2020 Fourth World Conference on Smart Trends in Systems, Security and Sustainability (WorldS4)*, *IEEE*, 449–453.

Andersen, J. B. (2017). History of communications/radio wave propagation from marconi to mimo. *IEEE Communications Magazine*, *55*(2), 6–10.

Balabadrapatruni, S. S. (2012). Performance evaluation of direction of arrival estimation using matlab. *Signal & Image Processing*, *3*(5), 57–72.

Balanis, C. A. (1969). Fundamental parameters and definitions for antennas. *IEEE Transactions on Antennas and Propagation*, *AP-17*(3), 3–56.

Balanis, C. A. (2016). *Antenna theory: Analysis and Design*. Hoboken, New Jersey: John wiley & sons Inc.

Barodia, B. (2017). Performance analysis of music algorithm for DoA estimation. *International Research Journal of Engineering and Technology (IRJET)*, *4*(2), 1667–1670.

Bellofiore, S., Balanis, C. A., Foutz, J., & Spanias, A. S. (2002). Smart-antenna systems for mobile communication networks. Part 1. Overview and antenna design. *IEEE Antennas and Propagation Magazine*, *44*(3), 145–154.

Bhalla, M. R., & Bhalla, A. V. (2010). Generations of mobile wireless technology: A survey. *International Journal of Computer Applications*, *5*(4), 26–32.

Bhobe, A. U., & Perini, P. L. (2001). An overview of smart antenna technology for wireless communication. *2001 IEEE Aerospace Conference Proceedings (Cat. No. 01Th8542)*, *2*(1), 875–883.

Bhuiya, S., Islam, F., & Matin, M. (2012). Analysis of direction of arrival techniques using uniform linear array. *International Journal of Computer Theory and Engineering*, *4*(6), 931–934.

Bush, D., & Xiang, N. (2017). n-tuple coprime sensor arrays. *The Journal of the Acoustical Society of America*, *142*(6), EL567–EL572.

Chen, Z., Fan, C., & Huang, X. (2020). Virtual array interpolation for coprime arrays: a signal reconstruction perspective. *Electronics Letters*, *56*(22), 1213–1215.

Chung, P.-J., Viberg, M., & Yu, J. (2014). DoA estimation methods and algorithms. In *Academic Press Library in Signal Processing*, *3*, 599–650.

Dai, H., Cherniakov, M., & Hong, J. (2006). Link budget analysis in mobile communication system. In *2006 International Conference on Communication Technology*, *IEEE*, 1–4.

Devendra, M., & Manjunathachari, K. (2015). DoA estimation of a system using music method. In *2015 International Conference on Signal Processing and Communication Engineering Systems*, *IEEE*, 309–313.

Dhande, P. (2009). Antennas and its applications. *DRDO Science Spectrum*, 66–78.

Dhope, T. S., Simunic, D., & Zentner, R. (2013). Comparison of DoA estimation algorithms in SDMA system. *Automatika: Journal for Control, Measurement, Electronics, Computing and Communications*, *54*(2), 199–209.

Dong, Y.-Y., Dong, C.-x., Liu, W., Chen, H., & Zhao, G.-q. (2017). 2-D DoA estimation for L-shaped array with array aperture and snapshots extension techniques. *IEEE Signal Processing Letters*, *24*(4), 495–499.

Dongarsane, C. R., & Jadhav, A. (2011). Simulation study on DoA estimation using MUSIC algorithm. *International Journal of Technology And Engineering System (IJTES)*, *2*(1), 54–57.

Falciasecca, G., & Valotti, B. (2009). Guglielmo marconi: The pioneer of wireless communications. In *2009 European Microwave Conference (EuMC)*, *IEEE*, 544–546.

Gentilho, E., Scalassara, P. R., & Abrão, T. (2020). Direction-of-arrival estimation methods: A performance-complexity tradeoff perspective. *Journal of Signal Processing Systems*, *92*(2), 239–256.

Giordani, M., Polese, M., Mezzavilla, M., Rangan, S., & Zorzi, M. (2020). Toward 6G networks: Use cases and technologies. *IEEE Communications Magazine*, *58*(3), 55–61.

Gong, P., Zhang, X., & Zheng, W. (2018). Unfolded coprime L-shaped arrays for two-dimensional direction of arrival estimation. *International Journal of Electronics*, *105*(9), 1501–1519.

Grant, M., Boyd, S., & Ye, Y. (2009). *CVX: Matlab software for disciplined convex programming*. Retrieved December 20, 2020, from http://www.stanford.edu/~boyd/cvx.

Guo, M., Zhang, Y. D., & Chen, T. (2018). DoA estimation using compressed sparse array. *IEEE Transactions on Signal Processing*, *66*(15), 4133–4146.

Gupta, P., & Kar, S. (2015). MUSIC and improved MUSIC algorithm to estimate direction of arrival. In *2015 International Conference on Communications and Signal Processing (ICCSP)*, *IEEE*, 0757–0761.

Hassan, T. U., Gao, F., Jalal, B., & Arif, S. (2018). Direction of arrival estimation using augmentation of coprime arrays. *Information*, *9*(11), 277.

He, W., Yang, X., & Wang, Y. (2020). A high-resolution and low-complexity DoA estimation method with unfolded coprime linear arrays. *Sensors*, *20*(1), 218.

Hosseini, S. M., & Sebt, M. A. (2017). Array interpolation using covariance matrix completion of minimum-size virtual array. *IEEE Signal Processing Letters*, *24*(7), 1063–1067.

Hu, B., Lv, W., & Zhang, X. (2015). 2D-DoA estimation for co-prime L-shaped arrays with propagator method. In *2015 4th National Conference on Electrical, Electronics and Computer Engineering*, *Atlantis Press*, 1551–1556.

Hu, N., Ye, Z., Xu, X., & Bao, M. (2013). DoA estimation for sparse array via sparse signal reconstruction. *IEEE Transactions on Aerospace and Electronic Systems*, *49*(2), 760–773.

Ilderem, V. (2019). 1.4 5G wireless communication: An inflection point. In *2019 IEEE International Solid-State Circuits Conference-(ISSCC)*, *IEEE*, 35–39.

Jaafer, Z., Goli, S., & Elameer, A. S. (2018). Best performance analysis of doa estimation algorithms. In *2018 1st Annual International Conference on Information and Sciences (AiCIS)*, *IEEE*, 235–239.

Joshi, R., & Dhande, A. (2014). Direction of arrival estimation using music algorithm. *International Journal of Research in Engineering and Technology*, *3*(3), 633–636.

Kiani, S., & Pezeshk, A. M. (2015). A comparative study of several array geometries for 2d doa estimation. *Procedia Computer Science*, *58*, 18–25.

Kubba, Z. M. J., & Hoomod, H. K. (2019). The internet of everything based smart systems: Applications and challenges. In *2019 1st AL-Noor International Conference for Science and Technology (NICST)*, *IEEE*, 58–62.

Kwizera, E., Mwangi, E., & Konditi, D. (2017). Direction of arrival estimation based on music algorithm using uniform and non-uniform linear arrays. *Journal of Engineering Research and Application ISSN*, 2248–9622.

Lakshmi, T. J., & Sivvam, S. (2017). Smart antennas for wireless communication. *International Journal of Applied Engineering Research ISSN 0973-4562*, *12*(1), 100–105.

Lavate, T. B., Kokate, V., & Sapkal, A. (2010). Performance analysis of music and esprit doa estimation algorithms for adaptive array smart antenna in mobile communication. In *2010 Second International Conference on Computer and Network Technology*, *IEEE*, 308–311.

Lee, W. C. (1986). Elements of cellular mobile radio systems. *IEEE Transactions on Vehicular Technology*, *35*(2), 48–56.

Li, F., Liu, H., & Vaccaro, R. J. (1993). Performance analysis for doa estimation algorithms: unification, simplification, and observations. *IEEE Transactions on Aerospace and Electronic Systems*, *29*(4), 1170–1184.

Li, J., Li, Y., & Zhang, X. (2018). Two-dimensional off-grid doa estimation using unfolded parallel coprime array. *IEEE Communications Letters*, *22*(12), 2495–2498.

Li, J., & Zhang, X. (2017). Direction of arrival estimation of quasi-stationary signals using unfolded coprime array. *IEEE access*, *5*, 6538–6545.

Li, W., Mao, X., Yu, W., & Yue, C. (2014). An effective technique for enhancing direction finding performance of virtual arrays. *International journal of antennas and propagation*, *2014*(728463), 1–7.

Liu, A., Yang, Q., Zhang, X., & Deng, W. (2017). Direction-of-arrival estimation for coprime array using compressive sensing based array interpolation. *International Journal of Antennas and Propagation*, *2017*(6425067), 1–10.

Liu, C.-L., Vaidyanathan, P., & Pal, P. (2016). Coprime coarray interpolation for doa estimation via nuclear norm minimization. In *2016 IEEE International Symposium on Circuits and Systems (ISCAS)*, *IEEE*, 2639–2642.

Liu, Z.-M., Zhang, C., & Philip, S. Y. (2018). Direction-of-arrival estimation based on deep neural networks with robustness to array imperfections. *IEEE Transactions on Antennas and Propagation*, *66*(12), 7315–7327.

Miraz, M. H., Ali, M., Excell, P. S., & Picking, R. (2015). A review on internet of things (iot), internet of everything (ioe) and internet of nano things (iont). In *2015 Internet Technologies and Applications (ITA)*, *IEEE*, 219–224.

Misra, G., Agarwal, K., Agarwal, A., Ghosh, K., & Agarwal, S. (2018). Smart antenna for wireless cellular communication-a technological analysis on architecture, working mechanism, drawbacks and future scope. In *2018 2nd International Conference on I-SMAC (IoT in Social, Mobile, Analytics and Cloud)(I-SMAC) I-SMAC (IoT in Social, Mobile, Analytics and Cloud)(I-SMAC), 2018 2nd International Conference on*, *IEEE*, 37–41.

Pal, P., & Vaidyanathan, P. P. (2011). Coprime sampling and the music algorithm. In *2011 Digital Signal Processing and Signal Processing Education Meeting (DSP/SPE)*, *IEEE*, 289–294.

Qin, S., Zhang, Y. D., & Amin, M. G. (2015). Generalized coprime array configurations for direction-of-arrival estimation. *IEEE Transactions on Signal Processing*, *63*(6), 1377–1390.

Ramiro, J., & Hamied, K. (2011). *Self-organizing networks: self-planning, self-optimization and self-healing for GSM, UMTS and LTE*. The Atrium, Southern Gate, Chichester, West Sussex, PO19 8SQ, United Kingdom: John Wiley & Sons.

Reaz, K., Haque, F., & Matin, M. (2012). A comprehensive analysis and performance evaluation of different direction of arrival estimation algorithms. In *2012 IEEE Symposium on Computers & Informatics (ISCI)*, *IEEE*, 256–259.

Renukadas, B. B., & Beed, G. (2016). Smart antennas for mobile communications. *Journal of Electronics and Communication Engineering*, *11*(4), 69–72.

Santacruz, J. P., Morales, A., Rommel, S., Johannsen, U., Navas, A. J., & Monroy, I. T. (2020). Experimental assessment of modulation formats for beyond 5g mm-wave arof systems. In *2020 European Conference on Networks and Communications (EuCNC)*, *IEEE*, 300–304.

Saunders, S. R., & Aragón-Zavala, A. (2007). *Antennas and propagation for wireless communication systems*. The Atrium, Southern Gate, Chichester, West Sussex, PO19 8SQ, England: John Wiley & Sons.

Sharma, B., Singh, G., & Sarkar, I. (2015). Study of doa estimation using music algorithm. *International Journal of Scientific & Engineering Research*, *6*, 594–603.

Sun, F., Lan, P., & Zhang, G. (2018). Reduced dimension based two-dimensional doa estimation with full dofs for generalized co-prime planar arrays. *Sensors*, *18*(6), 1725–1735.

Tayem, N., & Kwon, H. M. (2005). L-shape 2-dimensional arrival angle estimation with propagator method. *IEEE transactions on antennas and propagation*, *53*(5), 1622–1630.

Vaidyanathan, P. P., & Pal, P. (2010). Sparse sensing with co-prime samplers and arrays. *IEEE Transactions on Signal Processing*, *59*(2), 573–586.

Vaidyanathan, P. P., & Pal, P. (2011). Sparse sensing with co-prime samplers and arrays. *IEEE Transactions on Signal Processing*, *59*(2), 573–586.

Wang, Z., Xiaofei, Z., & Zhan, S. (2017). Two-dimensional direction of arrival estimation for coprime planar arrays via a computationally efficient one-dimensional partial spectral search approach. *IET Radar, Sonar & Navigation*, *11*(10), 1581–1588.

Yan, F.-G., Chen, Z.-K., Sun, M.-J., Shen, Y., & Jin, M. (2015). Two-dimensional direction-of-arrivals estimation based on one-dimensional search using rank deficiency principle. *International Journal of Antennas and Propagation*, *2015*(127621), 1–8.

Yang, D.-l., Liu, W.-t., Cheng, Q.-l., Xia, Z.-x., & Zhang, X.-f. (2017). 2D-DOA Estimation for Coprime L-shaped Arrays with MUSIC Algorithm. *DEStech Transactions on Computer Science and Engineering*, *CECE2017*(ISBN: 978-1-60595-476-9), 275–281.

Zhang, D., Zhang, Y., Zheng, G., Deng, B., Feng, C., & Tang, J. (2018). Two-dimensional direction of arrival estimation for coprime planar arrays via polynomial root finding technique. *IEEE Access*, *6*, 19540–19549.

Zhang, K., Shen, C., Li, H., Li, Z., Wang, H., Chen, X., & Chen, J. (2020). Direction of arrival estimation and robust adaptive beamforming with unfolded augmented coprime array. *IEEE Access*, *8*, 22314–22323.

Zhang, Z., Guo, Y., Huang, Y., & Zhang, P. (2019). A 2-D DOA Estimation Method With Reduced Complexity in Unfolded Coprime L-Shaped Array. *IEEE Systems Journal*, *15*(1), 407–410.

Zhang, Z., Wang, W., Huang, Y., & Liu, S. (2017). Decoupled 2-d direction of arrival estimation in l-shaped array. *IEEE Communications Letters*, *21*(9), 1989–1992.

Zhao, P., Wang, K., Hu, G., & Wan, L. (2019). Underdetermined doa estimation using unfold coprime array from the perspective of sum-difference co-array. *IEEE Access*, *7*, 168557–168564.

Zhou, C., Shi, Z., Gu, Y., & Shen, X. (2013). Decom: Doa estimation with combined music for coprime array. In *2013 International Conference on Wireless Communications and Signal Processing*, *IEEE*, 1–5.

Zoltowski, M. D., & Wong, K. T. (2000). Esprit-based 2-d direction finding with a sparse uniform array of electromagnetic vector sensors. *IEEE Transactions on Signal Processing*, *48*(8), 2195–2204.

APPENDICES

Appendix 1: Acronyms and Abbreviations

1D	One Dimensional
2D	Two Dimensional
3D	Three Dimensional
5G	Fifth Generation
BER	Bit Error Rate
CLA	Coprime Linear Array
CLSA	Coprime L-shaped Arrays
CPA	Coprime Planar Arrays
CRB	Cramer-Rao Bound
CRLB	Cramer-Rao Lower Bound
CSA	Cross shaped Array
CVX	Matlab Software for Disciplined Convex Programming
DECOM	Decomposition and Combination
DOA	Direction of Arrival
DOF	Degrees of Freedom
DS	Delay-and-Sum
ESPRIT	Estimation of Signal Parameters via Rotational Invariance Techniques
EVD	Eigenvalue Decomposition
GHz	Gega Hertz

IoE	Internet of Everything
IoT	Internet of Things
LSA	L-shaped Array
MHA	Minimum Hole Arrays
ML	Maximum Likelihood
MRA	Minimum Redundancy Arrays
MUSIC	Multiple Signal Classification
MVDR	Minimum Variance Distortionless Response
NCLA	Nonuniform Coprime Linear Array
QoS	Quality of Service
RMSE	Root Mean Square Error
SNR	Signal to Noise Ratio
SULA	Sparse Uniform Linear Array
UCA	Uniform Circular Array
UCLA	Unfolded Coprime Linear Array
UCLSA	Unfolded Coprime L-shaped Array
ULA	Uniform Linear Array
VSNLA	Virtual Symmetric Nonuniform Linear Array
VULA	Virtual Uniform Linear Array
Wi-Fi	Wireless Fidelity
WSF	Weighted Subspace Fitting
ZB	Zetabytes

Appendix 2: Symbols

$\vert \cdot \vert$	Absolute value
$[\cdot]^H$	Transpose conjugate
$[\cdot]^T$	Transpose
$\in$	Is member of a given set
λ	Wavelength
$\Vert\cdot\Vert$	Frobenius norm
$\mathbb{A}$	Set A
$\mathbb{C}$	Set of complex numbers
$O(\cdot)$	Bachmann-Landau or asymptotic notation
ϕ	Predominantly used to refer to azimuth angle
σ	Signal or noise standard deviation
$\subseteq$	Is a subset of
$\mathbf{I}$	Identity matrix
$\mathbf{O}$	Null matrix
θ	Predominantly used to refer to elevation angle
Bold letters	Vectors (matrices)
$diag[\cdot]$	Diagonal matrix
$E[\cdot]$	Statistical expectation
Hatted letters	Approximated values
$\Vert\cdot\Vert_*$	Nuclear norm
σ^2	Signal or noise (variance) power